

Computing Spin Networks

Annalisa Marzuoli

Dipartimento di Fisica Nucleare e Teorica, Università degli Studi di Pavia and
Istituto Nazionale di Fisica Nucleare, Sezione di Pavia,
via A. Bassi 6, 27100 Pavia (Italy)
annalisa.marzuoli@pv.infn.it

and

Mario Rasetti

Dipartimento di Fisica and Istituto Nazionale di Fisica della Materia,
Politecnico di Torino,
corso Duca degli Abruzzi 24, 10129 Torino (Italy)
rasetti@isi36a.isi.it

Abstract

We expand a set of notions recently introduced providing the general setting for a universal representation of the quantum structure on which quantum information stands. The dynamical evolution process associated with generic quantum information manipulation is based on the (re)coupling theory of $SU(2)$ angular momenta. Such scheme automatically incorporates all the essential features that make quantum information encoding much more efficient than classical: it is fully discrete; it deals with inherently entangled states, naturally endowed with a tensor product structure; it allows for generic encoding patterns. The model proposed can be thought of as the non-Boolean generalization of the *quantum circuit* model, with unitary gates expressed in terms of $3nj$ coefficients connecting inequivalent binary coupling schemes of $n + 1$ angular momentum variables, as well as Wigner rotations in the eigenspace of the total angular momentum. A crucial role is played by elementary j -gates ($6j$ symbols) which satisfy algebraic identities that make the structure of the model similar to "state sum models" employed in discretizing Topological Quantum Field Theories and quantum gravity. The spin network simulator can thus be viewed also as a Combinatorial QFT model for computation. The semiclassical limit (large j) is discussed.

PACS numbers: 03.67.Lx, 03.65.Fd, 11.10.Kk

Keywords: Quantum Computation, Spin Networks, Topological Quantum Field Theory.

1 Introduction

It is by-now a generally accepted fact that the laws of quantum theory provide in principle a radically novel, and more powerful way to process information than any classically operated device [1]. In the past few years a big deal of activity has been devoted to devise and to implement schemes for taking actual advantage from such quantum extra power. In particular in Quantum Computation (QC) the states of a quantum system \mathcal{S} are used for encoding information in such a way that the final state, obtained by the appropriate unitary time evolution of \mathcal{S} , encodes the solution to a given computational problem. A system \mathcal{S} with state-space \mathcal{H} (the *Quantum Computer*) supports universal QC if any unitary transformation $U \in \mathcal{U}(\mathcal{H})$ can be approximated with arbitrarily high accuracy by a sequence (the *network*) of simple unitaries (the *gates*) that the experimenter is supposed to be able to implement. The case in which \mathcal{S} is a multi-partite system is the most relevant, as it allows for entanglement, a unique quantum feature that is generally believed to be one of the crucial elements from which quantum speed-up (polynomial or possibly exponential) is generated [2].

In the above picture of QC the realization of the quantum network is achieved at the physical level by turning on and off external fields coupled to \mathcal{S} as well as local interactions among the subsystems of \mathcal{S} . In other words the experimenter "owns" a basic set of time-dependent Hamiltonians that she/he activates at will to perform the necessary sequences of quantum logic gates.

At variance with such a standard dynamical view of QC, more recently several authors considered geometrical and topological approaches [3]–[7]. The peculiarity of these proposals is far reaching: over the manifold \mathcal{C} of quantum codewords one can have a trivial Hamiltonian, for example $H|_{\mathcal{C}} = 0$, yet obtain nevertheless a non-trivial quantum evolution due to the existence of an underlying geometrical/topological global structure. The quantum gates – or parts thereof – in this latter case are realized in terms of operations having a purely geometrical/topological nature. Besides being conceptually intriguing on their own, these schemes have some built-in fault-tolerant features. This latter attractive characteristic stems out of the fact that often certain topological as well as geometrical quantities are inherently stable against local perturbations. This in turn allows for quantum information processing inherently stable against special classes of computational errors.

There has been a number of proposals suggesting general conceptual schemes of interpretation of quantum computation. Most of them are in-

deed based on topological notions, even though this is not always explicitly stated. Among these, anyonic quantum computation [3], fermionic quantum computation [8], localised modular functor quantum field computation [4], holonomic quantum computation [9], [10] have mostly attracted attention. However, such models appear to be simply different realizations of a unique conceptual scheme that incorporates all of them as particular instances (once one focuses on their suitable "discretized" counterparts).

We propose here, expanding a set of notions introduced in [11], a general setting for a universal representation of the very quantum structure on which quantum information stands. The associated dynamical evolution process, giving rise to information manipulation, is based on the (re)coupling theory of $SU(2)$ angular momenta (see [12], [13] Topic 12, [14]). The scheme automatically incorporates all the essential features that make quantum information encoding so much more efficient than classical: it is fully discrete (both for space-like and time-like variables); it deals with inherently entangled states, naturally endowed with a (non associative) tensor product structure; it allows for generic encoding patterns. The minimal set of requirements listed by Feynman [15] as essential for the proper characterisation of an efficient quantum simulator is automatically satisfied: i) locality of interactions; ii) number of "computer" elements proportional to a function which is at most polynomial in the space-time volume of the physical system; iii) time discreteness (time is itself "simulated" in the computer by computational steps).

Key element of our argument is the fact that all such basic features are typical of spin networks. It should be emphasized that by *spin networks* we mean here – contrary to what happens in solid state physics, but somewhat in the spirit of combinatorial approach to quantum space-time representation [16] – graphs the node and edge sets of which can be labelled by quantum numbers associated with $SU(2)$ irreducible representations and by $SU(2)$ recoupling coefficients, respectively. For this reason spin networks can be thought of as an ideal candidate conceptual framework for dealing with tensorial transformations and topological effects in groups of observables. The idea is to exploit to their full extent the discreteness hypotheses ii) and iii), by modelling the computational space in terms of a set of combinatorial and topological rules that mimic space-time features in a way that automatically includes quantum mechanics.

The model proposed can be thought of as a non-Boolean generalization of the *quantum circuit* model, with unitary gates expressed in terms of: a) recoupling coefficients ($3nj$ symbols) between inequivalent binary coupling

schemes of $N = n + 1$ $SU(2)$ -angular momentum variables (j -gates); b) Wigner rotations in the eigenspace of the total angular momentum (M -gates). These basic ingredients of the spin network simulator, namely computational Hilbert spaces and admissible elementary gates, are discussed in details in Sections 2 and 3, respectively. The picture does contain the Boolean case as the particular case when all N angular momenta are spin $\frac{1}{2}$.

In Section 4 both the architecture and the computational capabilities of the simulator are described in full extent. On the kinematical side (Section 4.1), the computational space is shown to be modeled as an $SU(2)$ -decorated graph or, more precisely, as a fiber space structure over a discrete base space – the Rotation graph – which encodes all possible computational Hilbert spaces as well as gates for any fixed number N of incoming angular momenta. A crucial role is played by elementary j -gates (Racah transforms, related to $6j$ symbols of $SU(2)$) which satisfy suitable algebraic identities [14] and make the structure of the model similar to "state sum models" employed in discretizing Topological Quantum Field Theories (TQFT) and quantum gravity (see Section 5). In Section 4.2, after a discussion of the hypotheses of Feynman [15], general circuit-type computation processes on the spin network are described and classified into *computing classes*. Virtual, polylocal Hamiltonians are generated by the simulator which evolves in an intrinsic discrete time variable. Section 4.3 deals with questions in (quantum) computational complexity which turn out to be closely related to graph combinatorics. We argue that our new framework, when implemented on the basis of explicit encoding schemes [17], could be suitable to handle "combinatorially hard" problems more efficiently than any classical machine.

The key ingredient of Section 5 is the Ponzano–Regge asymptotic formula [18] for the $6j$ symbol which plays a twofold role. On the one hand, it gives a precise meaning to the semiclassical analog of a j -gate providing, together with the asymptotics of Wigner rotation matrices [13] (Topic 9), the notion of "approaching a classical simulator" out of a quantum one. Moreover, as stated in [11], the whole conceptual scheme of spin network computing can be reformulated in terms of density matrix formalism, namely resorting no longer to sharp eigenstates of angular momenta but rather to generalised multipole moments (see *e.g.* [19], Ch. 7.7). Such generalisations can be summarised in the following diagram

SEMICLASSICAL SIMULATOR

 \Uparrow (large quantum numbers) \Uparrow

SPIN NETWORK QU-SIMULATOR

 \Downarrow (extension to) \Downarrow

MIXED STATES COMPUTING MACHINE

On the other hand, the Ponzano–Regge asymptotic formula opens the intriguing possibility of bridging the quantum theory of angular momenta to Euclidean gravity in dimension three. More precisely, a *state sum functional* for triangulated 3–dimensional space–time manifolds, built up by associating a $6j$ symbol with each tetrahedron, is shown to correspond, in the asymptotic limit, to the semiclassical partition function of gravity [18] with a classical action representing the discretized counterpart of the Einstein–Hilbert action of general relativity [20]. Since quantum gravity in dimension three is strictly related to a TQFT with an $SU(2)$ Chern–Simons–type action (see references quoted at the end of Section 5 and at the beginning of Section 6) we present in this part of the paper some known results concerning spin networks viewed as “Combinatorial Quantum Field Theories”, to be interpreted as discretized versions of TQFTs based on $SU(2)$ –decorated triangulations. At the end of Section 5 we compare the discrete partition functions of Ponzano–Regge gravity with the partition functions introduced in Section 4.2 in connection with the simulator’s dynamics. We conclude that a spin network simulator working by switching on j –gates acting on states with N incoming spins is able to simulate some subclasses of triangulated surfaces and possibly some subclasses of triangulated 3–manifolds but, since partition functions for quantum field theories must be “sums over all configurations” (apart from regularization), we cannot infer the possibility of fully simulating Combinatorial QFT (unless we take some sort of thermodynamical limit for $N \rightarrow \infty$ which does not sound good when dealing with quantum circuit schemes for computation).

We start Section 6 (Spin network and topological quantum computation) by reviewing some basic definitions on TQFTs. Section 6.1 addresses holonomic quantum computation and we give indications that the discrete setting developed in Section 4 could support also such kind of computational

processes. In Section 6.2 we compare the spin network approach with the approach of Freedman and collaborators [4]. We provide a (not unique) mapping between the spin network and the modular functor approach by introducing combinatorial marked 2-disks which display localised interactions between spins. The algebraic structures of the two approaches, summarised in the Yang–Baxter identity for the standard topological one and in the (hexagon + pentagon) identities for the spin network, suggest that the partition functions of the two models are related to each other in the same way as the regularized version of Ponzano–Regge functional corresponds to a double Chern–Simons partition function.

In Appendix A we present the graph–theoretical rationale underlying spin network combinatorics by collecting results spread over a number of references in discrete mathematics, binary couplings and recoupling theory of angular momenta, complexity theory. Binary coupling trees are defined in Appendix A1, Twist–Rotation and Rotation graphs in A2 and some results in (classical) combinatorial complexity theory are summarised in A3. Appendix B contains (standard) technical results concerning the composition of Wigner rotation matrices (B1) and U–rotation matrices (B2) which are employed in Section 3.2 (M –gates).

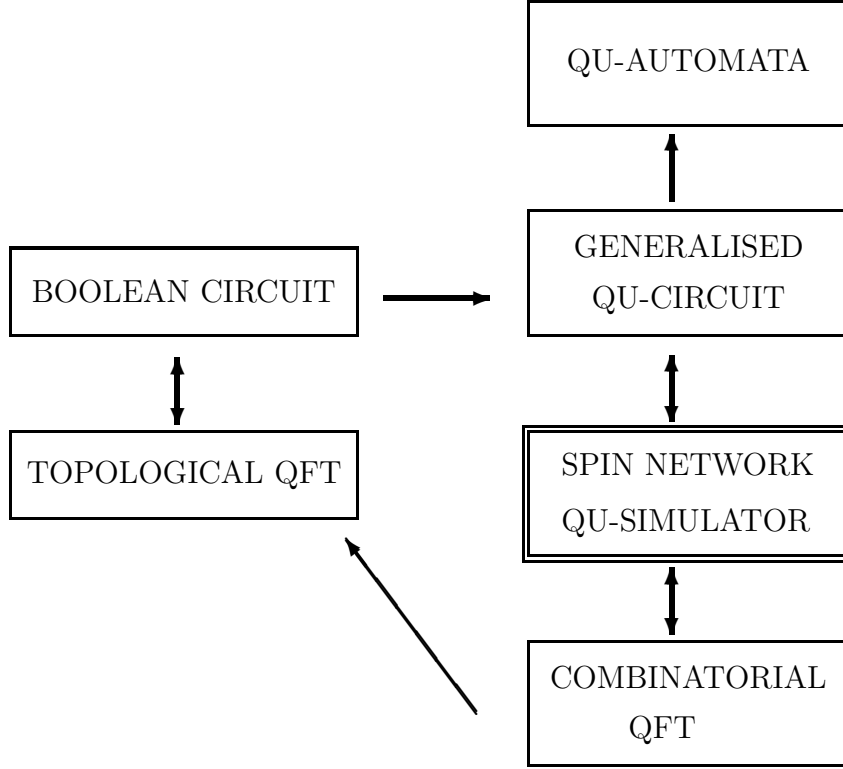
The twofold possible interpretation of the deliberately ambiguous title we have chosen for the paper should have become clear at this point:

- on the one hand, spin networks are computing devices supporting simulations of the dynamical behaviour of composite quantum systems described in terms of pure angular momentum eigenstates;
- such computing devices, on the other hand, are able to simulate classes of extended geometrical objects modeled as spin networks.

We may summarise the content of the paper in the following diagram, where the spin network simulator may be viewed both as a generalised quantum circuit and as a Combinatorial QFT model for computation. The standard Boolean quantum circuit (shown to be equivalent to the topological approach [4]) is a particular case of this general scheme for computation. To complete the picture, the combinatorial approach can be suitably mapped into the purely topological one as discussed in Section 6.2.

We plan to develop in the next future the upper connection which points toward “quantum automata” since our framework seems quite promising to address such issues like quantum languages and grammars, quantum encoding [17] and quantum complexity classes of algorithms, naturally related here

to enumerative combinatorics of graphs.



2 Computational Hilbert spaces

Following [13] (Topic 12) let us consider $N = n + 1$ mutually commuting angular momentum operators of the algebra of $SU(2)$

$$\mathbf{J}_1, \mathbf{J}_2, \mathbf{J}_3, \dots, \mathbf{J}_{n+1} \equiv \{\mathbf{J}_i\}$$

and the corresponding components

$$\{J_{i(z)}\}_{i=1,2,\dots,n+1}$$

along the quantization axis. For each $i = 1, 2, \dots, n + 1$ the simultaneous eigenstates of the complete sets \mathbf{J}_i^2 and $J_{i(z)}$ are

$$\begin{aligned}\mathbf{J}_i^2 |j_i m_i\rangle &= j_i(j_i + 1) |j_i m_i\rangle \\ J_{i(z)} |j_i m_i\rangle &= m_i |j_i m_i\rangle,\end{aligned}\tag{1}$$

where we set $\hbar = 1$ and the eigenvalues range over

$$\begin{aligned}j_i &= 0, \frac{1}{2}, 1, \frac{3}{2}, \dots; \\ -j_i &\leq m_i \leq j_i \text{ (integer steps)}.\end{aligned}\tag{2}$$

Denoting by

$$\mathcal{H}^{j_i} \doteq \text{span} \{ |j_i m_i\rangle \}$$

the $(2j_i + 1)$ -dimensional Hilbert space supporting the j_i -th irreducible representation of $SU(2)$, the tensor product

$$\begin{aligned}\mathcal{H}^{j_1} \otimes \mathcal{H}^{j_2} \otimes \mathcal{H}^{j_3} \otimes \dots \otimes \mathcal{H}^{j_n} \otimes \mathcal{H}^{j_{n+1}} \\ \doteq \text{span} \{ |j_1 m_1\rangle \otimes \dots \otimes |j_{n+1} m_{n+1}\rangle \}\end{aligned}\tag{3}$$

represents the simultaneous eigenspace of the $2(n + 1)$ operators $\{\mathbf{J}_i^2; J_{i(z)}\}$ and may be used *e.g.* to describe the state of $N = (n + 1)$ kinematically independent particles. By setting $j_1 = j_2 = \dots = j_{n+1} = 1/2$ in (3) we would get $\otimes^N \mathbb{C}^2$, namely the N -qubits space of the Boolean quantum circuit model.

To address the interacting case, we make explicit the basic assumptions on which the model of simulator discussed in this paper relies:

1. The simulator computational states are suitable pure $(n + 1)$ -angular momenta states (to be described below) in Wigner-coupled Hilbert spaces of the total angular momentum operator

$$\mathbf{J}_1 + \mathbf{J}_2 + \mathbf{J}_3 + \dots + \mathbf{J}_{n+1} \doteq \mathbf{J}\tag{4}$$

and of its projection J_z . The corresponding quantum numbers, J and $M \equiv m_1 + m_2 + \dots + m_{n+1}$ ($-J \leq M \leq J$ in integer steps), label the resulting representation spaces (which are referred to as JM -representations).

2. Interactions are not fixed *a priori* but rather are generated by the simulator itself as polylocal virtual Hamiltonian operators (see Section 4.2).
3. The admissible interactions are modeled on (a finite number of) combinations of the following basic types:
 - binary couplings of the computational states which involve only the spin quantum numbers;
 - actions of rotation operators over states in JM -representations involving the total magnetic quantum number and depending on continuous sets of parameters (*e.g.* Euler angles).

Given \mathbf{J} as in (4), the simultaneous eigenspace of the operators \mathbf{J}^2 and J_z (namely a JM -representation space for any fixed J)

$$\begin{aligned}\mathbf{J}^2 |JM\rangle &= J(J+1) |JM\rangle \\ J_z |JM\rangle &= M |JM\rangle\end{aligned}\tag{5}$$

turns out to be degenerate. The degeneracy is partially removed by noticing that $\mathbf{J}_1^2, \mathbf{J}_2^2, \dots, \mathbf{J}_{n+1}^2$ commute with \mathbf{J}^2 and J_z and thus j_1, j_2, \dots, j_{n+1} still are good quantum numbers (while the individual m_1, m_2, \dots, m_{n+1} are not). The ket vectors $|JM\rangle$ in (5) can be rewritten for the moment as $|j_1, j_2, \dots, j_{n+1}; JM\rangle$, namely in terms of $(n+1) + 2$ quantum numbers.

The complete removal of the degeneracy would be achieved by introducing a new set of $(n-1)$ Hermitean operators – commuting with each other and with the previous ones – in order to get a total amount of $2(n+1)$ quantum numbers (this number equals the number of operators needed to specify the eigenstates in the factorized Hilbert space (3)). The most effective way to reach the goal is to consider *equivalently*:

- binary coupling schemes in the sequence

$$\mathbf{J}_1 + \mathbf{J}_2 + \mathbf{J}_3 + \dots + \mathbf{J}_{n+1} = \mathbf{J}\tag{6}$$

- binary bracketings on the factorized Hilbert space

$$\mathcal{H}^{j_1} \otimes \mathcal{H}^{j_2} \otimes \mathcal{H}^{j_3} \otimes \dots \otimes \mathcal{H}^{j_n} \otimes \mathcal{H}^{j_{n+1}}.\tag{7}$$

As a simple example, consider the case $(n + 1) = 3$: the binary coupling schemes are $(\mathbf{J}_1 + \mathbf{J}_2) + \mathbf{J}_3 = \mathbf{J}$; $\mathbf{J}_1 + (\mathbf{J}_2 + \mathbf{J}_3) = \mathbf{J}$; $(\mathbf{J}_1 + \mathbf{J}_3) + \mathbf{J}_2 = \mathbf{J}$, and the corresponding binary bracketings are $(\mathcal{H}^{j_1} \otimes \mathcal{H}^{j_2}) \otimes \mathcal{H}^{j_3}$; $\mathcal{H}^{j_1} \otimes (\mathcal{H}^{j_2} \otimes \mathcal{H}^{j_3})$; $(\mathcal{H}^{j_1} \otimes \mathcal{H}^{j_3}) \otimes \mathcal{H}^{j_2}$, respectively.

The crucial point is to realize that each binary coupling in (6) generates – by using the Clebsch–Gordan series of $SU(2)$ – an intermediate angular momentum operator whose quantum number will be added to the set $\{j_1, j_2, \dots, j_{n+1}; JM\}$. In the case $(n + 1) = 3$ the first coupling scheme $(\mathbf{J}_1 + \mathbf{J}_2) + \mathbf{J}_3 = \mathbf{J}$ splits into

$$\begin{aligned} (\mathbf{J}_1 + \mathbf{J}_2) &= \mathbf{J}_{12} \\ \mathbf{J}_{12} + \mathbf{J}_3 &= \mathbf{J} \end{aligned} \tag{8}$$

with $|j_1 - j_2| \leq j_{12} \leq j_1 + j_2$ and $J = j_{12} + j_3$, while the second coupling scheme $\mathbf{J}_1 + (\mathbf{J}_2 + \mathbf{J}_3) = \mathbf{J}$ splits into

$$\begin{aligned} (\mathbf{J}_2 + \mathbf{J}_3) &= \mathbf{J}_{23} \\ \mathbf{J}_1 + \mathbf{J}_{23} &= \mathbf{J} \end{aligned} \tag{9}$$

with $|j_2 - j_3| \leq j_{23} \leq j_2 + j_3$ and $J = j_1 + j_{23}$.

The reformulation of the same example in terms of binary bracketings on (7) leads to the expressions

$$\begin{aligned} &((\mathcal{H}^{j_1} \otimes \mathcal{H}^{j_2})_{j_{12}} \otimes \mathcal{H}^{j_3})_J \\ &(\mathcal{H}^{j_1} \otimes (\mathcal{H}^{j_2} \otimes \mathcal{H}^{j_3})_{j_{23}})_J \end{aligned} \tag{10}$$

where the inner brackets have been labeled by the q-numbers associated with the corresponding intermediate angular momentum operators and we have added an overall bracket labeled by the total J . Note that these Hilbert spaces, although isomorphic, are not identical since they actually correspond to (partially) different complete sets of physical observables, namely $\{\mathbf{J}_1^2, \mathbf{J}_2^2, \mathbf{J}_{12}^2, \mathbf{J}_3^2, \mathbf{J}^2, J_z\}$ and $\{\mathbf{J}_1^2, \mathbf{J}_2^2, \mathbf{J}_3^2, \mathbf{J}_{23}^2, \mathbf{J}^2, J_z\}$ respectively (in particular, \mathbf{J}_{12}^2 and \mathbf{J}_{23}^2 cannot be measured simultaneously). On the mathematical side this remark reflects the fact that the tensor product \otimes is not an associative operation.

Coming to the general case, a counting argument explained in Appendix A1 (based on combinatorics of rooted labeled binary trees) shows that the number of binary bracketings one can accommodate on the $(n+1)$ -fold tensor product in (7) is $(n-1)$, plus the external bracket $(\dots)_J$. Thus we get exactly the number of intermediate angular momenta operators we need to remove completely the degeneracy in the JM space (5). More precisely, given a particular binary bracketing structure (for the moment we can think of an ordered sequence of incoming angular momenta $\{\mathbf{J}_1, \mathbf{J}_2, \mathbf{J}_3, \dots, \mathbf{J}_{n+1}\}$), we get a unique set of (ordered) mutually commuting operators denoted by

$$\mathbf{K}_1, \mathbf{K}_2, \mathbf{K}_3, \dots, \mathbf{K}_{n-1} \quad (11)$$

with quantum numbers $k_1, k_2, k_3, \dots, k_{n-1}$, each running over a suitable finite range (*cfr.* (8) and (9)).

An explicit example of one possible bracketing structure is given by

$$(\dots(((\mathcal{H}^{j_1} \otimes \mathcal{H}^{j_2})_{k_1} \otimes \mathcal{H}^{j_3})_{k_2} \otimes \dots \otimes \mathcal{H}^{j_n})_{k_{n-2}} \otimes \mathcal{H}^{j_{n+1}})_{k_{n-1}})_J \quad (12)$$

where the incoming angular momenta are coupled sequentially. To denote the basis vectors belonging to such a space we could write either

$$\{|j_1, j_2, j_3, \dots, j_{n+1}; k_1, \dots, k_{n-1}; JM\rangle, -J \leq M \leq J\} \quad (13)$$

(where both the sequences of quantum numbers j 's and k 's are ordered) or

$$\{ |(\dots(((j_1, j_2)_{k_1}, j_3)_{k_2}, \dots), j_{n+1})_{k_{n-1}})_J; JM\rangle, -J \leq M \leq J\}, \quad (14)$$

where the binary bracketing structure $(\cdot \otimes \cdot)_k$ of (12) has been exactly transferred on the string of quantum numbers inside the symbol $|\dots\rangle$ as $(\cdot, \cdot)_k$.

However, when dealing with other types of binary bracketing structures none of the above notations turns out to be well suited. First, we would like to consider any permutation of the incoming angular momenta quantum numbers $\{j_1, j_2, j_3, \dots, j_{n+1}\}$ and not just a sequence with a fixed ordering. It is clear that the notation adopted in (13) is not flexible in this respect. Secondly, we have to get rid of all possible binary arrangements of the incoming variables and at the same time of the resulting (partially ordered) set

of intermediate k 's which appears in the example (14) as subscripts under brackets.

According to the above remarks we shall denote from now on a binary coupled basis of $(n + 1)$ angular momenta in the JM -representation (and the corresponding Hilbert space) as

$$\begin{aligned} & \{ |[j_1, j_2, j_3, \dots, j_{n+1}]^{\mathfrak{b}}; k_1^{\mathfrak{b}}, k_2^{\mathfrak{b}}, \dots, k_{n-1}^{\mathfrak{b}}; JM \rangle, -J \leq M \leq J \} \\ & = \mathcal{H}_n^J(\mathfrak{b}) \doteq \text{span} \{ |\mathfrak{b}; JM \rangle_n \}, \end{aligned} \quad (15)$$

where the string inside $[j_1, j_2, j_3, \dots, j_{n+1}]^{\mathfrak{b}}$ is not necessarily an ordered one, \mathfrak{b} indicates the current binary bracketing structure and the k 's are uniquely associated with the chain of pairwise couplings given by \mathfrak{b} .

As explained in details in Appendix A1, the combinatorial structure underlying the above computational Hilbert spaces (for fixed n and for any J) is provided by *rooted labeled binary trees* with:

- $(n + 1)$ terminal nodes (or leaves) labeled by $\{j_1, j_2, j_3, \dots, j_{n+1}\}$;
- $(n - 1)$ internal nodes labeled by $\{k_1, k_2, k_3, \dots, k_{n-1}\}$;
- the root, labeled by J .

For instance, the binary coupling tree structure corresponding to (12) and (14) is depicted in Fig. 12 of Appendix A1.

As shown in the following Section, processing information through changes of binary coupling schemes of the Hilbert spaces (15) involves only spin quantum numbers (*cfr.* the first assumption in point 3.) and can be modeled on other types of combinatorial structures, Twist-Rotation and Rotation graphs as discussed in Section 4.1.

On the other hand, the quantum number M can be activated by noticing that a vector in $\mathcal{H}_n^J(\mathfrak{b})$ is expressed in terms of the basis (15) as

$$|\mathfrak{b}; J \rangle_n = \sum_{M=-J}^J {}^{(\mathfrak{b})}a_M^J |\mathfrak{b}; JM \rangle_n, \quad (16)$$

where ${}^{(\mathfrak{b})}a_M^J$ ($M = -J, -J + 1, \dots, J - 1, J$) represent the (complex) components of the vector. The natural unitary transformations acting on the

M -dependence of basis vectors and components (Wigner rotation operators $D_{MM'}^J(\alpha\beta\gamma)$ introduced in Section 3.2) are not discrete, but rather depend on continuous parameters as claimed in the second assumption of 3..

Remark 2.1. A more fundamental question arising in connection with assumptions 1., 2., and 3. is the following: we could have included the factorized states (3) too in the set of computational states of the simulator, *e.g.* as non interacting input states. Then any binary coupled state (15) could be generated by means of a suitable sequence of Clebsch–Gordan coefficients representing a unitary transformation depending on the whole set of quantum numbers $\{j_1, j_2, \dots, j_{n+1}; m_1, m_2, \dots, m_{n+1}; k_1, k_2, \dots, k_{n-1}; J, M\}$ (see [13], Topic 12). For instance, a vector in the binary basis associated with (8) is obtained from the factorized basis through

$$\begin{aligned} & |((j_1, j_2)_{j_{12}}, j_3)_J; JM\rangle \\ &= \sum_{m_1 m_2 m_3} C_{j_{12} m_{12} j_3 m_3}^{JM} C_{j_1 m_1 j_2 m_2}^{j_{12} m_{12}} |j_1 m_1\rangle \otimes |j_2 m_2\rangle \otimes |j_3 m_3\rangle, \end{aligned} \quad (17)$$

where there appear two Clebsch–Gordan coefficients. This expression can obviously be inverted, providing us with one factorized basis vector in terms of a combination of binary coupled states in the JM -representation.

However, such kind of procedure – namely going through the factorized basis at each step of "computation" – is not satisfactory in many respects and certainly very cumbersome when dealing with many spins. Even if we could assume that the input state of the simulator is indeed a factorized, non-interacting one (and thus a transformation of the type (17) is certainly allowed), any further unitary computing step would force us to deal with (pure angular momenta) *coupled states*. Now, quantum theory of angular momentum gives us a powerful framework to manipulate the *binary* coupled states of the type we are considering: other kinds of couplings (*e.g.* symmetrical) cannot be efficiently manipulated since the degeneracy in the total JM -representation space cannot be completely removed for $N \equiv n + 1 > 3$ (see the remark at the end of [13], Topic 12).

Summing up, a model of simulator whose computational states are binary coupled ones actually relies on the most exhaustive theory we have at our disposal in order to deal with many-angular momenta quantum systems whose interactions are modeled (or can be well approximated) by polylocal two-body-type interactions. It is worth noting that two-body interactions were

shown to be sufficient to implement universal quantum computation in the decoherence-free subspaces approach according to [21] (see other references therein). \blacktriangle

3 Gates

3.1 j -gates

By j -gates we mean unitary transformations on the computational Hilbert spaces (15) which act on the set of the spin variables $\{j_1, j_2, j_3, \dots, j_{n+1}, k_1, k_2, k_3, \dots, k_{n-1}\}$ of the eigenstates without changing the quantum numbers J and M .

According to the recoupling theory of angular momenta [12], [13] (Topic 12), [14] (see also [22], [23]) the most general unitary transformation between two computational states characterised by different binary coupling schemes \mathbf{b} and \mathbf{b}'

$$\begin{aligned} & |[j_1, j_2, j_3, \dots, j_{n+1}]^{\mathbf{b}}; k_1^{\mathbf{b}}, k_2^{\mathbf{b}}, \dots, k_{n-1}^{\mathbf{b}}; JM\rangle \longmapsto \\ & \longmapsto |[j_1, j_2, j_3, \dots, j_{n+1}]^{\mathbf{b}'}; k_1^{\mathbf{b}'}, k_2^{\mathbf{b}'}, \dots, k_{n-1}^{\mathbf{b}'}; JM\rangle \end{aligned} \quad (18)$$

is a recoupling coefficient of $SU(2)$ (or $3nj$ -symbol) denoted by

$$\mathcal{U}_{3nj} \begin{bmatrix} k_1^{\mathbf{b}} & \dots & k_{n-1}^{\mathbf{b}} \\ k_1^{\mathbf{b}'} & \dots & k_{n-1}^{\mathbf{b}'} \end{bmatrix} \doteq \mathcal{U}_{3nj} [\mathbf{b}; \mathbf{b}'], \quad (19)$$

where the variables $\{j\}$, $\{k^{\mathbf{b}}\}$, $\{k^{\mathbf{b}'}\}$, J , M appearing in states (18) have been partially or totally dropped (*cfr.* the shorthand notation for Hilbert spaces and state vectors introduced in (15)). According to this definition, $|\mathcal{U}_{3nj} [\mathbf{b}; \mathbf{b}']|^2$ represents the probability that a quantum system prepared in the state $|\mathbf{b}; JM\rangle_n$ is measured in the state $|\mathbf{b}'; JM\rangle_n$.

Note that (19) is a reduced tensor operator, namely the magnetic quantum numbers do not appear at all in its expression in view of the Wigner-Eckart theorem [19]. More explicitly, by looking at the *re*-coupling between two states of the type (18) –but with different M, M' – we would get

$$\langle [j_1, \dots, j_{n+1}]^{\mathbf{b}'}; k_1^{\mathbf{b}'}, \dots, k_{n-1}^{\mathbf{b}'}; JM' | [j_1, \dots, j_{n+1}]^{\mathbf{b}}; k_1^{\mathbf{b}}, \dots, k_{n-1}^{\mathbf{b}}; JM \rangle$$

$$= \delta_{MM'} \langle [\dots]^{\mathbf{b}'}; k_1^{\mathbf{b}'}, \dots, k_{n-1}^{\mathbf{b}'}; JM' || [\dots]^{\mathbf{b}}; k_1^{\mathbf{b}}, \dots, k_{n-1}^{\mathbf{b}}; JM \rangle, \quad (20)$$

where δ is the Kronecker delta and the symbol $\langle \dots || \dots \rangle$ denotes the reduced operator (which coincides with $\mathcal{U}_{3nj} [\mathbf{b}; \mathbf{b}']$ in (19) for $M = M'$).

For each fixed n there exist inequivalent types of $3nj$ symbols (up to degenerate cases and phase transforms, see below): one $6j$ symbol, one $9j$, two $12j$ symbols, five $15j$'s, eighteen $18j$'s etc. [12]. The recoupling coefficients classified as *type I* and *type II* may be expressed through single sums of products of $6j$ symbols, while *types III, IV, V, ...* (appearing for $n \geq 5$) may be represented either by single sums of more complex products of $6j$ and $9j$ symbols or by multiple sums of products of symbols of lower orders. In the present context we do not really need any such complicated expressions since we take advantage of the results illustrated in details in [13] (Topic 12) and collected in the following:

Theorem (Biedenharn–Louck).

For each n any $\mathcal{U}_{3nj} [\mathbf{b}; \mathbf{b}']$ is the composition of (a finite number of) two elementary unitary transformations, namely

- Racah transform

$$\mathcal{R} : | \dots ((ab)_d c)_f \dots; JM \rangle \mapsto | \dots (a(bc)_e)_f \dots; JM \rangle, \quad (21)$$

- Phase transform

$$\Phi : | \dots (ab)_c \dots; JM \rangle \mapsto | \dots (ba)_c \dots; JM \rangle, \quad (22)$$

where we are using Latin letters a, b, c, \dots to denote both incoming (j 's in the previous notation) and intermediate (k 's) spin quantum numbers.

The explicit expression of (21) reads

$$|(a(bc)_e)_f; M\rangle = \sum_d (-1)^{a+b+c+f} [(2d+1)(2e+1)]^{1/2} \begin{Bmatrix} a & b & d \\ c & f & e \end{Bmatrix} |((ab)_d c)_f; M\rangle, \quad (23)$$

where there appears the Racah–Wigner $6j$ symbol of $SU(2)$ and the weights $(2d+1)$, $(2e+1)$ are the dimensions of the irreps labeled by d and e , respectively.

Recall that the $6j$ symbol may be expressed in turn as a sum over magnetic quantum numbers of the product of four Clebsch–Gordan coefficients with entries in the set $\{a, b, c, d, e, f; m_a, m_b, m_c, m_d, m_e, m_f\}$, where m_a ($-a \leq m_a \leq a$ in integer steps) is the magnetic quantum number associated with the spin variable a (and similarly for the others) [14]. The numerical value of the $6j$ symbol depends on normalization: we are tacitly assuming through the whole paper the standard Condon–Shortley conventions.

Finally, the phase transform (22) reads

$$|\dots (ab)_c \dots; JM\rangle = (-1)^{a+b-c} |\dots (ba)_c \dots; JM\rangle. \quad \blacktriangle \quad (24)$$

Summing up, the unitary transformations $\{\mathcal{U}_{3nj}[\mathbf{b}; \mathbf{b}']\}$ connecting any pair of computational states $|\mathbf{b}'; JM\rangle_n$, $|\mathbf{b}; JM\rangle_n$ are identified as j –gates in the present computational context and the theorem stated above naturally single out two types of universal *elementary* j –gates. In particular, the Racah transform switches the current coupling scheme to a physical inequivalent one (*cfr.* the explicit expression (23)).

As a further remark note that the elementary unitary j –gates (21) and (22) are in one–to–one correspondence with elementary topological operations between pairs of rooted labeled binary trees, Rotations and Twists respectively (*cfr.* Appendix A2 and pay attention to the fact that “rotation” will be used in the following part of the present Section in a totally different way).

3.2 M –gates

As anticipated in Section 1, M –gates are implemented –inside each computational Hilbert space $\mathcal{H}_n^J(\mathbf{b})$ introduced in (15)– by the Wigner D –functions $D_{MM'}^J$, namely the matrix elements of the (unitary) rotation operator $\mathfrak{D}_{MM'}^J$ in the JM representation. By using Euler angles α, β, γ to specify the rotation, the Wigner D –functions –or W –rotation matrices– are defined by

$$\langle JM | \mathfrak{D}_{MM'}^J(\alpha\beta\gamma) | J'M'\rangle \doteq \delta_{JJ'} D_{MM'}^J(\alpha\beta\gamma), \quad (25)$$

where $0 \leq \alpha < 2\pi$; $0 \leq \beta \leq \pi$ or $2\pi \leq \beta \leq 3\pi$; $0 \leq \gamma < 2\pi$ and we adopt in this Section the notations of [14] (see also [19] for a general treatment of

$SU(2)$ representation theory). A W -matrix can be always expressed as

$$D_{MM'}^J(\alpha\beta\gamma) = e^{-iM\alpha} d_{MM'}^J(\beta) e^{-iM'\gamma}, \quad (26)$$

where $d_{MM'}^J(\beta)$ is the *reduced* W -matrix.

Generally speaking, W -rotation matrices appears when we look at transformations of the wave function of a quantum mechanical system under a coordinate rotation. Given a basis vector of $\mathcal{H}_n^J(\mathfrak{b})$ as in (15), its dependence on polar coordinates (θ, ϕ) is better described if we change our previous notation according to

$$|\mathfrak{b}; JM\rangle_n \rightsquigarrow {}^{(\mathfrak{b})}\psi_M^J(\theta, \phi) \quad (27)$$

where we dropped the subscript n for simplicity. Then the action of a W -matrix (25) on any such basis vector is expressed by

$${}^{(\mathfrak{b})}\psi_{M'}^J(\theta', \phi') = \sum_{M=-J}^{+J} {}^{(\mathfrak{b})}\psi_M^J(\theta, \phi) D_{MM'}^J(\alpha\beta\gamma), \quad (28)$$

where (θ, ϕ) and (θ', ϕ') are polar angles in the initial and rotated coordinate systems, respectively. The action of a rotation on the components of vectors (*cfr.* the decomposition written in (16)) involves the Hermitean conjugate $\tilde{D}_{M'M}^J$ of the corresponding $D_{MM'}^J$, namely ${}^{(\mathfrak{b})}a_{M'}^J = \sum \tilde{D}_{M'M}^J {}^{(\mathfrak{b})}a_M^J$, where the sum is over M as in (28).

It is worth to recall that in the general case (N any integer and j_1, j_2, \dots, j_{n+1} chosen in $\{0, 1/2, 1, 3/2, \dots\}$) the *reducible* $(2J+1) \times (2J+1)$ W -rotation matrix $D_{MM'}^J$ will admit a block diagonal decomposition into irreducible rotation matrices of lower ranks. On the other hand, by changing N and/or the values of the incoming spins, the resulting $D_{\bar{M}\bar{M}'}^{\bar{J}}$ will decompose into different elementary blocks. From the computational viewpoint this provides a more general notion of *universal* set of elementary M -gates than that currently adopted in (Boolean) quantum information schemes, typically given in terms of 2×2 and/or 4×4 unitary matrices [24].

However, as described in details in Appendix B1, each matrix element of any $D_{MM'}^J$ can be *factorized* in a well-defined way, and this procedure is independent of the binary bracketing structure of $\mathcal{H}_n^J(\mathfrak{b})$. The explicit expression of such factorisation given in (135) can be written symbolically as in (136), namely

$$\begin{aligned}
& \mathbf{D}^J (\alpha \beta \gamma) = \\
& \sum_{\{m, m'\}} \prod_{i=1}^N \left(\mathbf{C}_{\kappa_{i-1} j_i}^{\kappa_i} \mathbf{D}^{j_i} (\alpha \beta \gamma) \mathbf{C}_{\kappa_{i-1} j_i}^{\kappa_i} \right), \quad (29)
\end{aligned}$$

where we dropped the matrix indices M, M', m_i, m'_i on the W-matrices $\mathbf{D}^J, \mathbf{D}^{j_i}$ ($i = 1, 2, \dots, N \equiv n + 1$) and similarly $\mathbf{C}_{\bullet\bullet}^{\bullet}$'s are Clebsch–Gordan coefficients with m -type entries omitted. The summation is over all magnetic quantum numbers of the angular momentum operators $\{\mathbf{J}_i\}$, while $\{\kappa_i\}$ are spin quantum numbers associated with the intermediate operators defined in (130).

In (29) there appear N ($\equiv \#$ of incoming spins) factors, each containing a W-matrix in the irreducible j_i -th representation of dimension $(2j_i + 1)$, and a total amount of $2N$ Clebsch–Gordan coefficients. As explained at the end of Appendix B1, each matrix element of \mathbf{D}^{j_i} may be further factorized into the (sum of) product of $2j_i$ W-matrices in the fundamental $j = 1/2$ representation of $SU(2)$. The explicit form of $D_{m m'}^{\frac{1}{2}}$ ($m, m' \in \{\frac{1}{2}, -\frac{1}{2}\}$) reads

$$D_{m m'}^{\frac{1}{2}} (\alpha \beta \gamma) = \begin{pmatrix} e^{-i\alpha/2} \cos(\beta/2) e^{-i\gamma/2} & -e^{-i\alpha/2} \sin(\beta/2) e^{i\gamma/2} \\ e^{i\alpha/2} \sin(\beta/2) e^{-i\gamma/2} & e^{i\alpha/2} \cos(\beta/2) e^{i\gamma/2} \end{pmatrix}. \quad (30)$$

As a consequence of the above remarks we conclude that the "elementary factors" appearing in the right hand side of (29) needed to determine one matrix element of \mathbf{D}^J , namely $D_{M M'}^J (\alpha \beta \gamma)$ for some MM' , are

$2N$ C–G coefficients

$$2J \equiv 2 \sum_{i=1}^N j_i \text{ W-matrices } D_{m m'}^{\frac{1}{2}} \quad (31)$$

and the number of factors one needs in order to evaluate the whole \mathbf{D}^J amounts to $[2(J+N)]^{(2J+1)^2}$. These estimates represent in fact upper bounds on the number of factors, since we may reduce the number of elementary W-matrices by employing some 3×3 matrices \mathbf{D}^1 of the $j = 1$ irrep. Moreover,

by considering a purely fermionic (bosonic) symmetric N -multiplet, the expression (29) does not contain C-G coefficients anymore and the number of elementary factors to be taken into account in (31) is simply $2J \equiv N$ ($J \equiv N$, respectively), as discussed in Appendix B1.

Remark 3.1. Our framework turns out to be much richer than the Boolean case, but contains the usual Boolean gates as particular examples. Note also that $D_{mm'}^{\frac{1}{2}}$ is an *elementary* gate in any situation; it is also *universal* for the two particular cases discussed above. In particular, the N spin- $\frac{1}{2}$ case is compatible with the scheme proposed in [21], Sect.VII.

Remark 3.2. In each representation labeled by J the W -matrices form a group under multiplication, namely

$$\mathbf{D}^J(\alpha_1\beta_1\gamma_1) \mathbf{D}^J(\alpha_2\beta_2\gamma_2) = \mathbf{D}^J(\alpha\beta\gamma), \quad (32)$$

where $(\alpha\beta\gamma)$ are related to $(\alpha_1\beta_1\gamma_1)$ and $(\alpha_2\beta_2\gamma_2)$ by quite involved expressions (see [14] Ch. 1.4.7).

Remark 3.3. Instead of W -matrices we could have used other parametrisations for rotations, for instance the matrices $U_{MM'}^J$ defined in terms of rotation axis and rotation angle. For completeness we collect in Appendix B2 some standard formulas relating these two types of transformations together with some explicit examples [14]. ▲

4 Spin Network Quantum Circuit

By exploiting the basic ingredients introduced in the previous sections (computational Hilbert spaces, j -gates and M -gates) we present here the structural setting of a quantum simulator \mathfrak{M} —the spin network simulator—modeled as a generalised (*i.e.* not Boolean) quantum circuit model. In a broader sense such a computing machine could be reinterpreted as a concrete realization of what should be a Quantum Automaton (see *e.g.* [25], [26]), namely a theoretical framework able to deal consistently with quantum languages and grammars [17].

4.1 Combinatorial kinematics

The computational space of the simulator \mathfrak{M} turns out to be modeled on an $SU(2)$ -decorated graph (or *spin network*, according to Penrose's similar structures introduced in [16]).

For each fixed n the underlying network structure is denoted for the moment by $\mathbf{G}_n(V, E)$, where V and E are the vertex and edge sets of the graph, respectively. Both the vertices and the edges (arcs connecting pairs of vertices) of $\mathbf{G}_n(V, E)$ are decorated by algebraic objects from $SU(2)$ -representation theory we introduced previously. The vertices are in one-to-one correspondence with the set of computational Hilbert spaces $\mathcal{H}_n^J(j_1, j_2, \dots, j_{n+1}; k_1, k_2, \dots, k_{n-1}; JM) \doteq \mathcal{H}_n^J(\mathfrak{b})$ introduced in (15)

$$\text{vertex set } V \longleftrightarrow \{\mathcal{H}_n^J(\mathfrak{b})\} \quad (33)$$

and since each $\mathcal{H}_n^J(\mathfrak{b})$ has dimension $(2J+1)$ over \mathbb{C} there exists one isomorphism

$$\mathcal{H}_n^J(\mathfrak{b}) \cong_{\mathfrak{b}} \mathbb{C}^{2J+1} \quad (34)$$

for each admissible binary coupling scheme \mathfrak{b} of $(n+1)$ incoming spins. Thus each vertex in the spin network is decorated with a copy of \mathbb{C}^{2J+1}

$$\mathbb{C}^{2J+1} \rightsquigarrow v(\mathfrak{b}) \in V, \quad (35)$$

where each $v \in V$ is labeled by the unique corresponding \mathfrak{b} .

The construction of the graph proceeds by establishing the connections between vertices. The edge set $E = \{e\}$ of $\mathbf{G}_n(V, E)$ is a subset of the Cartesian product $(V \times V)$ selected by the action of elementary j -gates. More precisely, an (undirected) arc between two vertices $v(\mathfrak{b})$ and $v(\mathfrak{b}')$

$$e(\mathfrak{b}, \mathfrak{b}') \doteq (v(\mathfrak{b}), v(\mathfrak{b}')) \in (V \times V) \quad (36)$$

exists if, and only if, the underlying Hilbert spaces are related to each other by one of elementary unitary operations defined in Biedenharn–Louck Theorem of Section 3.1. Note that at the kinematical level the resulting decorated edges in the net are to be considered undirected since any such operation is invertible.

This general combinatorial structure can be concretized in two different ways, depending on what types of binary bracketing schemes –associated

with the vertex set of $\mathbf{G}_n(V, E)$ as stated in (33)– we are going to consider as inequivalent (we refer to Appendix A2 for more details on the combinatorics of the resulting graphs). If we distinguish pairs \mathbf{b}, \mathbf{b}' which differ either by a Racah transform \mathcal{R} (21) or by a Phase transform Φ (22), then the structure we get is a Twist–Rotation graph

$$\mathbf{G}_n^{TR}(V, E) \doteq \hat{\mathfrak{G}}_n(V, E) \quad (37)$$

with

$$\begin{aligned} \hat{\mathfrak{G}}_n \supset V &= \{v(\mathbf{b}), \text{ all admissible } \mathbf{b}\} \\ \hat{\mathfrak{G}}_n \supset E &= \{e(\mathbf{b}, \mathbf{b}') \leftrightarrow \mathcal{R}, \Phi\}. \end{aligned} \quad (38)$$

For each n the Twist–Rotation graph is a regular, cubic (trivalent) graph representing pictorially all possible types of $3nj$ symbols introduced in Section 3.1 and extensively analysed in literature (*cfr.* [22], [23], [13], [27]). In Fig. 21 of Appendix A2 the Twist–Rotation graph $\hat{\mathfrak{G}}_3$ (binary coupling schemes of four angular momenta and associated $9j$ symbols) is depicted.

Since quantum states which differ by phase transformations give rise to the same physical probabilities of observables, it seems quite natural to consider a combinatorial structure in which \mathbf{b}, \mathbf{b}' correspond to different vertices only if the states are related by a Racah transform (recall that in this case there is a change of one intermediate spin variable). This reduction operation on the Twist–Rotation graph (37) involves an equivalence relation to be imposed on the vertex set. Moreover, each of the surviving edges turns out to be associated with a Racah transform \mathcal{R} , but there could appear some additional weights and/or phase factors in its explicit expression (23). With these premises we define the Rotation graph

$$\mathbf{G}_n^R(V, E) \doteq \mathfrak{G}_n(V, E) \quad (39)$$

with

$$\begin{aligned} \mathfrak{G}_n \supset V &= \{\text{equivalence classes of } v(\mathbf{b})\} \\ \mathfrak{G}_n \supset E &= \{e(\mathbf{b}, \mathbf{b}') \leftrightarrow \mathcal{R}, \text{ mod weights/phases}\}. \end{aligned} \quad (40)$$

Figure 1

A picture of \mathfrak{G}_3 is given in Fig. 1, while more details on the above construction are collected in Appendix A2. Here we just recall that the Rotation graph \mathfrak{G}_n is a regular (not planar) $2(n-1)$ -valent graph with a number of vertices given by

$$|V| \equiv \text{card } V = (2n-1)!! \quad (41)$$

where $()!!$ denotes the double factorial number. In the following we shall deal mainly with the Rotation graph structure, but we point out in advance that applications of such combinatorial machinery in the computing context work on the Twist-Rotation graph as well.

On the spin network the action of a j -gate defined by a recoupling coefficient $\mathcal{U}_{3nj}[\mathfrak{b}; \mathfrak{b}']$ introduced in (19) is represented formally by a *piecewise path* in \mathfrak{G}_n connecting the vertices $v(\mathfrak{b})$ and $v(\mathfrak{b}')$

$$v(\mathfrak{b}) \xrightarrow{\mathcal{U}_{3nj}[\mathfrak{b}; \mathfrak{b}']} v(\mathfrak{b}'). \quad (42)$$

Two state vectors (*e.g.* basis vectors, for simplicity, with the same value of the q -number M) in the Hilbert spaces (33) attached to the vertices labeled by \mathfrak{b} (the initial point) and \mathfrak{b}' (the terminal point) are denoted by

$$|\mathfrak{b}; JM\rangle_n \doteq |\text{in}(\mathfrak{b}); JM\rangle_n \quad \text{and} \quad |\mathfrak{b}'; JM\rangle_n \doteq |\text{out}(\mathfrak{b}'); JM\rangle_n, \quad (43)$$

and can be interpreted consistently "in" and "out" as referring to an initial state (input) and a final state (output), respectively.

To deal with the formal expression (42) we need some results from angular momenta recoupling theory summarised in the following

Theorem (see [12], [13] Topic 12, and the original references therein).

Consider all possible paths in \mathfrak{G}_n connecting two states as in (43). Then the transition probability amplitudes for *any* pair of paths with given end-points, say γ_1 and γ_2 , are equal

$$\langle \text{in}(\mathfrak{b}); JM | \text{out}(\mathfrak{b}'); JM \rangle_{\gamma_1} = \langle \text{in}(\mathfrak{b}); JM | \text{out}(\mathfrak{b}'); JM \rangle_{\gamma_2} \quad (44)$$

since we can freely deform such paths one into each other. As a consequence of that, probabilities too turn out to be equal owing to the fact that

$$|\mathcal{U}_{3nj}[\mathfrak{b}; \mathfrak{b}']|^2 \equiv |\langle \text{in}(\mathfrak{b}); JM | \text{out}(\mathfrak{b}'); JM \rangle|^2 \quad (45)$$

is actually the probability that a quantum system prepared in the state "in" will be measured in the state "out". The proof of (44) relies on the existence of fundamental algebraic identities involving $6j$ symbols, namely

- the Biedenharn–Elliott identity

$$\begin{aligned} \sum_x (-)^{R+x} (2x+1) \begin{Bmatrix} a & b & x \\ c & d & p \end{Bmatrix} \begin{Bmatrix} c & d & x \\ e & f & q \end{Bmatrix} \begin{Bmatrix} e & f & x \\ b & a & r \end{Bmatrix} \\ = \begin{Bmatrix} p & q & r \\ e & a & d \end{Bmatrix} \begin{Bmatrix} p & q & r \\ f & b & c \end{Bmatrix}; \end{aligned} \quad (46)$$

- the Racah identity

$$\sum_x (-)^{p+q+x} (2x+1) \begin{Bmatrix} a & b & x \\ c & d & p \end{Bmatrix} \begin{Bmatrix} a & b & x \\ d & c & q \end{Bmatrix} = \begin{Bmatrix} a & c & q \\ b & d & p \end{Bmatrix}, \quad (47)$$

where the spin variables $\{a, b, c, \dots, x\}$ run over $\{0, \frac{1}{2}, 1, \frac{3}{2}, \dots\}$ and must satisfy suitable triangular inequalities inside each $6j$ symbol (otherwise the symbol itself would vanish). The weight $(2x+1)$ is the dimension of the representation labeled by the quantum number x , the sum over x is constrained only by the triangular conditions quoted above and R in the phase factor of the first identity is the combination $(a+b+c+d+e+f+p+q+r)$. Note that these identities, together with the orthogonality relation

$$\sum_x (2x+1) \begin{Bmatrix} a & b & x \\ c & d & p \end{Bmatrix} \begin{Bmatrix} c & d & x \\ a & b & q \end{Bmatrix} = \frac{\delta_{pq}}{(2p+1)}, \quad (48)$$

define uniquely the Racah–Wigner $6j$ symbol (considered as the hypergeometrical polynomial which generates the Askey hierarchy [28]).

Without entering into details about the proof of the above theorem, we collect below some remarks which should make the rationale of its proof as clear as possible.

- The spin network \mathfrak{G}_2 (see Fig. 22 in Appendix A2) is a closed loop of triangular shape: the vertices correspond to the three inequivalent binary couplings of $(n+1) = 3$ spins and each edge is associated with a Racah transform. Then Racah identity (47) ensures that we may implement the transition from one vertex ("in") to another ("out") traversing either the edge connecting them directly or the other two.

- The spin network \mathfrak{G}_3 shown in Fig. 1 is characterised by triangular and pentagonal closed loops (bounding triangular and pentagonal plaquettes). Triangles are associated with Racah identity (47) (as happens for \mathfrak{G}_2), while pentagonal plaquettes turns out to correspond to the Biedenharn–Elliott identity (46): if the chosen path embraces two edges of a pentagon, one can freely deform it traversing the other three edges (and viceversa). By using both (46) and orthogonality relation (48) we can also deform a piece of path connecting two contiguous vertices into a path which touches the other four edges of the pentagon (and viceversa). Thus we conclude that the improvement of (44) for \mathfrak{G}_3 relies on all the three algebraic identities written above.
- The spin networks \mathfrak{G}_n ($n > 3$) display plaquettes with other types of polygonal boundaries. Each type of plaquette can be associated with a suitable algebraic identity which can be derived from the fundamental ones by making use of the explicit expression for the $3nj$ symbol involved. The procedure for improving (44) goes on as in the previous cases.

As a final comment on the equi-amplitudes of paths in \mathfrak{G}_n under the action of pure j -gates, notice that such result holds as far as we are dealing with the computational space of the simulator at the kinematical level. When we shall ask the spin network to perform a computation by means of a sequence of j -gates such an invariance will be broken (as we are going to explain in the following section). \blacktriangle

In order to include in the combinatorial setting the action of M -gates (see Section 3.2) we may employ either the Wigner rotation matrices (25) parametrised by Euler angles or U -matrices written in terms of rotation axis and rotation angle introduced in Appendix B2: here we agree to making use of the former ones as in the rest of the main text. By analogy with the formal expression (42) representing a j -gate on the spin network, we write formally the action of an M -gate on \mathfrak{G}_n as

$$v(\mathfrak{b}) \xrightarrow{\mathcal{D}^J(\alpha\beta\gamma)} v(\mathfrak{b}), \quad (49)$$

where we drop the matrix indices M, M' by using the operatorial notation as in (25). Since rotations do not alter the binary bracketing structure of

the computational Hilbert space $\mathcal{H}_n^J(\mathfrak{b})$ we may activate an M -gate independently at any vertex $v(\mathfrak{b}) \subset \mathfrak{S}_n$. To recover the explicit expression of the action of an M -gate we have to pick up a vector in $\mathcal{H}_n^J(\mathfrak{b})$, change back our notation as in (27) (to make the angular dependence explicit) and finally recover the expression given in (28). However, in order to have at our disposal a unified notation for states to be considered as "input" and "output" in a quantum circuit framework, we are forced here to use a hybrid notation by setting

$$\mathcal{H}_n^J(\mathfrak{b}) \doteq \{\text{span } |\mathfrak{b}; \theta, \phi; JM\rangle_n\}. \quad (50)$$

With this convention we write down the action of an M -gate (for a given choice of the parameters α, β, γ) on an input (basis) state as

$$\mathcal{D}^J(\alpha\beta\gamma) : |\mathfrak{b}; \text{in}(\theta, \phi; M)J\rangle_n \rightarrow |\mathfrak{b}; \text{out}(\theta', \phi'; M')J\rangle_n \quad (51)$$

where the output state is

$$|\mathfrak{b}; \text{out}(\theta', \phi'; M')J\rangle_n = \sum_{M=-J}^J D_{MM'}^J(\alpha\beta\gamma) |\mathfrak{b}; \theta, \phi; JM\rangle_n \quad (52)$$

and the input basis state appears in the combination on the right-hand side with its particular M -label.

The actions of both types of gates on the spin network can be visualised by looking at Fig. 2: we can move from one vertex to a different one along an edge as in (42) (without changing M) or choose to perform a rotation (49) inside the computational Hilbert space associated with a vertex.

Figure 2

According to (50) and (16), a suitable unified notation for generic state vectors to be used in actual computations should be

$$|\mathfrak{b}; \theta, \phi; J\rangle_n \quad (53)$$

and consequently input/output states in the particular cases (43) and (51) have to be set in the form

$$|\text{in}(\mathfrak{b}; \theta, \phi); J\rangle_n; |\text{out}(\mathfrak{b}; \theta', \phi'); J\rangle_n \quad (54)$$

possibly with additional M -labels if basis vectors are considered.

Summing up, the kinematical ingredients of the spin network simulator based on the Rotation graph $\mathfrak{G}_n(V, E)$ are

$$\begin{aligned} V &= \{v(\mathfrak{b})\} \leftrightarrow \{\mathcal{H}_n^J(\mathfrak{b})\} \\ E &= \{e(\mathfrak{b}, \mathfrak{b}')\} \leftrightarrow \text{elementary } j\text{-gates} \\ \{\mathcal{D}^J : \mathcal{H}_n^J(\mathfrak{b}) \rightarrow \mathcal{H}_n^J(\mathfrak{b}')\} &\leftrightarrow M\text{-gates} \end{aligned} \quad (55)$$

where the discrete structure encoded in (V, E) is endowed with transformations \mathcal{D}^J depending on both discrete and continuous parameters (*cfr.* the points discussed in Section 2).

Remark 4.1. The combinatorial setting described above can be interpreted as a fiber space structure $(V, \mathbb{C}^{2J+1}, SU(2)^J)$ where

- $V = \{v(\mathfrak{b})\}$ is the (discrete) base space;
- \mathbb{C}^{2J+1} is the typical fiber, a copy of which is attached to each $v(\mathfrak{b})$ through the isomorphisms given in (34);
- $SU(2)^J$ is the automorphism group of the fiber realized by the $(2J+1) \times (2J+1)$ W-matrices which form a group under the composition law (32);
- $E = \{e(\mathfrak{b}, \mathfrak{b}')\}$ are arcs connecting pairs of contiguous vertices in the base space (*cfr.* (36)), but they may be also considered as mappings

$$\begin{aligned} V \times \mathbb{C}^{2J+1} &\rightarrow V \times \mathbb{C}^{2J+1} \\ (v(\mathfrak{b}), \mathcal{H}_n^J(\mathfrak{b})) &\mapsto (v(\mathfrak{b}'), \mathcal{H}_n^J(\mathfrak{b}')) \end{aligned} \quad (56)$$

connecting each given decorated vertex to one of its nearest $2(n-1)$ vertices.

In such a vector bundle framework one could take advantage of the above transport prescriptions (W-matrices along the fiber and maps (56) along horizontal sections) to get a notion of "connection" in the total fiber space $V \times \mathbb{C}^{2J+1}$ as illustrated in more details in [29]. This remark opens the possibility of discussing relations between the spin network scheme and the holonomic q-computation approach. We shall come back on this point in Section 6.1. \blacktriangle

4.2 Dynamics and computing

The kinematical structure of the spin network \mathfrak{M} complies with all the requisites of an universal q-simulator as defined by Feynman [15], namely

- *locality*, reflected in the binary bracketing structure of the computational Hilbert spaces, which –together with the action of W -rotations – bears on the existence of local interactions;
- *discreteness of the computational space*, reflected in the combinatorial structure of \mathfrak{G}_n ;
- *discreteness of time*, to be discussed below;
- *universality*, guaranteed by the properties of gates we described in Section 3: any unitary transformation operating on computational Hilbert spaces can be reconstructed by taking a finite sequence of Racah transforms (and possibly phases) followed by the application of a finite number of W -rotations.

Thus we have explicitly defined the class of "exact imitators" of any finite, discrete quantum system (described by pure angular momentum states) with no need of resorting to the notions coming from the (inherently classical) Boolean circuit theory.

In order to describe the dynamical behavior of the spin network, we notice preliminarily that the rule to "move" from a state (say a vector (53)) to a nearest one have been already established: apply either one j -gate or one particular M -gate (for fixed α, β, γ). Thus a natural discrete time unit, denoted by τ , can be associated with one elementary step in such a cellular automaton scheme. However, as pointed out by Feynman himself, this naive assumption can at best make the simulator to "imitate" time. If we pretend the spin network \mathfrak{M} to "simulate" time, we have to go through a genuine space-time dynamics providing Hamiltonians and intrinsical evolution in actual time intervals.

Generally speaking, the basic data to implement computation in a circuit model are an input state and a program \mathcal{P} giving instructions to manipulate information stored in the machine states: output states must belong to the set of "accepted" states (if computation halts, as we are tacitally assuming).

In the spin network \mathfrak{G}_n the choice of a particular program \mathcal{P} is interpreted as the selection of a subset of unitary transformations

$$\mathcal{P} \longleftrightarrow \{\mathfrak{U}_{\mathcal{P}}\} \subset \{\mathfrak{U}\} \quad (57)$$

among all the kinematically allowed $\{\mathfrak{U}\}$. Since we are going to deal with sequences of states we are forced to change again our last notation (53) into a simplified one, namely

$$|\mathfrak{b}; \theta, \phi; J\rangle_n \rightsquigarrow |\mathfrak{v}\rangle_n. \quad (58)$$

Then a computation based on the program \mathcal{P} , represented formally as

$$|\mathfrak{v}_{\text{in}}\rangle_n \xrightarrow{\mathfrak{U}_{\mathcal{P}}} |\mathfrak{v}_{\text{out}}\rangle_n \quad (59)$$

is a collection of directed paths in \mathfrak{G}_n , all starting from the input state $|\mathfrak{v}_{\text{in}}\rangle_n$ and ending in some accepted $|\mathfrak{v}_{\text{out}}\rangle_n$. By a directed path we mean a (time) ordered sequence of states

$$|\mathfrak{v}_{\text{in}}\rangle_n \equiv |\mathfrak{v}_0\rangle_n \rightarrow |\mathfrak{v}_1\rangle_n \rightarrow \cdots \rightarrow |\mathfrak{v}_s\rangle_n \rightarrow \cdots \rightarrow |\mathfrak{v}_L\rangle_n \equiv |\mathfrak{v}_{\text{out}}\rangle_n \quad (60)$$

where $s = 0, 1, 2, \dots, L$ is the lexicographical labelling of the states along the given path and L is the length of the path, which turns out to be proportional to the time duration of the computation process $L \cdot \tau \doteq T$ in units of the discrete time step τ . The integer L characterising the particular directed path in (60) represents the number of time-ordered elementary operations (computational steps) needed to get $|\mathfrak{v}_{\text{out}}\rangle_n$ from $|\mathfrak{v}_{\text{in}}\rangle_n$ by employing the program \mathcal{P} . It should be clear that from the same input $|\mathfrak{v}_{\text{in}}\rangle_n$ the program \mathcal{P} could select different paths to get (possibly) different output states. For instance we may represent by

$$|\mathfrak{v}_{\text{in}}\rangle_n \equiv |\mathfrak{v}_0\rangle_n \rightarrow |\mathfrak{v}'_1\rangle_n \rightarrow \cdots \rightarrow |\mathfrak{v}'_s\rangle_n \rightarrow \cdots \rightarrow |\mathfrak{v}'_{L'}\rangle_n \equiv |\mathfrak{v}'_{\text{out}}\rangle_n \quad (61)$$

another path of length L' in the collection (59) ending in an accepted $|\mathfrak{v}'_{\text{out}}\rangle_n$. Each arrow in (60) or (61) stands for one of the elementary operations (Racah transforms, Wigner rotations) described in the previous sections (*cfr.* also Fig. 2). Using our current notation an elementary computational step is

$$\begin{aligned} & \text{either } |\mathbf{v}_s\rangle_n \xrightarrow{\mathcal{R}} |\mathbf{v}_{s+1}\rangle_n \\ & \text{or } |\mathbf{v}_s\rangle_n \xrightarrow{\mathcal{D}(\alpha\beta\gamma)} |\mathbf{v}_{s+1}\rangle_n \end{aligned} \quad (62)$$

and the expression of a particular unitary transformation $\mathfrak{U}_{\mathcal{P}}$ (of length L) in (59) turns out to be a well defined time-ordered composition

$$\mathfrak{U}_{\mathcal{P}} = \mathcal{U}_L \circ \mathcal{U}_{L-1} \circ \cdots \circ \mathcal{U}_2 \circ \mathcal{U}_1, \quad (63)$$

where each \mathcal{U} is given by one of the operations (62).

The framework developed so far is an extremely flexible and powerful circuit modelization of quantum computing and we shall examine later on in this section the range of different types of computations that can be actually carried out. However, to complete the dynamical setting based on the identification made in (57) and (59) of a program \mathcal{P} with a collection of directed paths in \mathfrak{G}_n , we have to call into play algorithms. Then the program $\mathcal{P}(\mathcal{A})$ to perform a particular algorithm \mathcal{A} is the specification of a suitable directed path in the collection (59), starting from a given $|\mathbf{v}_{\text{in}}\rangle_n$ and ending in one particular $|\mathbf{v}_{\text{out}}\rangle_n$. The associated unitary transformation is denoted by

$$\mathcal{P}(\mathcal{A}) \longleftrightarrow \mathfrak{U}_{\mathcal{P}(\mathcal{A})} \subset \{\mathfrak{U}_{\mathcal{P}}\} \quad (64)$$

and for the path itself we may use the same notation as in (60). Alternatively, by broadening the meaning of the symbol $\mathcal{P}(\mathcal{A})$, we agree that it represents also an ordered sequence of labelings

$$\mathcal{P}(\mathcal{A}) \longleftrightarrow \{s = 0, 1, 2, \dots, L(\mathcal{P}(\mathcal{A}))\} \quad (65)$$

which turns out to be in one-to-one correspondence with the states $\{|\mathbf{v}_s\rangle_n, s = 0, 1, 2, \dots, L(\mathcal{P}(\mathcal{A}))\}$. The time lapse required to get the output is nothing but the length of the path in units of the discrete time step τ , namely

$$T(\mathcal{P}(\mathcal{A})) = L(\mathcal{P}(\mathcal{A})) \cdot \tau. \quad (66)$$

A circuit-type computation process in \mathfrak{G}_n based on a program \mathcal{P} performing the algorithm \mathcal{A} (which could be formally written as in (59)) is actually

represented by the expectation value of the unitary operator (64) evaluated between the given input and output

$$\langle \mathbf{v}_{\text{out}} | \mathfrak{U}_{\mathcal{P}(\mathcal{A})} | \mathbf{v}_{\text{in}} \rangle_n. \quad (67)$$

This quantity gives the physical transition probability amplitude to get $|\mathbf{v}_{\text{out}}\rangle_n$ by acting with $\mathfrak{U}_{\mathcal{P}(\mathcal{A})}$ on $|\mathbf{v}_{\text{in}}\rangle_n$ and obviously its square modulus is the quantum probability to be assigned to the corresponding computation. By taking advantage of the possibility of decomposing $\mathfrak{U}_{\mathcal{P}(\mathcal{A})}$ uniquely into an ordered sequence of elementary operators (gates), (67) becomes

$$\langle \mathbf{v}_{\text{out}} | \mathfrak{U}_{\mathcal{P}(\mathcal{A})} | \mathbf{v}_{\text{in}} \rangle_n = \llbracket \prod_{s=0}^{L-1} \langle \mathbf{v}_{s+1} | \mathcal{U}_{s,s+1} | \mathbf{v}_s \rangle_n \rrbracket_{\mathcal{P}(\mathcal{A})} \quad (68)$$

with $L \equiv L(\mathcal{P}(\mathcal{A}))$ for short. The symbol $\llbracket \rrbracket_{\mathcal{P}(\mathcal{A})}$ denotes the ordered product along the path $\mathcal{P}(\mathcal{A})$ and provides a sort of superselection rule which induces destructive interference of the forbidden (*i.e.*, not leading to the correct result) paths in \mathfrak{G}_n . Each elementary operation introduced in the generic expression (63) is now better denoted by $\mathcal{U}_{s,s+1}$ to stress its "one-step" character with respect to computation. Consequently, each elementary transfer matrix in (68) turns out to be associated with a local Hamiltonian operator arising from

$$\langle \mathbf{v}_{s+1} | \mathcal{U}_{s,s+1} | \mathbf{v}_s \rangle_n = \exp \{ i \mathbf{H}_n(s, s+1) \cdot \tau \} \quad (69)$$

and representing the unitary evolution of the simulator in one unit of its intrinsic time variable ($s = 0, 1, 2, \dots, L(\mathcal{P}(\mathcal{A}))$). We indicate with the shorthand notation $(s, s+1)$ the dependence of \mathbf{H}_n on its variables to make clear the local nature of this operator with respect to the computational space \mathfrak{G}_n (a more detailed description should involve the quantum numbers characterising both states and operation). When (69) is inserted in (68), such *virtual* Hamiltonians generally do not commute with each other but nonetheless the whole computational process may be identified with a well defined unitary evolution of the simulator in the internal time interval given in (66).

The above remarks justify the statement made at the beginning of this section, namely that the spin network simulates intrinsically time evolution (without resorting to *ad hoc* external Hamiltonians as happens for instance in the Universal Quantum Simulator model proposed in [30]). Moreover, by changing the program \mathcal{P} (and the algorithm \mathcal{A}) the machine is able to

select different types of dynamical behaviors, and thus to simulate complex poly-local many angular momenta interactions modeled as binary couplings and Wigner rotations (see the assumptions discussed in Section 2). What we mean in particular is that different types of evolutions in \mathfrak{G}_n can be grouped into "computing classes" based on the choice of gates that each program has to employ. Then a program \mathcal{P} (defined in (59) and associated with a collection of directed paths as in (60) or, equivalently, with decompositions into a number of gates as in (63)) may be based on either M -gates alone, or j -gates alone, or some fixed sequence of M and j -gates.

◆ An *M -computing class* contains programs which employ only M -gates at each step in their associated directed paths. The binary bracketing structure of the computational Hilbert spaces described in Section 2 is not involved, and it is not difficult to realize that such kind of computation, when applied to $N \frac{1}{2}$ -spins, reproduces the usual Boolean quantum circuit (*cfr.* the end of Section 3.2 and Appendices B1 and B2).▲

◆ A *j -computing class* includes programs which employ only j -gates at each computational step. This class is particularly interesting since it shares many features with suitable types of discretized field theories (the so-called state sum models, to be discussed in Section 6) as we already noticed in [11]. Now the combinatorial structure of Rotation graphs becomes prominent owing to the existence of an one-to-one correspondence between allowed elementary operations and the edge set E of \mathfrak{G}_n , for each n (*cfr.* (40) and more generally Appendix A2).

In the present framework it is convenient to switch back to notations used in the first part of Section 4.1. Then states will be labeled again by $|\mathfrak{b}\rangle_n$ as in (43) (dropping JM) and a program \mathcal{P} is represented formally as

$$\mathcal{U}_{3nj} [\mathfrak{b}_{\text{in}} \xrightarrow{\mathcal{P}} \mathfrak{b}_{\text{out}}] : |\mathfrak{b}_{\text{in}}\rangle_n \longrightarrow |\mathfrak{b}_{\text{out}}\rangle_n, \quad (70)$$

where, as before, $|\mathfrak{b}_{\text{in}}\rangle_n$ is fixed and $|\mathfrak{b}_{\text{out}}\rangle_n$ is an accepted state. The set of operators $\mathfrak{U}_{\mathcal{P}}$ in (59) has been replaced by the unitary operators \mathcal{U}_{3nj} introduced in (19) and already used in (42). The collection of directed paths associated with (70) is defined as in (60) and a particular path of length L corresponding to a time-ordered sequence of states is represented as

$$|\mathfrak{b}_{\text{in}}\rangle_n \equiv |\mathfrak{b}_0\rangle_n \rightarrow |\mathfrak{b}_1\rangle_n \rightarrow \cdots \rightarrow |\mathfrak{b}_s\rangle_n \rightarrow \cdots \rightarrow |\mathfrak{b}_L\rangle_n \equiv |\mathfrak{b}_{\text{out}}\rangle_n \quad (71)$$

Each arrow corresponds now to the first type of operation in (62), namely a Racah transform (possibly up to weights/phases). When one particular path is chosen we would recover expressions similar to (64)–(69), referring to a computation process based on a program \mathcal{P} performing an algorithm \mathcal{A} .

However, in the j -computing class one may address other types of problems, namely: selected two states in \mathfrak{G}_n , say $|\mathfrak{b}_{\text{in}}\rangle_n$ and $|\mathfrak{b}_{\text{out}}\rangle_n$, consider all possible $\mathcal{P}(\mathcal{A})$ that compute $|\mathfrak{b}_{\text{out}}\rangle_n$ as the result of the application of some

$$\mathcal{U}_{3nj} [\mathfrak{b}_{\text{in}} \xrightarrow{\mathcal{P}(\mathcal{A})} \mathfrak{b}_{\text{out}}] \quad (72)$$

to $|\mathfrak{b}_{\text{in}}\rangle_n$. The functional on \mathfrak{G}_n which takes care of such multiple choices is a "path sum" (a discretized Feynman's path integral) which may be written as

$$\mathbf{Z}[\mathfrak{b}_{\text{in}}, \mathfrak{b}_{\text{out}}] = \sum_{\mathcal{P}(\mathcal{A})} W_{\mathcal{P}(\mathcal{A})} \langle \mathfrak{b}_{\text{out}} | \mathcal{U}_{3nj} [\mathfrak{b}_{\text{in}} \xrightarrow{\mathcal{P}(\mathcal{A})} \mathfrak{b}_{\text{out}}] | \mathfrak{b}_{\text{in}} \rangle_n, \quad (73)$$

where the summation is over all paths with fixed endpoints and $W_{\mathcal{P}(\mathcal{A})}$ is a weight to be assigned to each path.

Notice that if we should give the same weight, say $W_{\mathcal{P}(\mathcal{A})} = 1$ to each path, then the results on equi-probability amplitudes collected in the theorem of Section 4.1 ensure us that the functional (73) is a combinatorial invariant, namely it is actually independent of the particular path connecting \mathfrak{b}_{in} and $\mathfrak{b}_{\text{out}}$. On the other hand, if we insert non trivial weights in (73), we may naturally address questions about most efficient algorithms and time complexity. For instance we could weigh paths with the inverse of their lengths $L(\mathcal{P}(\mathcal{A}))$; then the minimum-length path (the optimal algorithm) will be dynamically singled out in the path sum. As a matter of fact, even such simple example turns out to be highly non trivial owing to the combinatorial complexity of \mathfrak{G}_n . We shall come back on such issues in the following Section 4.3. \blacktriangle

◆ An *altered j -computing class* is a modification of the j -class obtained on applying just one Wigner rotation (M -gate) to the input state. A typical directed path in this class can be represented by mixing our previous notations (see (53), (58), (60) and (71)) to get

$$\begin{aligned} |\mathfrak{v}_{\text{in}}\rangle_n &\equiv |\mathfrak{b}_0; \theta, \phi; J\rangle_n \rightarrow |\mathfrak{b}_0; \theta', \phi'; J\rangle_n \rightarrow |\mathfrak{b}_1\rangle_n \rightarrow |\mathfrak{b}_2\rangle_n \rightarrow \cdots \rightarrow \\ &\rightarrow |\mathfrak{b}_s\rangle_n \rightarrow \cdots \rightarrow |\mathfrak{b}_{L+1}; \theta', \phi'; J\rangle_n \equiv |\mathfrak{v}_{\text{out}}\rangle_n \end{aligned} \quad (74)$$

where the first arrow represents a Wigner rotation $\mathfrak{D}^J(\alpha\beta\gamma)$ and all the others are alterations of the binary bracketing structure while keeping the angular dependence of the states fixed. Such computing class seems sufficiently general and shares some features with the j -class for what concerns the path sum interpretation. The counterpart of the path sum functional (73) reads

$$\begin{aligned} \mathbf{Z}[\mathbf{v}_{\text{in}}, \mathbf{v}_{\text{out}}] &= \sum_{\mathcal{P}(\mathcal{A})} W_{\mathcal{P}(\mathcal{A})} \langle \mathbf{b}_{L+1} | \mathcal{U}_{3nj}[\mathbf{b}_0 \xrightarrow{\mathcal{P}(\mathcal{A})} \mathbf{b}_{L+1}] | \mathbf{b}_0 \rangle_n \\ &\quad \langle \mathbf{b}_0; \theta', \phi'; J | \mathcal{D}^J(\alpha\beta\gamma) | \mathbf{b}_0; \theta, \phi; J \rangle_n, \end{aligned} \quad (75)$$

from which we see in particular that combinatorial invariance is broken even if we assign to each path the same weight. \blacktriangle

◆ An *alternating computing class* includes programs which alternates M and j -gates and the length of each of the associated directed paths is an even number $L = 2\ell$. This class is quite general with respect to capability of simulating real physical systems and includes all the former computing categories since anyone of the elementary gates could eventually be realized by an identity transformation. \blacktriangle

4.3 Computational complexity

In view of the role that binary coupling trees play in our model for quantum computation we define an encoding map

$$\mathcal{H}_n^J(\mathbf{b}) \longrightarrow T(\mathbf{b}) \quad (76)$$

where, as in (15), the shorthand notation \mathbf{b} stands for the string of quantum numbers $([j_1, j_2, \dots, j_{n+1}]^{\mathbf{b}}; k_1^{\mathbf{b}}, k_2^{\mathbf{b}}, \dots, k_{n-1}^{\mathbf{b}})$, and $T(\mathbf{b})$ is the coupling tree uniquely associated with the computational Hilbert space \mathcal{H}_n^J for given J and n (see Appendix A1). This coding is intrinsically quantum, namely $T(\mathbf{b})$ in (96) is not a simple device in which classical information can be stored (as happens for instance when search trees are considered). The quantum behaviour of $T(\mathbf{b})$ emerges in particular when we look at the nature of the internal labelings. Recall from Section 2 that an intermediate angular momentum, say $\mathbf{K}_1 = \mathbf{J}_1 + \mathbf{J}_2$, has eigenvalue k_1 ranging between $|j_1 - j_2|$ and $j_1 + j_2$ and thus such *quantum trees* – even when equipped with definite values

of the incoming quantum numbers chosen in $\{0, \frac{1}{2}, 1, \frac{2}{3}, \dots\}$ – take care consistently of the range of different values that may be assigned to the internal nodes.

It is worth noting that the binary bracketing notations introduced in (12) and (14) of Section 2 can be interpreted as the quantum counterpart of the "word construction" outlined in Remark A.1 of Appendix A1 for a generic binary operation. To formalise this observation we introduce a new map – equivalent to (76) from a quantum mechanical point of view – which encodes information carried by the Hilbert space \mathcal{H}_n^J into a *quantum word*, namely a string of quantum numbers plus parenthesization. Denote formally this map by

$$\mathcal{H}_n^J(\mathbf{b}) \longrightarrow ([j_1, j_2, \dots, j_{n+1}]^{\mathbf{b}}; k_1^{\mathbf{b}}, k_2^{\mathbf{b}}, \dots, k_{n-1}^{\mathbf{b}}), \quad (77)$$

since a more explicit form as in (14) would force us to write down just one particular type of binary coupling. In our opinion a closer inspection of the encoding map (77) (instead of (76) which will be exploited in the following) could represent a promising starting point to establish a truly quantum Formal Theory including languages, grammars, Gödel numberings and related automaton models [17].

Coming back to the encoding map (76), and referring to the topological transformations on binary coupling trees discussed in Appendix A2, we easily recognise that a Racah transform \mathcal{R} defined in (21) is encoded in a rotation (more precisely, the explicit expression given in (23) is encoded into the operation depicted at the bottom of Fig. 19). On the other hand, a phase transform Φ defined in (22) turns out to be encoded into a twist (compare *e.g.* the explicit expression (24) with the twist depicted at the bottom of Fig. 20). Consequently,

$$\begin{aligned} \text{Racah transform } \mathcal{R} &\longrightarrow \text{Rotation} \\ \text{Phase transform } \Phi &\longrightarrow \text{Twist} \end{aligned} \quad (78)$$

represent encoding maps associating the two types of unitary elementary j -gates introduced in Section 3.1 with basic topological moves on quantum trees. The role of these two sets of operations is specular also for what concerns composition, since the Biedenharn–Louck Theorem (Section 3.1) has its counterpart in the fact that any pair of binary coupling trees can be connected by a sequence of rotations and twists (see Appendix A2).

The quantum encoding maps (76), (78) make manifest that combinatorics of (Twist)–Rotation graphs (Appendix A2) and of the computational space of the simulator (Section 4.1) share identical features, at least as far as j –computing classes (Section 4.2) are implemented. This crucial remark justifies the fact that we may speak about combinatorial and computational complexity questions by employing a common language and concepts. Note however that these similarities can be exploited only to some extent since combinatorial complexity of graphs is usually addressed in a classical information theory context (see Appendix A3). In the remaining part of this section we shall illustrate in brief the computational potentialities of the spin network simulator. Going beyond questions in number theory, we argue that our model is suitable to deal with $\#\mathbf{P}$ (“hard enumerative/combinatorial”) problems more efficiently than any classical machine.

For what concerns space complexity capacity of the spin network simulator in the sense of capability of storing information, we realize that it behaves as the cardinality of the (Twist)–Rotation graphs (*cfr.* (114), (115), (116), Table 2 and Table 3 of Appendix A1). When the number n of incoming angular momenta grows, the number of states which becomes accessible for computation increase at least exponentially. To quantify these asymptotic growth, consider first the Catalan numbers (96) which represent some sort of lower bound for the various enumerations of rooted labeled binary trees shown in Table 3 of Appendix A1. They have the following asymptotic expansion for $n \rightarrow \infty$ [31]

$$C_n \approx \frac{e^{n \ln 4}}{\sqrt{\pi n(n+1)^2}} \left\{ 1 - \frac{1}{8n} + \frac{1}{128n^2} + \dots \right\} \quad (79)$$

where $\ln = \log_e$. On the other hand, we may estimate approximatively rates of growth of the double factorial D_n in (116) and of the quadruple factorial \hat{C}_n in (115) by using Stirling formula. We get

$$D_n \approx n^n \exp \{n \ln 2 - n\} \quad (80)$$

$$\hat{C}_n \approx n^n \exp \{2n \ln 2 - n\} \quad (81)$$

where the subleading terms are decreasing (increasing) exponentials, respectively. Thus the case considered in Section 4.1, namely the computational space modeled on the Rotation graph \mathfrak{G}_n , turns out to exhibit for large n space complexity of factorial class $\approx n!$ as in (80).

To address analogously *time complexity*, we need first the notion of "input length" (for an instance of some given problem) which turns out to be related with the encoding scheme employed. By using the map (76) we may say that a typical input length is the number of symbols required to specify a (quantum) labeled tree, namely $(2n+1)$ (terminal nodes, intermediate nodes and the root). Thus it seems natural to assume such a number as a typical measure of the size of the input (note however that in order to specify one particular quantum state we should choose also a value for the total magnetic number M). Although the input length is linear in the number of symbols, the quantum nature of the computational space is reflected by the fact that the size of the configuration space accessible for computation grows factorially with n as discussed in the previous remark.

With these premises and by exploiting the estimate on the Diameter of the rotation graph \mathfrak{G}_n given in (128) of Appendix A3, we assert that the (time) complexity function for any possible algorithm running over the spin network simulator can be expected to be polynomially bounded as a function of the input size n . An effective discussion of both space and time complexity, however, requires of course reference to a specific algorithm, which in turn can be formulated only provided the necessary encoding scheme is defined. Work is in progress along these lines [17].

5 Semiclassical simulator and $SU(2)$ state sum models

According to the Bohr correspondence principle, classical concepts become increasingly valid in the regime where quantum numbers are large. In handling with angular momenta variables measured in units of \hbar , the classical limit $\hbar \rightarrow 0$ implies that, for finite angular momenta, both the j -quantum numbers and the magnetic ones are much bigger than one. For what concerns pure angular momentum states – and in particular the computational Hilbert spaces introduced in Section 2 and involved in dynamical processing as illustrated in Section 4.2 – when approaching classical limit all the components of the operators $\{\mathbf{J}_i (i = 1, 2, \dots, n+1), \mathbf{J}\}$ are confined to narrower ranges around specific values. Thus geometrical concepts typical of the semiclassical vector model arise naturally and the corresponding physical quantities have

to be thought as averaged out. As we shall see below, angular momentum functions such as Racah transforms and Wigner rotation matrices admit well defined *asymptotic limits*, whose absolute squares (probabilities) correspond to *classical limits* of the related physical quantities.

With these preliminary remarks, and on the basis of [18] and [13], Topic 9 (in which a self contained discussion of the various asymptotics is given, together with the list of original references), we are going to set up a semi-classical counterpart of the spin network simulator which represents, to our knowledge, the first explicit example of a quantum circuit model mapped onto a (classical) probabilistic automaton scheme.

Let us focus for the moment on probabilities, namely on asymptotic expansions of absolute squares of transition amplitudes. Consider an elementary j -gate, namely a Racah transform expressed in terms of a $6j$ symbol as in (23). When all the six angular momenta in the $6j$ become $\gg 1$ in \hbar units, the square of the symbol has the limiting value given by the Wigner formula

$$\left\{ \begin{matrix} a & b & d \\ c & f & e \end{matrix} \right\}^2 \sim \frac{1}{12\pi V} \quad (82)$$

where V is the Euclidean volume of the tetrahedron formed by the six angular momentum vectors whose lengths are the arguments of the coefficient (V^2 can be computed from (a, b, c, d, e, f) by using the Cayley determinant). This result can be exploited to find the probability of measuring a coupling scheme $(a(bc)_e)_f$ having prepared the system in the scheme $((ab)_d c)_f$. Denoting by $P(e)$ this probability and using (23) and (82) we get

$$P(e) = \frac{(2e+1)(2d+1)}{12\pi V}. \quad (83)$$

Coming to elementary M -gates, and in particular to the expression (26) for a W -rotation matrix in terms of Euler angles, we see that

$$|D_{M'M}^J(\alpha\beta\gamma)|^2 = |d_{M'M}^J(\beta)|^2 \quad (84)$$

and this quantity is symmetric in M' and M . Following the step illustrated in [13] (Topic 9, Section 2) we limit ourselves to analyse the case of an input quantum state characterised in the original reference frame by a total angular momentum \mathbf{J} maximally oriented along the z -axis, namely $M = J$.

the probability that the angular momentum projection along the rotated z' -axis has the value $M' = M$ is given by

$$P(M) = [d_{M'M}^J(\beta)]^2 = \binom{2J}{J-M} \left(\cos \frac{\beta}{2}\right)^{2(J+M)} \left(\sin \frac{\beta}{2}\right)^{2(J-M)}. \quad (85)$$

In the classical limit the most probable value of M is distributed around the classical value $M_0 = J \cos \beta$ with some fixed value of the classical probability $P(M_0)$. Then it can be shown that the limiting value of (85) for $J \gg 1$ and $J \pm M_0 \gg (M - M_0)$ reads

$$P(M) \sim P(M_0) \exp \left\{ -\frac{1}{J} \left(\frac{M - M_0}{\sin \beta} \right)^2 \right\}. \quad (86)$$

Thus the probability for M is a Gaussian distribution around the classical value M_0 and the dispersion in the variable $(M - M_0)$, $\sqrt{J} \sin \beta$, is of the order \sqrt{J} by the assumption made above. The simplicity of this result is due to the choice of $|JJ\rangle$ as original states. More general types of classical limits and asymptotics are discussed in [13] (Topic 9, Section 10) and collected also in [14].

Without entering into further technical details, the rationale underlying our approach should have become clear: anyone of the computing classes of the quantum simulator introduced in Section 4.2 as finite sequences of elementary unitary j - and/or M -gates can be mapped onto a corresponding (classical) non-deterministic circuit-type computing process based on combinations of (83) and/or (86). We argue that such a semiclassical model could be able to simulate physical systems made up by many interacting constituents such as polyatomic molecules described by pure states of some suitable angular momentum-type variables for high values of q -numbers.

In order to complete our semiclassical picture we have to include the treatment of asymptotic limits of the transition amplitudes associated with the elementary gates employed in the quantum model. As we shall see, the resulting setting is closely related to $SU(2)$ *state sum models* introduced in a completely different context, namely topological quantum field theories (TQFT) and Euclidean quantum gravity defined on triangulated 3-dimensional manifolds (see [32], [33] for extended reviews on such topics).

The key point is the interpretation of the Ponzano–Regge asymptotic formula for the $6j$ symbol which reads [18]

$$\begin{Bmatrix} a & b & d \\ c & f & e \end{Bmatrix} \sim \frac{1}{\sqrt{24\pi V}} \exp \left\{ i \left(\sum_{r=1}^6 \ell_r \theta_r + \frac{\pi}{4} \right) \right\} \quad (87)$$

where the limit is taken for all entries $\gg 1$ (recall that $\hbar = 1$) and $\ell_r \equiv j_r + 1/2$ with $\{j_r\} = \{a, b, c, d, e, f\}$. V is the Euclidean volume of the tetrahedron with edges of lengths $\{\ell_r\}$ (note the shift $j \rightarrow j + 1/2$ with respect to the variables employed in calculating the volume in (82)) and finally θ_r is the angle between the outer normals to the faces which share the edge ℓ_r .

- From a purely quantum mechanical point of view, the probability amplitude (87) has the form of a semiclassical (wave) function since the factor $1/\sqrt{24\pi V}$ is slowly varying with respect to the spin variables while the exponential is a rapidly oscillating dynamical phase. Such behavior complies with the fact that the square of the modulus of the asymptotic (87) reproduces Wigner’s expression (82). Moreover, according to Feynman path sum interpretation of quantum mechanics, the argument of the exponential represents a classical action, and indeed it can be read as $\sum p \dot{q}$ for pairs (p, q) of canonical variables (angular momenta and conjugate angles).
- There exists another intriguing physical interpretation of (87) if we recognise that the expression in the exponential represents the classical Regge action [20] – namely the discretized version of Einstein–Hilbert action of General Relativity – for the tetrahedron associated with the $6j$ symbol in the asymptotic regime.

In Regge’s approach the edge lengths of a triangulated spacetime are taken as discrete counterparts of the metric tensor appearing in the usual action for gravity and angular variables (deficit angles) are related to the scalar curvature obtained from the Riemann tensor. Strictly speaking, a “triangulated spacetime” is a piecewise linear (PL) manifold of dimension D dissected into simplices, namely triangles in $D = 2$, tetrahedra in $D = 3$, 4-simplices in $D = 4$ and so on. Inside each simplex either an Euclidean or a Minkowskian metric can be assigned: accordingly, spacetime manifolds obtained by gluing together D -dimensional simplices acquire an overall PL metric of Riemannian or Lorentzian signature.

The Regge Calculus formalism became in the early 80's the starting point for a novel approach to quantization of General Relativity known as Simplicial Quantum Gravity (see the review [34] and references therein). The quantization procedure most commonly adopted is the Euclidean path sum approach, namely the discretized version of Hartle–Hawking path integral describing D -dimensional, locally Euclidean geometries undergoing "quantum fluctuations", possibly with the constraint of keeping some $(D - 1)$ -dimensional boundaries fixed.

Coming back to the interpretation of (87), we conclude that it represents the semiclassical functional – to be intended as the semiclassical limit of a sum over all quantum fluctuations – associated with a very simple 3-dimensional "spacetime", the Euclidean tetrahedron.

On the basis of the remark above, we pass to describe in brief the Ponzano–Regge state sum model representing the (quantized) partition function of simplicial Euclidean 3-gravity. Denote by

$$\mathcal{T}^3(j) \rightarrow \mathcal{M}^3 \quad (88)$$

a particular triangulation of a closed 3-dimensional PL manifold \mathcal{M}^3 (of fixed topology) obtained by assigning $SU(2)$ "spin variables" $\{j\}$ to the edges of \mathcal{T}^3 . The assignment must satisfy a number of conditions which can be more easily illustrated if we introduce the *state functional* associated with $\mathcal{T}^3(j)$, namely

$$\mathbf{Z}[\mathcal{T}^3(j) \rightarrow \mathcal{M}^3; L] = \Lambda(L)^{-N_0} \prod_{A=1}^{N_1} (-1)^{2j_A} \mathbf{w}_A \prod_{B=1}^{N_3} \phi_B \left\{ \begin{matrix} j_1 & j_2 & j_3 \\ j_4 & j_5 & j_6 \end{matrix} \right\}_B \quad (89)$$

where N_0, N_1, N_3 denote the number of vertices, edges and tetrahedra in $\mathcal{T}^3(j)$, $\Lambda(L) = 4L^3/3C$ (C an arbitrary constant), $\mathbf{w}_A \doteq (2j_A + 1)$ are the dimensions of irreducible representations of $SU(2)$ which weigh the edges, $\phi_B = (-1)^{\sum_{p=1}^6 j_p}$ and $\left\{ \begin{matrix} a & b & c \\ d & e & f \end{matrix} \right\}$ are $SU(2)$ $6j$ symbols to be associated with the tetrahedra of the triangulation. The Ponzano–Regge *state sum* is obtained by summing over triangulations corresponding to all assignments of spin variables $\{j\}$ bounded by the cut-off L , namely

$$\mathbf{Z}_{PR}[\mathcal{M}^3] = \lim_{L \rightarrow \infty} \sum_{\{j\} \leq L} \mathbf{Z}[\mathcal{T}^3(j) \rightarrow \mathcal{M}^3; L], \quad (90)$$

where we formally remove the cut-off by taking the limit in front of the sum. As already noted in [18], the above state sum is a topological invariant owing to the fact that its value is actually independent of the particular triangulation, namely does not change under suitable topological transformations (the bistellar moves). These moves are expressed algebraically in terms of the Biedenharn-Elliott identity (46) –representing the moves $(2 \text{ tetrahedra}) \leftrightarrow (3 \text{ tetrahedra})$ – and of both the Biedenharn-Elliott identity and the orthogonality conditions (48) for $6j$ symbols, which represent the barycentric move together its inverse, namely $(1 \text{ tetrahedra}) \leftrightarrow (4 \text{ tetrahedra})$.

The state sum (90) (and, more generally, geometric partition functions of this type built up in any dimension D [35]) resembles the functional (73) introduced in dealing with the j -computing class of the spin network simulator (Section 4.2). This is due to the fact that the amplitude of the $3nj$ symbol in (73) can be factorized according to the general prescription (68) into sums over intermediate angular momenta of products of $6j$ symbols weighted by suitable factors and phases (*cfr.* (23), (24)). These two partition functions share the property of being combinatorially invariant under topological moves expressed in terms of algebraic identities of the $6j$ symbols. However, on the one hand, the Racah identity (47) does not appear in the Ponzano-Regge framework since it would correspond to a topological transformation $(1 \text{ tetrahedron}) \leftrightarrow (2 \text{ tetrahedra})$ which is forbidden in the PL category. On the other hand, in the spin network framework it is not required *a priori* that the $6j$ symbols match together to give rise to a triangulation of a 3-dimensional manifold. Moreover, if we fix n to get a specific computational space modeled on the graph \mathfrak{G}_n , we would not catch in \mathfrak{G}_n all possible triangulations of a given PL 3-manifold. Although we may be tempted to claim that the spin network is able to simulate $SU(2)$ -coloured 3-dimensional quantum gravity, we should bear in mind that we are actually dealing with a graphical device which encodes all types of $3nj$ symbols for any fixed n [22]. In this perspective it is interesting to recall that Ponzano and Regge themselves [18] noted that the topology of a $9j$ symbol corresponds to the real projective space \mathbb{RP}^2 , in the same sense that the $6j$ has the topology of the 2-sphere bounding the tetrahedron. Indeed any particular type of $3nj$ symbol may be associated with a closed, not necessarily oriented, surface representing the boundary of a 3-dimensional polyhedron [36] obtained by duality from the graphical representations introduced in [12]. In this sense the claim that the simulator can simulate some classes of extended triangulated objects is certainly true in dimension 2.

Remark 5.1. In [37] a regularized version of (90) –based on representation theory of a quantum deformation of the group $SU(2)$ – was proposed and shown to be a well-defined (finite) *quantum invariant* for closed 3-manifolds. Its expression reads

$$\mathbf{Z}_{TV}[\mathcal{M}^3; q] = \sum_{\{j\}} \mathbf{w}^{-N_0} \prod_{A=1}^{N_1} \mathbf{w}_A \prod_{B=1}^{N_3} \left| \begin{array}{ccc} j_1 & j_2 & j_3 \\ j_4 & j_5 & j_6 \end{array} \right|_B, \quad (91)$$

where the summation is over all colourings $\{j\}$ labeling highest weight irreps of $SU(2)_q$ ($q = \exp\{2\pi i/r\}$, with $\{j = 0, 1/2, 1, \dots, r-1\}$), $\mathbf{w}_A \doteq (-1)^{2j_A} [2j_A + 1]_q$ where $[]_q$ denote a quantum integer, $\mathbf{w} = 2r/(q - q^{-1})^2$ and $| \cdot |_B$ represents the q -6j symbol whose entries are the angular momenta j_ℓ , $\ell = 1, \dots, 6$ associated with tetrahedron B . In [38] the invariant (91) is shown to equal the square of the modulus of the Reshetikhin–Turaev invariant, which in turn represents the Chern–Simons partition function written for a closed oriented manifold \mathcal{M}^3 equipped with a surgery presentation. We may write schematically

$$\mathbf{Z}_{TV}[\mathcal{M}^3; q] \longleftrightarrow |\mathbf{Z}_{CS}[\mathcal{M}^3; k]|^2, \quad (92)$$

where the level $k = 2(r-1)$ of the Chern–Simons functional is related to the deformation parameter q and also to the cosmological constant of the underlying Euclidean gravity model (*cfr.* [33] (Ch 7) and [39] for reviews on Chern–Simons theory and its relations with 3-dimensional gravity).

As we shall see in the following section, functors derived from $SU(2)$ Chern–Simons theory are the basic ingredients for implementing computation in the topological approach [4]. It will be shown that the spin network dynamics based on j -gates can be mapped into the functorial approach in a way that resembles the correspondence (92). \blacktriangle

6 Spin network and topological quantum computation

We begin this section by introducing some basic ingredients of Chern–Simons-type Topological Quantum Field Theories (CS TQFTs) in order to deal with

the topological approach to quantum computation. Our presentation will be necessarily sketchy, and we refer the reader to [40], [41], [42] for general reviews on TQFTs, while the 3-dimensional CS case is extensively addressed in [32], [33], [39].

TQFTs are particular types of gauge theories, namely field theories quantized through the (Euclidean) path integral prescription starting from a classical Yang–Mills action defined on a suitable D -dimensional space(time). TQFTs are characterized by observables (correlation functions) which depend only on the global features of the space on which these theories live, namely they are independent of any metric which may be used to define the underlying classical theory. The geometrical and topological generating functionals and correlation functions of such theories are computable by standard techniques in quantum field theory and provide novel representations of certain global invariants (for D -manifolds and/or for particular submanifolds embedded in the ambient space) which are of prime interest in mathematics. In the 3-dimensional case, theories based on Chern–Simons-type actions (see below) have been shown to incorporate significant generalizations of previously known invariants for both 3-manifolds (Witten–Reshetikhin–Turaev invariant) and knots/links (Jones polynomial). In particular, the Jones polynomials [43] can be obtained as correlation functions of Wilson line operators along closed loops in the CS framework [44]. While these mathematical advances are self-evident, CS theory also provides a unifying 3-dimensional viewpoint for 2-dimensional Conformal Field Theory as well as new results on 3-dimensional quantum gravity.

Since TQFTs are quite generally soluble, they could provide a testing ground for new approaches to the quantum theory of fields. It has been conjectured that TQFTs may represent different “phases” –in which general covariance is unbroken– of their more conventional counterparts.

Denote by Σ_1 and Σ_2 a pair of 2-dimensional manifolds and by \mathcal{M}^3 a generic 3-dimensional manifold with boundary $\partial\mathcal{M}^3 = \Sigma_1 \cup \Sigma_2$ (all manifolds here are compact, smooth and oriented). A unitary 3-dimensional quantum field theory corresponds to the assignment of

i) finite dimensional Hilbert spaces (endowed with non-degenerate bilinear forms) \mathcal{H}_{Σ_1} and \mathcal{H}_{Σ_2} to Σ_1 and Σ_2 , respectively;

ii) a map ("functor") connecting such Hilbert spaces

$$\mathcal{H}_{\Sigma_1} \xrightarrow{\mathbf{Z}[\mathcal{M}^3]} \mathcal{H}_{\Sigma_2} \quad (93)$$

where \mathcal{M}^3 is a manifold which interpolates between Σ_1 (incoming boundary) and Σ_2 (outgoing boundary). Without entering into details concerning a few more axioms (diffeomorphism invariance, factorisation *etc.*) we just recall that unitarity implies that

iii) if $\bar{\Sigma}$ denotes the surface Σ with the opposite orientation, then $\mathcal{H}_{\bar{\Sigma}} = \mathcal{H}_{\Sigma}^*$, where $*$ stands for complex conjugation;

iv) the functors (93) are unitary and $\mathbf{Z}[\bar{\mathcal{M}}^3] = \mathbf{Z}^*[\mathcal{M}^3]$, where $\bar{\mathcal{M}}^3$ denote the manifold with the opposite orientation.

In Chern–Simons theory the functor (93) is the partition function \mathbf{Z}_{CS} associated with the classical action

$$S_{CS}(A) = \int_{\mathcal{M}^3} \left(A dA + \frac{2}{3} A \wedge A \wedge A \right) \quad (94)$$

written for simplicity for a closed manifold \mathcal{M}^3 , $\partial\mathcal{M}^3 = \emptyset$. Here A is an $SU(2)$ –connection, namely a 1–form on the principal $SU(2)$ –bundle over \mathcal{M}^3 , d is the exterior differential and \wedge is the wedge product of differential forms. The partition function is obtained functionally by integrating the exponential of the classical action (94) over the space of all $SU(2)$ connections. We formally write

$$\mathbf{Z}_{CS}[\mathcal{M}^3; k] = \int [DA] \exp \left\{ \frac{ik}{4\pi} S_{CS}(A) \right\} \quad (95)$$

where the coupling constant k (the level of the theory) must be an integer. It can be shown that the partition function (95) actually represents a topological invariant for closed 3–manifolds, related in turn to the Turaev–Viro invariant (91) by the correspondence (92) (where $|\mathbf{Z}_{CS}[\mathcal{M}^3]|^2$ stands for $\mathbf{Z}_{CS}[\mathcal{M}^3] \mathbf{Z}_{CS}^*[\mathcal{M}^3]$).

The extension of (95) to the case $\partial\mathcal{M}^3 \neq \emptyset$ requires modifications of the classical action (94) by suitable (Wess–Zumino–type) boundary terms [39]. In view of applications in a computational context it is sufficient to note that for a boundary component Σ , $\mathbf{Z}_{CS}[\mathcal{M}^3](\Sigma)$ can be realized as restriction to invariant subspace $W \subseteq \mathcal{H}_{\Sigma}$ of transformations of the form $\prod_i g_i$ on the subspace of computational states of a quantum computer, where the g_i ,

interpreted as gates in a quantum circuit scheme, can be written as "words" in the standard generators (Dehn's twists) of the *Mapping Class Group* of the surface Σ . Also in the computational framework the "observables" of the theory turn out to be represented by Wilson loops as discussed in [45] and in the following paragraph. The explicit expression of Wilson loops operators $\mathcal{W}_k(K)$, namely holonomies of the connection 1-form evaluated on closed curves K in \mathcal{M}^3 , read

$$\mathcal{W}_k(K) = \int_{A/\mathcal{G}} [DA] e^{\frac{ik}{4\pi} S_{CS}(A)} \text{Tr}(\text{hol } K) / \int_{A/\mathcal{G}} [DA] e^{\frac{ik}{4\pi} S_{CS}(A)} \quad (96)$$

where $\text{hol } K \doteq \mathcal{P} \exp \int_K A$, \mathcal{P} is the path ordering, and A is now thought of as the connection over the \mathcal{G} -bundle of Lie algebra-valued 1-forms tangent to \mathcal{M}^3 (\mathcal{G} being the gauge group).

It is worth to recall that the evaluation of Jones polynomials – appearing in expressions like (96) – was shown to be computationally $\#P$ [46] (namely essentially the enumerative equivalent of NP -complete [47]).

6.1 Holonomic Quantum Computation

Holonomic Quantum Computation (HQC) is an all-geometrical approach to quantum information processing. In the HQC strategy information is encoded in degenerate eigenspaces of a parametric family of Hamiltonians. The computational network of unitary quantum gates is realized by driving adiabatically the Hamiltonian parameters along loops in a control manifold. By properly designing such loops the non-trivial curvature of the underlying bundle geometry gives rise to unitary transformations, *i.e.* holonomies that implement the desired unitary transformations. Conditions necessary for universal QC are stated in terms of the curvature associated to the non-Abelian gauge potential over the control manifold. In view of their geometrical nature the holonomic gates are robust against several kind of perturbations and imperfections. This, along with the adiabatic fashion in which gates are operated, makes in principle HQC an appealing way towards universal fault-tolerant QC.

HQC as introduced in [9], [10], is based on a novel gauge-theoretic framework in which one is supposed to be able to control a set of parameters

$\lambda \in \mathcal{L}$, on which depends an iso-degenerate family \mathcal{F} of quantum Hamiltonians $\{H(\lambda)\}$. Information is encoded in a ν -dimensional eigenspace \mathcal{C} of a specific $H(\lambda_0) \in \mathcal{F}$. Universal QC [48] over \mathcal{C} can be then obtained by adiabatically driving the control parameters along suitable loops γ rooted at λ_0 . The key physical ingredient is provided by the appearance in such quantum evolutions of non-Abelian geometrical contributions [49] $U_\gamma \in U(\nu)$ ($\nu > 1$) given by holonomies associated with a gauge potential A valued in the algebra of $U(\nu)$ [50], [51]. In other words quantum computation in the HQC approach is nothing but the parallel transport of states in \mathcal{C} realized by the connection A . Therefore the computational power in the HQC approach relies on the non-triviality of the geometry of the bundle of eigenspaces of \mathcal{F} over the manifold of control parameters, \mathcal{L} : in this sense HQC is fully geometrical. It is worth observing that the computational subspace \mathcal{C} can be thought of as the lowest-energy manifold of a highly symmetric quantum system; from this point of view HQC is a kind of ground-state computation. This last remark points out the potential existence of a fault-tolerant [52] feature of HQC due to energy gaps and even spontaneous relaxation mechanisms. Further fault-tolerant characteristics of HQC are related to the fact that the holonomies U_γ realizing quantum computations typically turn out to depend just on the areas of the surfaces that the generating loops γ span on certain 2-dimensional submanifolds. When this area is given one can consider even very large, *i.e.* "far" from the identity deformations of γ , but as long as they are area-preserving no errors are induced. Moreover as far as the adiabaticity condition holds, U_γ does not depend on the rate at which the control loops are driven. Hence, even with respect the issue of timing, HQC can be expected to be robust.

The evolution of the quantum system is thought of as actively driven by the parameters λ , over which the experimenter is assumed to have direct access and control, being able to drive by a dynamical control process the parameter configuration $\lambda \in \mathcal{L}$ through a path $\gamma : [0, T] \rightarrow \mathcal{L}$. Hence, a one-parameter (time-dependent) family

$$\mathcal{F}_\gamma \doteq \{H(t) \equiv H[\Phi \circ \gamma(t)] | t \in [0, T]\} \subset \mathcal{F}, \quad (97)$$

is defined for all $\Phi : \mathcal{L} \mapsto U(\mathcal{N})$, $\mathcal{N} = \dim \mathcal{C}$, Φ being a smooth mapping, and $\dim(U(\mathcal{N})) = \mathcal{N}^2$. The quantum evolution associated to the family \mathcal{F}_γ is described by the time-dependent Schrödinger equation $i\partial_t |\psi(t)\rangle =$

$H(t)|\psi(t)\rangle$ and hence it has the operator form

$$U_\gamma \doteq \mathbf{T} \exp \left\{ -i \int_0^T dt H(t) \right\} \in U(\mathcal{N}) , \quad (98)$$

where \mathbf{T} denotes chronological ordering. The above time-dependent quantum evolution, for a given map Φ , depends in general on the path γ and *not* just on the curve $\gamma([0, T])$, namely the image of γ in the control manifold. In other words the unitary transformation U_γ contains a *dynamical* as well as a *geometrical* contribution, the former depends on the rate at which $\gamma([0, T])$ is traveled along whereas the latter depends merely on the geometrical characteristics of the curve.

Non-Abelian holonomies are a natural generalization of the Abelian Berry phases. The basic assumption is that \mathcal{F} is an iso-degenerate Hamiltonian family, *i.e.* all the elements of \mathcal{F} have the same degeneracy structure. When the system control parameters are driven adiabatically, slowly with respect to any time-scale associated to the system dynamics, along a loop γ in \mathcal{L} any initially prepared state $|\psi_{in}\rangle \in \mathcal{H}$ will be mapped after the period T onto the state

$$|\psi_{out}\rangle = U_\gamma |\psi_{in}\rangle , \quad U_\gamma = \bigoplus_{\ell=1}^R e^{i\phi_\ell} \Gamma_{A_\ell}(\gamma) , \quad (99)$$

where $\phi_\ell \doteq \int_0^T d\tau \varepsilon_\ell(\lambda_\tau)$ is the dynamical phase ($\varepsilon_\ell(\lambda)$ denoting the degenerate Hamiltonian eigenvalues) whereas the matrices $\Gamma_{A_\ell}(\gamma)$ represent the geometrical contributions. They are unitary mappings of \mathcal{H}_ℓ onto itself and they can be expressed by the following path ordered integrals

$$\Gamma_{A_\ell}(\gamma) \doteq \mathcal{P} \oint_\gamma A_\ell \in U(n_\ell) , \quad \ell = 1, \dots, R , \quad (100)$$

n_ℓ denoting the number of degenerate states of energy ε_ℓ , and R the number of degeneracies. These are the *holonomies* associated with the loop γ , and the *adiabatic connection forms* A_ℓ . The latter have an explicit matrix form given by

$$A_\ell = \sum_\mu A_{\ell,\mu} d\lambda_\mu , \quad (A_{\ell,\mu})^{\alpha,\beta} \doteq \langle \psi_\ell^\alpha(\lambda) | \frac{\partial}{\partial \lambda^\mu} | \psi_\ell^\beta(\lambda) \rangle , \quad (101)$$

with $\{\lambda_\mu\}_{\mu=1}^d$ the local coordinates on \mathcal{L} , and $\mathcal{H}_\ell = \text{span}\{\psi_\ell^\alpha(\lambda)\}_{\alpha=1}^{n_\ell}$, $\psi_\ell^\alpha(\lambda)$ denoting the eigenstates of $H(\lambda)$ corresponding to eigenvalue $\varepsilon_\ell(\lambda)$. The connection forms A_ℓ are nothing but the non-Abelian gauge potentials enabling the parallel transport over \mathcal{L} of vectors of the fiber \mathcal{H}_ℓ .

The combinatorial setting of the spin network simulator, and in particular of its fiber space structure over \mathfrak{G}_n (see Remark 4.1 at the end of Section 4.1 and [29]), appears to provide the natural structure for a discrete-time implementation of HQC, at least when the Hamiltonian defined in (69) exhibit the required degeneracy.

6.2 Combinatorial setting of Topological Quantum Computation

The approach to quantum computation of Freedman and collaborators [4] is based on an extension of Chern–Simons functor at level $k = 3$ (CS3) to particular types of 2-dimensional boundary objects, namely closed disks with some marked points. Denote by $(D^2, 3 \text{ pts})$ a closed disk –namely a set topologically equivalent to the standard 2-disk $\{(x, y) \in \mathbb{R}^2 \mid x^2 + y^2 \leq 1\}$ – with three points lying in the interior of D^2 . These points, together with the boundary ∂D^2 of the disk, are marked by four labels $\{a, b, c, d\}$ chosen in the set $\{0, 1, 2, \dots, k\}$, which reduces to $\{0, 1, 2, 3\}$ in the present case $k = 3$. Notice that the convention adopted by the authors of [4] is different from ours: the level $k = 3$ here corresponds to their $k = 5$.

The disk considered so far and depicted in Fig. 3 (left) is the support of the so-called “topological qubit”. More precisely, a topological qubit corresponds to the image of the usual 1-qubit space \mathbb{C}^2 into the Hilbert space $\mathcal{H}_{CS3}(D^2, 3 \text{ pts})$ derived from CS theory. The inclusion

$$\begin{aligned} i : \mathbb{C}^2 &\hookrightarrow \mathcal{H}_{CS3}(D^2, 3 \text{ pts}) \\ \text{with } i(\mathbb{C}^2) &\doteq V(D^2, 3 \text{ pts}) \end{aligned} \tag{102}$$

induces on the label set $\{a, b, c, d\}$ the identifications $a \equiv b \equiv c \equiv 1$ and $d \equiv 0$, namely a mapping onto the binary digits $\{0, 1\}$ (see Fig. 3, right).

Figure 3

In the present framework 1-qubit gates are implemented by considering – instead of the full Chern–Simons functor (93) – a unitary action of the braid group B_3 on the strands generated in the ambient space by "evolution" of the marked points.

Figure 4

If

$$B_3 \times (D^2, 3 \text{ pts}) \rightarrow (D^2, 3 \text{ pts}) \quad (103)$$

denotes the action of the braid group B_3 on the topological support (see Fig. 4) then we formally write the induced unitary functor between Hilbert spaces as

$$V_1(D^2, 3 \text{ pts}) \xrightarrow{\mathbf{Z}_{B_3}} V_2(D^2, 3 \text{ pts}). \quad (104)$$

A configuration of N qubits is supported by a 2-disk with $3N$ marked points $(D^2, 3N \text{ pts})$ and the associated Hilbert space is $V(D^2, 3N \text{ pts})$, namely the image of $(\mathbb{C}^2)^{\otimes N}$ in $\mathcal{H}_{CS5}(D^2, 3N \text{ pts})$, where the image is defined as in (102). An N -qubit gate is represented by a unitary map

$$V_1(D^2, 3N \text{ pts}) \xrightarrow{\mathbf{Z}_{B_{3N}}} V_2(D^2, 3N \text{ pts}), \quad (105)$$

where B_{3N} is the braid group acting on the $3N$ strands generated by the marked points.

We may summarise the main results of the series of papers [4] as follows. It is shown that their $CS5$ -functor (and also any other CSk -functor, $k \geq 3, k \neq 4$) is universal for quantum computation and in particular that 1 and 2-qubits topological gates are sufficient to reconstruct all other gates of the type (105). The resulting model is polynomially equivalent to the usual Boolean quantum circuit and, conversely, it is actually shown that there exists (at least) a class of TQFTs which can be simulated on a quantum machine (*cfr.* the diagram at the end of Section 2). There are however some open problems in this approach, mainly due to the fact that it is difficult to "localise" topological objects (such as the marked points on disks) in order to provide local Hamiltonian operators.

Remark 6.1. It may be useful to recall some basic properties of the Artin braid group B_n (see for instance [32]). B_n has n generators, denoted for the moment by $\{\sigma_1, \sigma_2, \dots, \sigma_n\}$, which satisfy the relations

$$\begin{aligned} \sigma_i \sigma_j &= \sigma_j \sigma_i \quad \text{if } |i - j| > 1 \\ \sigma_i \sigma_{i+1} \sigma_i &= \sigma_{i+1} \sigma_i \sigma_{i+1} \quad (i = 1, 2, \dots, n). \end{aligned} \quad (106)$$

This group acts naturally on topological sets of n disjoint strands – running downward and labeled from left to right – in the sense that each generator σ_i corresponds to a crossing of two contiguous strands labeled by i and $(i + 1)$, respectively (if σ_i stands for the crossing of the i -th strand over the $(i + 1)$ -th one, then σ_i^{-1} represents the inverse operation and $\sigma_i \sigma_i^{-1} = \sigma_i^{-1} \sigma_i = \text{Identity}$). By slightly changing notations, denote by R_{ij} the (over)crossing operation acting on two strands the endpoints of which are labeled by i and j . Then the second relation in (106) can be recasted into the form

$$R_{12} R_{13} R_{23} = R_{23} R_{13} R_{12} \quad (107)$$

and represented pictorially as in Fig. 5, where operations are ordered downward. Note that this picture can be viewed as a portion of an n -strands configuration (and thus $\{1, 2, 3\}$ may actually represent labels attached to any triad of contiguous strands) since the first relation in (106) ensures that other kinds of crossing are trivial. The relation (107) (or, alternatively, (106)) is the algebraic Yang–Baxter equation which characterises the algebraic structure of a number of models in statistical mechanics and field theory.

Figure 5

The Artin braid group –which arises naturally in the CS-framework and consequently in the topological setting for quantum computation described above– plays a crucial role also in the approach recently proposed in [53] where unitary representations of B_4 are shown to be universal gates for Boolean quantum computation. We shall come back on this point at the end of this section, after the analysis of the algebraic structure underlying the spin network model. ▲

We come now to describe the algebraic content of the theory underlying the spin network simulator by showing explicitly how binary coupling trees

can be embedded into "combinatorial" 2-disks with marked points whose associated transformations satisfy the Racah and the Biedenharn–Elliott identities (46) and (47) (instead of the Yang–Baxter equation (107) characterising the standard topological approach).

Recall from Appendix A1 (see in particular Fig. 18) that the fundamental binary trees on $(n + 1) = 3$ labeled leaves are of three types (twists are inessential). Choose for instance the tree T_{12} corresponding to the bracketing scheme

$$T_{12} \longleftrightarrow ((j_1 j_2)_{j_{12}} j_3)_J \quad (108)$$

and pay attention to the fact that in the drawings we further simplify labels by setting $j_1 \equiv 1$; $j_2 \equiv 2$; $j_{12} \equiv 12$; $j_3 \equiv 3$ while J is left unchanged. Since now we have always placed the labels onto the nodes (following the notations of [13] (Topic 12)) but here we switch to the conventions of [12] by labeling edges. Thus the tree acquires a new edge springing from the vertex formerly labeled by J and becomes a 3-valent graph –denoted by t_{12} – as shown in Fig. 6. We may interpret the vertices of such new graphs as "interaction vertices" for the pair of incoming spin variables.

Figure 6

The procedure to pass from t_{12} to a decorated 2-disk with marked points is carried out in a few steps illustrated below.

Step 1. A topological transformation can be performed on t_{12} (technically it corresponds to the action of a thickening functor, see *e.g.* [42]) which consists in "blowing inside" the graph and smoothing the corners. The resulting topological 2-manifold, depicted in Fig. 7, is a 2-sphere S^2 with boundaries represented by four circles (a "punctured" sphere). We label such boundary circles by arbitrary labels $\{a, b, c, d\}$ and denote such a surface by $(S^2; a, b, c, d)$.

Figure 7

Step 2. Fill up $(S^2; a, b, c, d)$ with an open set $\subset \mathbb{R}^3$: the resulting 3-space is (a portion of) a "precursor" of a handlebody \mathcal{M}^3 (a handlebody is a closed oriented 3-manifold –the complement of a link in the 3-sphere

S^3 – obtained by gluing tubular neighbourhoods of the link along the boundary 2–disks). Here we simply glue closed 2–disks along the boundary circles of $(S^2; a, b, c, d)$ to get a 3–manifold with boundary –topologically equivalent to the 3–ball bounded by a 2–sphere– denoted by $(D^3, S^2)_{(a,b,c,d)}$, where (a, b, c, d) may be thought of as labelings for 2–disks. The corresponding picture can be visualised by looking at the configuration in Fig. 7 as representing a "solid" object with 2–dimensional disks placed over the circles a, b, c, d .

Step 3. Consider an oriented embedding

$$i_t : \mathbf{t}_{12} \hookrightarrow (D^3, S^2)_{(a,b,c,d)} \quad (109)$$

which can be realized as a smooth map by splitting the 3–valent vertices in \mathbf{t}_{12} according to the rule illustrated in Fig. 8.

Figure 8

Then the image of \mathbf{t}_{12} into $(D^3, S^2)_{(a,b,c,d)}$ is obtained by requiring that $1 \hookrightarrow a$, $2 \hookrightarrow b$, $3 \hookrightarrow c$, $J \hookrightarrow d$ as shown in Fig. 9 (we agree to drop out the auxiliary labels on the boundary 2–disks once the map i_t in (109) has been implemented).

Figure 9

Having started from the fundamental binary tree of (108) we end up with a set of three (embedded) disjoint strands with crossings. In TQFTs configurations of this type represent "precursors" of knots/links, which are the observables of the theory as explained in the introductory remarks of this section.

We may note that the procedure outlined so far depends on the choice of the embedding map (109) and thus it is not uniquely defined. As discussed in [42] (Ch. 7) is always possible to establish a bijection between TQFTs belonging to the categories FCx^{0+1} (graphs) and $SDif^{1+1}$ (smooth surfaces) but the construction is not well defined since one should actually consider "categories of all possible choices of embeddings and regular neighbourhoods, and get an induced TQFT by taking inverse limits over these categories".

Step 4. By taking "time slicings" on the configuration of embedded strands in Fig. 9 equipped with the downward orientation we get the picture shown in Fig. 10, where points and boundaries of disks inherit consistent labelings.

Figure 10

The final configuration (at the bottom of Fig. 10) represents a 2-disk (D^2 ; $j_1, j_2, j_3; j_{12}; J$) with three marked points and one marked circle inside (binary marked 2-disk for short). Note that

- $SU(2)$ -labelings of marked points $(1, 2, 3) \equiv (j_1, j_2, j_3)$ can be freely chosen;
- the labelings of the internal circle ($12 \equiv j_{12}$) and of the boundary of the disk (J) have suitable ranges (*cfr.* (8)) and are induced by the original tree structure.

Step 5. If we take into account all the three fundamental binary coupling trees (each mapped into a suitable binary marked 2-disk) we realize that the algebraic structure relating the associated Hilbert spaces is encoded into the Racah identity (see the explicit expression (47)) which we write down schematically (apart from weights/phases) as

$$\mathcal{R}(j_{12}, j_{31}) = \sum_{j_{23}} \mathcal{R}(j_{12}, j_{23}) \mathcal{R}(j_{23}, j_{31}) \quad (110)$$

The pictorial representation of (110) acting on (the Hilbert spaces of) binary marked 2-disks is given by the triangular commutative diagram of Fig. 11 which has the same content of the triangular graph shown in Fig. 22 of Appendix A2 (where the edges are thought of as topological moves on binary trees).

Figure 11

Step 6. By taking into account the different binary coupling schemes of $(n+1) = 4$ angular momenta we would get a combinatorial picture based on binary 2-disks with four marked points and two marked circles, each associated with its own computational Hilbert space defined in (15). Then the natural algebraic structure linking the five spaces (up to phases) is provided

by the Biedenharn–Elliott identity (46) encoded in the pentagonal diagram depicted in Fig. 23 of Appendix A2.

Remark 6.2. As is well known from representation theory of simple Lie algebras (see *e.g.* [54]), the multiple tensor products of irreducible modules can be handled formally by employing intertwiner spaces. More precisely, if $\Lambda, \Lambda', \Lambda'', \dots$ label highest weight representations of the algebra, the isomorphisms $V_\Lambda \otimes V_{\Lambda'} \cong V_{\Lambda'} \otimes V_\Lambda$ between the modules supporting (the tensor product of) the irreps Λ, Λ' is reflected into an isomorphism of intertwiner spaces

$$F : \Upsilon_{\Lambda\Lambda'}^{\Lambda_i} \longrightarrow \Upsilon_{\Lambda'\Lambda}^{\Lambda_i} \quad (111)$$

and the three-fold isomorphism $(V_\Lambda \otimes V_{\Lambda'}) \otimes V_{\Lambda''} \cong V_\Lambda \otimes (V_{\Lambda'} \otimes V_{\Lambda''})$ corresponds to an isomorphism

$$R : \sum_i \Upsilon_{\Lambda\Lambda'}^{\Lambda_i} \otimes \Upsilon_{\Lambda_i\Lambda''}^{\Lambda_j} \longrightarrow \sum_i \Upsilon_{\Lambda\Lambda_i}^{\Lambda_j} \otimes \Upsilon_{\Lambda'\Lambda''}^{\Lambda_i} \quad (112)$$

of suitably defined intertwiner spaces. It can be shown that in fact the isomorphisms (111) and (112) are all we need to treat arbitrary tensor products of (a finite number of) irreducible modules provided that three compatibility conditions are fulfilled, namely a so-called *pentagon* and two *hexagon* identities. In the case of the Lie algebra $\mathfrak{sl}(2)$ the pentagon relation is the Biedenharn–Elliott identity (46) while the two hexagon relations become identical and coincide with the Racah identity (47). Thus we recover the content of the Biedenharn–Louck Theorem of Section 4.1 stated on the basis of $SU(2)$ recoupling theory. \blacktriangle

Summing up, the algebraic structure underlying the kinematics of the spin network simulator encodes automatically the pentagon and hexagon relations without resorting to *ad hoc* hypotheses. We have also shown that this combinatorial model for computation can be mapped –not uniquely– into the topological approach [4] and is not affected by localisation problems typical of any “purely topological” setting. Finally, all the gates appearing in the spin network framework are unitary while unitary representations of the braid group must be carefully picked up to fit with the usual (Boolean) quantum circuit model (see [53]). For the convenience of the reader we collect

below a concise dictionary of the basic objects, spaces and maps employed in the two approaches.

We argue that the partition functions of the two models may be related to each other much in the same way as the (regularized) Ponzano–Regge functional corresponds to a double Chern–Simons (*cfr.* Remark 5.1 at the end of Section 5 and in particular (92)).

	combinatorial approach	topological approach
information encoded into	binary coupling trees on 3 leaves	topological qubits (D^2 , 3 pts)
computational Hilbert spaces	$\mathcal{H}_n^J(\mathfrak{b})$	$\mathcal{H}_{CS3}(D^2, 3 \text{ pts})$
gates	phase and Racah transforms	unitary actions of B_{3N}
compatibility conditions	B–E (pentagon) identity Racah (hexagon) identity	Yang–Baxter equation

Table 1: A dictionary containing the basic ingredients of the combinatorial and topological approaches.

Appendix A. Spin network combinatorics

The next two paragraphs are inspired by the basic reference [13] (Topic 12) where binary couplings of N $SU(2)$ angular momenta and unitary transformations between pairs of such schemes (recoupling coefficients) are explored on the basis of their underlying graphs combinatorics. The origin of such an approach based on graph theory dates back to the Russian school of nuclear physics ([55] and earlier references therein) and gave rise to diagrammatical methods of vast applicability [12], [14]. Fack and collaborators have recently discussed some improvements concerning the efficiency of calculations for $3nj$ symbols [22], [23]. The latter achievements are summarised in Appendix A3, together with other results exploited in Section 4.3 in connection with spin network computational complexity.

A1. Binary coupling trees

A *rooted binary coupling tree* on $(n + 1)$ leaves (terminal nodes) is a tree T –namely a connected graph with no cycles (closed loops)– characterised as follows.

i) There exists a special vertex, the root.▲

ii) The tree is binary, namely each of its nodes has zero or two “siblings”. More precisely, if we draw the tree with the root at the bottom and the leaves at the top as in all Figures of this section, the siblings of a particular node are the nodes lying in the nearest upper level which are connected to the given node by an edge. Thus the number of siblings (the out-degree) of both root and internal nodes is two, while each leaf has out-degree zero. The number of internal nodes of a rooted binary tree on $(n + 1)$ leaves is $(n - 1)$ and the total number of nodes is $2n + \text{root} \equiv 2n + 1$ which of course coincides with the cardinality of the tree as a graph.▲

iii) The leaves are decorated with $(n + 1)$ distinct labels.

Generally speaking, we may attach to the leaves labelings $\{i_1, i_2, i_3, \dots, i_{n+1}\}$ thought of as a permutation of the integers $\{1, 2, 3, \dots, n+1\}$. However, in the framework of the quantum theory of angular momenta, labels are to be interpreted as quantum numbers $\{j_{i_1}, j_{i_2}, j_{i_3}, \dots, j_{i_{n+1}}\}$ associated with a set of $(n + 1)$ mutually commuting angular momentum operators $\mathbf{J}_1, \mathbf{J}_2, \mathbf{J}_3, \dots, \mathbf{J}_{n+1}$. Once assigned any such a labeling to the leaves, we induce a consistent decoration on the other nodes by associating with them –moving downside along the tree– the quantum numbers of the intermediate angular

momentum operators arising from the pairwise couplings described by the tree. According to this rule the root acquires a label J , the quantum number of the total angular momentum $\mathbf{J} = \mathbf{J}_1 + \mathbf{J}_2 + \cdots + \mathbf{J}_{n+1}$. Referring to (6) and (7) of Section 2 it follows that rooted binary coupling trees on $(n+1)$ leaves represent in a faithful combinatorial way the structure of the computational Hilbert spaces $\mathcal{H}_n^J(\mathbf{b})$ given explicitly in (15).

As an example we sketch in Fig. 12 the rooted binary coupling tree corresponding to the particular binary bracketing structure of (12) or (14).▲

Figure 12

Remark A.1. As a matter of fact there exist other discrete structures in one-to-one correspondences with rooted binary trees and commonly used in theoretical computer science. Suppose you have a finite set of symbols S (*e.g.* letters in an alphabet $A = \{x, y, z, \dots\}$) endowed with a binary operation denoted by paired round parentheses

$$(x, y) \in (S \times S) \mapsto (xy) \quad (113)$$

In the most general case the operation is neither commutative $[(xy) \neq (yx)]$ nor associative $[((xy)z) \neq (x(yz))]$. Note that we may enlarge the set S to include also "(" and ")", but then we should require that the admissible words possess an equal number of left and right parentheses. As a particular example consider the case where $S = \{(\,)\}$, namely no other symbol except the parentheses themselves. The objects we obtain – with n "(" and n ")" – are called Dyck words of length $2n$ [*e.g.* $((\,))$ and $((\,(\,)))$ for $n = 3$] and are enumerated by Catalan numbers. More generally, the structure induced by a binary operation on a finite set S turns out to be faithfully encoded in binary trees. As shown in Fig. 13, we may represent any pairing of two symbols (xy) by labeling with x and y , from left to right, two nodes in the tree which meet in a third node, then pairing the resulting symbol with a $z \in S$ attached to another node, and so on (note that this procedure generates automatically a root in the tree).▲

Figure 13

For the convenience of the reader, we collect here some useful facts from the combinatorics of rooted binary trees (*crf.* [13], [22], [23] [31], [56] and references therein). Having in mind the definition of rooted binary tree given

in **i)-ii)** we are going to distinguish between "plane" and "not plane" unlabeled trees (here we use the adjective "plane" instead of "ordered" to avoid confusion with possible ordering of labels to be assigned to leaves: for the moment there is no labeling at all). A tree T is *plane* if its nodes –except the root– are put into an ordered partition of disjoint $\{T_1, T_2, T_3, \dots, T_m\}$ in the Euclidean plane, where each T_k is a plane tree. In other words, in plane trees we distinguish between left/right and left/right subtrees. In Fig. 14 all plane unlabeled trees on 3 and 4 leaves are depicted.

Figure 14

These trees (on $(n + 1)$ leaves) are enumerated by Catalan numbers

$$C_n = \frac{1}{n+1} \binom{2n}{n} = \frac{(2n)!}{(n+1)!n!}. \quad (114)$$

The first few terms in the sequence (114) are collected in Table 3 at the end of this paragraph, while more terms are listed in [56] (ID Number A000108). According to Remark A.1, an identical counting holds true also for Dyck words and – as illustrated in Exercise 6.19 of [31] – there is actually a plenty of discrete structures from many branches of mathematics whose enumeration involves Catalan numbers.

Not plane trees are obtained as equivalence classes of plane trees of the same size under reflections with respect to vertical axes through each node which is not a leaf. The resulting structures are known as "types" (of not plane trees) and enumerated by Wedderburn–Etherington (W–E) numbers B_{n+1} for which a closed form expression is not known. The first terms of this sequence are listed in Table 3 (see [56], ID Number A001190 for more terms). In Fig. 15 the trees of W–E–types on 3 and 4 leaves are shown.

Figure 15

The classification for unlabeled trees considered so far is summarised in the upper row of Table 2 at the end of the section.

We say that a tree is *labeled* when we assign some symbol to each of its leaves. Generally speaking, we may use either distinct labels (as in binary coupling trees, see **iii)** above) or a binary label $\{0, 1\}$ (as in search trees) or even a same label for each leaf.

Remark A.2. To illustrate the subtleties arising from assignments of no label, a same label or distinct labels to leaves of trees, let us consider Catalan trees again. According to our previous definition they should be unlabeled, but it is easily recognised that the same combinatorics is shared by two more plane binary tree structures (see Fig. 16), namely

- Trees with all leaves labeled by a same x . In this case the trees encode a non associative, partially commuting binary operation on the alphabet $\{x\}$. [“Partially commuting” means that inside each pairing (xx) commutativity is trivially ensured, but for instance $((x^2)x) \neq (x(x^2))$]. Note that the case of a non associative totally commuting binary operation corresponds to W–E–types labeled with a same x since we would get in that case $((x^2)x) = (x(x^2))$ as should be clear by looking at Fig. 15, top).
- Trees with a fixed sequence of distinct labels (*e.g.* ordered lexicographically from left to right) on their leaves.

In the following we shall refer to the above labeled structures as Catalan trees too. ▲

Figure 16

From now on we are dealing with distinct labelings, chosen for simplicity in a string of $(n + 1)$ Latin letters $\{a, b, c, d, \dots\}$.

Starting with the plane category, we have to decorate the leaves of Catalan trees with all possible permutations of labels. Thus the number of these objects for any n is given by $(n + 1)!C_n$, where C_n is the Catalan number defined in (114). This number, usually written as

$$\hat{C}_n = \frac{(2n)!}{n!}, \quad (115)$$

is the quadruple factorial and in Fig. 17 all labeled plane trees on $n + 1 = 3$ leaves are shown ($\hat{C}_2 = 3!C_2 = 12$). The first terms of this integer sequence are listed in Table 3 and more terms can be found in [56], ID Number A001813.

Figure 17

To enumerate labeled *not plane* trees on $(n + 1)$ leaves we realize that there exist n axes through the $(n - 1)$ internal nodes plus root. Thus, on the basis of (115) and looking also at Fig. 17, we have to drop out exactly 2^n configurations since the trees are binary (namely each of the former n nodes has exactly two siblings). The resulting counting reads

$$D_n \doteq \frac{\hat{C}_n}{2^n} = \frac{(2n)!}{n!2^n} = (2n - 1)!!, \quad (116)$$

where $(2n - 1)!! \equiv 1 \cdot 3 \cdot 5 \cdot 7 \dots$ is the double factorial (see Table 3 and [56], ID Number A001147). The combinatorics of this enumeration can be also understood by picking up each W–E type of unlabeled trees (see Fig. 15) and decorating consistently its leaves. Then

$$D_n = \sum_{b=1}^{B_{n+1}} p_{n+1}(b) \quad (117)$$

where $p_{n+1}(b)$ represents the number of ways to decorate leaves of type b trees with $(n + 1)$ distinct labels in such a way that $(xy) = (yx)$ for each binary parenthesization involving both nodes and subtrees. In Fig. 18 not plane labeled trees on 3 leaves are depicted ($D_2 = \hat{C}_2/2^2 = 3$): they arise from the unique W–E type shown in Fig. 15, top.

Figure 18

In the following Table 2 the combinatorial enumerations for all trees considered so far are summarised, while in Table 3 the first few terms of the four integer sequences are written down to give the reader an idea of their rates of growth.

	plane	not plane
unlabeled	<i>Catalan number</i> $C_n = \frac{(2n)!}{n!(n+1)!}$	<i>Wedderburn–Etherington number</i> B_{n+1}
labeled	<i>Quadruple factorial</i> $\hat{C}_n = \frac{(2n)!}{n!}$ $= \text{card}(\hat{\mathfrak{G}}_n(V, E))$	<i>Double factorial</i> $D_n = \frac{(2n)!}{n! 2^n} = (2n-1)!!$ $= \text{card}(\mathfrak{G}_n(V, E))$

Table 2: Enumerations of rooted binary trees on $(n + 1)$ leaves according to **plane/not plane** and **unlabeled/labeled** categories. In case of labeled trees the numbers represent the cardinalities of the Twist–Rotation and Rotation graphs, respectively (see Appendix A2).

n	1	2	3	4	5	6	7
B_{n+1}	1	1	2	3	6	11	23
C_n	1	2	5	14	42	132	429
D_n	1	3	15	105	945	10395	135135
\hat{C}_n	2	12	120	1680	30240	665280	17297280

Table 3: The first terms of the four integer sequences of Table 1 arranged according to their rate of grow. B_{n+1} are Wedderburn–Etherington numbers; C_n are Catalan numbers; D_n are double factorial numbers; \hat{C}_n are quadruple factorial numbers

A2. Twist-Rotation and Rotation graphs

Here we explain –keeping on using extensively graph–theoretical tools as in [13], [22]– the construction underlying the discrete computational space of the spin network simulator discussed in Section 4.1. For simplicity we do not change the notation used there, although many definitions and results can be applied also to larger classes of graphs (the so-called “distance graphs” see [57]).

Given a rooted binary tree T on $(n + 1)$ labeled leaves ($n \geq 2$), two kinds of topological operations (moves) can be considered, namely rotations and twists (“rotation” is not to be confused with rotation matrices or operators used in Sections 3.2, 4.1 and Appendices B). These moves represent

alterations in the shape of the tree generated around either an internal node (rotation) or a node which is not a leaf (twist) and all trees in a given class can be reached on applying admissible moves to an arbitrary tree chosen in that class (roughly speaking the moves are "ergodic").

Rotations around non-root internal nodes consist in swapping subtrees or nodes as shown in Fig. 19. In the upper region there appears on the left a generic (portion of a) tree T with subtrees A, B, C and a fourth subtree R containing the root: the rotation around the node x transforms T into T' and, conversely, the rotation around $x' \in T'$ changes back T' into T . In the lower region a rotation on a particular tree is shown, together with its inverse operation.

Figure 19

Since there are $(n - 1)$ internal nodes, $(n - 1)$ different rotations can be performed on any tree (with fixed labelings on its leaves). Note that a rotation alters the shape of the tree near the corresponding node but leaves the rest of its structure intact.

Twists around non terminal nodes consist in exchanging left and right subtrees (or nodes). We draw in Fig. 20 both a general twist around a node $x \in T$ and a particular twist on a specific tree.

Figure 20

There are n possible twists on a rooted labeled tree on $(n + 1)$ leaves and these transformations may alterate the global shape of the tree.

Coming back to combinatorics of labeled rooted binary trees (see Table 2), we realize that every category may support rotations but only "plane" trees (enumerated by the quadruple factorial \hat{C}_n) admit twists. For what concerns labeled Catalan trees in Fig. 16 (bottom) we see that they are actually connected by the rotation represented in Fig. 19, but no twist is allowed since the sequence of labels must be kept fixed. Looking at Fig. 17, where plane trees labeled in all possible ways are shown, we see clearly that both rotations and twists appear as admissible moves connecting pairs. Finally, not plane trees (enumerated by the double factorial D_n and shown in Fig. 18) undergo only rotations since they do not distinguish between left and right at each non terminal node. The further step consists in building up new graphs associated with each of the above categories (these structures

are called "distance graphs" and the reason for such terminology will become clear in the next paragraph, where distances will be introduced). Denote generally such a graph by $\mathbf{G}_n(V, E)$ (as in Section 4.1), where V and E are the vertex and the edge sets, respectively. The vertices are in one-to-one correspondence with rooted binary trees on $(n + 1)$ labeled leaves, namely

$$T^{(n)} \longleftrightarrow v \in V, \quad (118)$$

where $T^{(n)}$ stands for a tree in a given class. The edge set E is generated by linking pairs of vertices $v, v' \in V$ by an undirected edge $e(v, v')$ if, and only if, the corresponding trees are related to each other either by a rotation or by a twist. Formally

$$e(v, v') \in E \iff T_v^{(n)} \leftrightarrow T_{v'}^{(n)}, \quad (119)$$

where \leftrightarrow stands for one of the topological moves described above. According to the remarks on admissible moves acting in different categories of trees we specialise $\mathbf{G}_n(V, E)$ as follows.

• **Labeled plane trees** on $(n + 1)$ leaves represent the vertex set of the Twist-Rotation graph $\mathbf{G}_n^{TR}(V, E)$ denoted as in (37), namely

$$\mathbf{G}_n^{TR}(V, E) \doteq \hat{\mathfrak{G}}_n(V, E).$$

Its cardinality is the quadruple factorial number given in (115)

$$\text{card}(\hat{\mathfrak{G}}_n(V, E)) \doteq |V| = \hat{C}_n \quad (120)$$

and each edge represents either a rotation or a twist (*cfr.* also (38)).

For any $n \geq 2$ $\hat{\mathfrak{G}}_n(V, E)$ is an undirected regular cubic graph (namely there is no ordering on its vertices and each vertex has valence three). It is also a planar graph, *i.e.* it can be drawn onto the 2-dimensional sphere without crossings. For $n = 2$ $\text{card}(\hat{\mathfrak{G}}_2) = 12$ (*cfr.* the trees in Fig. 17) and $\hat{\mathfrak{G}}_2$ has the shape of a truncated tetrahedron made up of triangular and hexagonal faces. $\hat{\mathfrak{G}}_3$ has cardinality 120 and represents the graph of a 3-valent polyhedron made up of pentagons and hexagons. A portion of this graph is shown in Fig. 21 (reprinted from [27]) and its shape looks quite familiar since the discover of fullerene.

Figure 21

• **Labeled not plane trees** on $(n + 1)$ leaves represent the vertex set of the Rotation graph $\mathbf{G}_n^R(V, E)$ denoted as in (39), namely

$$\mathbf{G}_n^R(V, E) \doteq \mathfrak{G}_n(V, E).$$

Its cardinality is the quadruple factorial number given in (116)

$$\text{card}(\mathfrak{G}_n(V, E)) \doteq |V| = D_n \quad (121)$$

and each edge represents a rotation (*cfr.* also (40)). For any $n \geq 2$, $\mathfrak{G}_n(V, E)$ is an undirected regular graph of valence $2(n - 1)$ which turns out to be not planar for $n \geq 3$.

The graph \mathfrak{G}_2 with cardinality 3 shown in Fig. 22 is a trivial example from the combinatorial point of view but – by exploiting the encoding map (78) – we see that it shares the same content as the "triangular" Racah algebraic identity (47) introduced in Section 4.1.

Figure 22

The graph \mathfrak{G}_3 (whose vertices are trees on 4 leaves) is depicted in Fig. 1 of Section 4.1: from a topological point of view we see that some vertices have been doubled to avoid crossings; when we identify by an antipodal mapping opposite vertices and edges we realize that this graph lies in the real projective space \mathbb{RP}^2 (namely it is not planar). Other pictures of \mathfrak{G}_3 can be found in [22] and [23]. In Fig. 23 one of the pentagons belonging to both \mathfrak{G}_3 in Fig. 1 and $\hat{\mathfrak{G}}_3$ in Fig. 21 is depicted: edges represent rotations from a topological point of view and at the same time the figure is the diagram encoding through (78) the Biedenharn–Elliot (pentagon) identity (46).

Figure 23

• **Labeled Catalan trees** on $(n + 1)$ leaves represent the vertex set of the Rotation graph denoted by

$$\mathbf{G}_n^R(V, E) \doteq \mathfrak{g}_n(V, E) \quad (122)$$

to distinguish it from the previously defined \mathfrak{G}_n . $\mathfrak{g}_n(V, E)$ is a regular graph of valence $(n - 1)$ and its cardinality is given by the Catalan number (114), namely

$$\text{card}(\mathfrak{g}_n(V, E)) \doteq |V| = C_n. \quad (123)$$

Although this kind of Rotation graph is not suitable to model the computational space of the quantum simulator (Catalan coupling trees are not sufficiently general) we meet these structures in connection with issues on combinatorial complexity discussed in Section 4.3 and in the next paragraph.

A3. Combinatorial complexity

All graphs described in Section A2 are actually "distance graphs" [57] since they encode in their edge sets operations on the basic objects (trees) associated with their vertex sets. To evaluate quantitatively how far away pairs of rooted labeled binary trees are –and using standard terminology in discrete mathematics– we introduce explicitly Twist–Rotation and Rotation distances.

Given two binary trees $T_1^{(n)}, T_2^{(n)}$ –thought of as vertices in $\hat{\mathfrak{G}}_n, \mathfrak{G}_n, \mathfrak{g}_n$, respectively– their distance is the length of the shortest path joining them, namely the minimum number of topological operations needed to transform one tree into the other. With an obvious meaning of symbols we set

$$\begin{aligned} d^{TR}(T_1^{(n)}, T_2^{(n)}) &\doteq \min \{\text{lengths of paths } T_1^{(n)} \leftrightarrow T_2^{(n)} \text{ in } \hat{\mathfrak{G}}_n\} \\ d^R(T_1^{(n)}, T_2^{(n)}) &\doteq \min \{\text{lengths of paths } T_1^{(n)} \leftrightarrow T_2^{(n)} \text{ in } \mathfrak{G}_n\} \\ d^r(T_1^{(n)}, T_2^{(n)}) &\doteq \min \{\text{lengths of paths } T_1^{(n)} \leftrightarrow T_2^{(n)} \text{ in } \mathfrak{g}_n\}. \end{aligned} \quad (124)$$

The diameters of the above graphs are naturally defined in terms of distances according to

$$\begin{aligned} \text{Diam}(\hat{\mathfrak{G}}_n) &= \max \{d^{TR}(T_1^{(n)}, T_2^{(n)}) \mid T_1^{(n)}, T_2^{(n)} \in \hat{\mathfrak{G}}_n\} \\ \text{Diam}(\mathfrak{G}_n) &= \max \{d^R(T_1^{(n)}, T_2^{(n)}) \mid T_1^{(n)}, T_2^{(n)} \in \mathfrak{G}_n\} \\ \text{Diam}(\mathfrak{g}_n) &= \max \{d^r(T_1^{(n)}, T_2^{(n)}) \mid T_1^{(n)}, T_2^{(n)} \in \mathfrak{g}_n\}. \end{aligned} \quad (125)$$

In addressing combinatorial complexity we are primarily interested in computing or estimating such distance functions and diameters since in Section 4.3 we relate combinatorial complexity to computational complexity of the spin network simulator on the basis of the quantum encoding maps introduced in (76) and (78). In this respect it may be useful to collect here some known results from graph theory (addressed in a classical computational complexity framework).

- For what concerns Catalan trees equipped with rotation distance d^r , a major breakthrough was achieved in [58], where the authors proved the existence of a tight bound on the diameter of \mathfrak{g}_n given by

$$\text{Diam}(\mathfrak{g}_n) < 2n - 8 \quad (126)$$

for trees on $(n + 1)$ terminal nodes. Their elegant proof relies on the translation of the combinatorial problem for trees into an equivalent geometrical one, namely enumerating triangulations of a polygon with $(n + 1)$ edges and finding the maximum number of diagonal flips needed to convert one triangulation into another (diagonal flips are topological moves on 2-dimensional triangulations which transform a quadrilateral dissected into two triangles into the configuration generated by cutting along the other diagonal). The argument to get the final result involves the construction of 3-dimensional hyperbolic polyhedra and calls into play volume estimates in hyperbolic geometry.

- In [23], purely combinatorial counting tools used previously in [59] are improved to establish lower and upper bounds for the diameter of the Rotation graph \mathfrak{G}_n . The explicit form of the upper bound is ($\lg = \log_2$)

$$\text{Diam}(\mathfrak{G}_n) < n \lg(n) + n - 2 \lg(n) + 1 \quad (127)$$

which is compatible with older estimates (see *e.g.* [60]). Therefore we may conclude that the diameter of \mathfrak{G}_n grows no faster than polynomially in n , namely

$$\text{Diam}(\mathfrak{G}_n) \lesssim n \lg(n) + O(n). \quad (128)$$

- A crucial open question remains the complexity status of computing the rotation distance even for the simplest case of d^r on the graph \mathfrak{g}_n made up by unlabeled Catalan trees (binary search trees in computer science language). In particular (*cfr.* the recent papers [61], [62]) it is not known

- whether the problem is **NP**-complete;
- whether d^r can be determined in time polynomial in n (that is to say, whether there exists an efficient algorithm to compute it exactly).

There are however (classical) polynomial time algorithms which estimate this distance (or its lower/upper bounds) ([61], [63]).

- The two remarks above hold for the rotation distance d^R too, since \mathfrak{G}_n is much bigger than \mathfrak{g}_n : more precisely, if we think about "labeled" Catalan trees (as pointed out in Remark A.2, Appendix A1) then \mathfrak{g}_n is actually a subgraph of \mathfrak{G}_n . To our knowledge there is no algorithm for computing d^R in \mathfrak{G}_n , although we may consider lower and upper bounds on $\text{Diam}(\mathfrak{G}_n)$ [23] (which are both of order $n \lg(n)$) as an estimate of the number of elementary operations –Racah transforms– appearing in an "optimal" expansion of a $3nj$ symbol. (Note however that such optimal expansion does exist only if we could actually computing $d^R(T_1^{(n)}, T_2^{(n)})$ for arbitrary $T_1^{(n)}, T_2^{(n)} \in \mathfrak{G}_n$)

- In order to try to overcome the difficulties outlined above, a basic strategy emerges in current literature, namely the idea of introducing in \mathfrak{g}_n some more specific notion of distance function. In [64] a "restricted" rotation distance has been considered, and linear lower and upper bounds are estimated in terms of the number of interior nodes of trees. In [62] a "right-arm" rotation distance is shown to be computable by an efficient algorithm (in polynomial time $O(n^2)$ for trees on $(n + 1)$ leaves).

- In the field of molecular biology, phylogenetic trees (or dendograms) for groups of species turn out to be powerful tools to address the study of similarities and dissimilarities appearing in biological evolution (see *e.g.* [65] and references therein). Theoretical biologists use different kinds of definitions with respect to our previous classifications from discrete mathematics. In particular, their rooted binary phylogenetic trees may have labels only on leaves (the different species) while the role of internal nodes is secondary. The distance function which is commonly used in this context is the "nearest neighbour interchange" (nni) distance which is surely more restrictive than the rotation distances introduced in (124), although it is not so easy to establish connections with the restricted rotation distances considered in our previous remark. The authors of [65] claim to have proved the fact that computing the nni distance is **NP**-complete (both in the unlabeled and in the labeled cases) by a reduction from Exact Cover by 3-sets) (X3C) which is known to be an **NP**-complete problem [47].

Appendix B

B1. Composition of W–rotation matrices

In this Appendix, following the standard reference [14], we illustrate the derivation of the symbolic expression given in (29) which represents –in the language of quantum theory of angular momenta– the generalised Clebsch–Gordan expansion involving a finite number of W–rotation matrices with the same arguments.

Denote as usual by

$$\begin{aligned} &\mathbf{J}_1, \mathbf{J}_2, \mathbf{J}_3, \dots, \mathbf{J}_N; \\ &j_1, j_2, j_3, \dots, j_N, \\ &m_1, m_2, m_3, \dots, m_N, \\ &m'_1, m'_2, m'_3, \dots, m'_N \end{aligned} \tag{129}$$

an set of N commuting angular momentum operators and the corresponding sets of quantum numbers.

Consider the operators

$$\mathcal{K}_i \doteq \mathbf{J}_1 + \mathbf{J}_2 + \mathbf{J}_3 + \dots + \mathbf{J}_i \tag{130}$$

which are defined, for each $1 \leq i \leq N$, by taking any kind of binary coupling consistent with this vector addition rules. We use here \mathcal{K} 's instead of \mathbf{K} 's used in Section 2 to stress the fact that we can choose *anyone* of the schemes considered there (note that in (130) there appear also $\mathcal{K}_1 \equiv \mathbf{J}_1$ and $\mathcal{K}_N \equiv \mathbf{J}$, so that the counting of intermediate operators is not in contradiction with previous statements). The quantum numbers of these operators are denoted by

$$\kappa_1, \kappa_2, \kappa_3, \dots, \kappa_N, \tag{131}$$

while (two possible sets of) magnetic quantum numbers are given by

$$\begin{aligned} M_i &= m_1 + m_2 + m_3 + \dots + m_i \\ M'_i &= m'_1 + m'_2 + m'_3 + \dots + m'_i. \end{aligned} \tag{132}$$

Coming to the composition of W-matrices, we start by considering the Clebsch–Gordan series, namely the expansion of the product of two W-matrices (with the same arguments) labeled by j_1 and j_2 . It reads

$$D_{m_1 m'_1}^{j_1}(\alpha\beta\gamma) D_{m_2 m'_2}^{j_2}(\alpha\beta\gamma) = \sum_{J=|j_1-j_2|}^{j_1+j_2} \sum_{M M'} C_{j_1 m_1 j_2 m_2}^{J M} D_{M M'}^J(\alpha\beta\gamma) C_{j_1 m'_1 j_2 m'_2}^{J M}, \quad (133)$$

where we denote simply by \mathbf{J} the sum $\mathbf{J}_1 + \mathbf{J}_2$ and by J, M, M' the corresponding quantum numbers (leaving aside for the moment the notations introduced in (130), (131) and (132)). By using the orthogonality condition of the Clebsch–Gordan coefficients C_{\dots}^{\dots} we can invert (133) to get

$$D_{M M'}^J(\alpha\beta\gamma) = \sum_{\substack{m_1 m_2 \\ m'_1 m'_2}} C_{j_1 m_1 j_2 m_2}^{J M} D_{m_1 m'_1}^{j_1}(\alpha\beta\gamma) D_{m_2 m'_2}^{j_2}(\alpha\beta\gamma) C_{j_1 m'_1 j_2 m'_2}^{J M}, \quad (134)$$

where the j 's entries of each Clebsch–Gordan coefficient must fulfill the triangular inequality (here in particular we have just to require $|j_1 - j_2| \leq J \leq j_1 + j_2$).

The decomposition established above represents the starting point to address the more general case of $N > 2$ incoming angular momenta. By fully restoring the notations explained at the beginning of this section and applying successively (134) together with the orthogonality conditions whenever necessary, we get the *generalised* C–G expansion involving the product of N W-rotation matrices. Its explicit expression reads

$$D_{M_N M'_N}^{\kappa_N}(\alpha\beta\gamma) = \sum_{\substack{m_1 \dots m_N \\ m'_1 \dots m'_N}} \prod_{i=1}^N C_{\kappa_{i-1} M_{i-1} j_i m_i}^{\kappa_i M_i} D_{m_i m'_i}^{j_i}(\alpha\beta\gamma) C_{\kappa_{i-1} M'_{i-1} j_i m'_i}^{\kappa_i M'_i}, \quad (135)$$

where it has been assumed $\kappa_0 = M_0 = M'_0 = 0$ and all the triads $\{j_i, \kappa_{i-1}, \kappa_i\}$ satisfy triangular inequalities.

We may recast the previous expansion in a symbolic form (*cfr.* (29) in Section 3.2) by keeping only the dimensions of representations both in D 's and C 's (the typographical changes are introduced to remind that these objects are matrices)

$$\begin{aligned} \mathbf{D}^J(\alpha\beta\gamma) = \\ \sum_{\{m, m'\}} \prod_{i=1}^N \left(\mathbf{C}_{\kappa_{i-1} j_i}^{\kappa_i} \mathbf{D}^{j_i}(\alpha\beta\gamma) \mathbf{C}_{\kappa_{i-1} j_i}^{\kappa_i} \right). \end{aligned} \quad (136)$$

Here we set

$$\begin{aligned} \mathbf{J} &\doteq \mathbf{\kappa}_N \equiv \mathbf{J}_1 + \mathbf{J}_2 + \mathbf{J}_3 + \cdots + \mathbf{J}_N; \\ J &\doteq \kappa_N \end{aligned} \quad (137)$$

to comply with the notation used in the main text and in the particular case (133) (consequently the matrix indices of $\mathbf{D}^J(\alpha\beta\gamma)$ are intended to be $M = m_1 + m_2 + m_3 + \cdots + m_N$; $M' = m'_1 + m'_2 + m'_3 + \cdots + m'_N$). The summation over the magnetic numbers of the incoming \mathbf{J} 's which appears in front of (135) (or (136)) is a partial trace on the N -product of triples contained in round parenthesis: any such triple combination can be directly evaluated by substituting the numerical values of the "elementary" W-matrices and of the suitable pair of C-G coefficients.

The structure displayed in (135) is drastically simplified if we look at two particular cases.

• **Fermionic case** (N spins $= \frac{1}{2}$ in the symmetric multiplet)

For

$$j_1 = j_2 = j_3 = \cdots = j_N = 1/2$$

and

$$\kappa_{i+1} = \kappa_i + 1/2 \quad (\Rightarrow J \equiv \kappa_N = N/2)$$

the expansion (135) becomes

$$\Delta \cdot D_{M M'}^J (\alpha \beta \gamma) = \sum_{\substack{m_1 + \dots + m_N = M \\ m'_1 + \dots + m'_N = M'}} \prod_{i=1}^N D_{m_i m'_i}^{\frac{1}{2}} (\alpha \beta \gamma) \quad (138)$$

where the weight Δ is given by

$$\sqrt{(J+M)!(J-M)!(J+M')!(J-M')!} / (2J)! \quad (139)$$

and each factor $D_{m m'}^{\frac{1}{2}}$ represents the W-matrix in the fundamental representation written in terms of the Euler angles $\alpha \beta \gamma$, namely

$$D_{m m'}^{\frac{1}{2}} (\alpha \beta \gamma) = \begin{pmatrix} e^{-i\alpha/2} \cos(\beta/2) e^{-i\gamma/2} & -e^{-i\alpha/2} \sin(\beta/2) e^{i\gamma/2} \\ e^{i\alpha/2} \sin(\beta/2) e^{-i\gamma/2} & e^{i\alpha/2} \cos(\beta/2) e^{i\gamma/2} \end{pmatrix}. \quad (140)$$

• **Bosonic case** (N spins = 1 in the symmetric multiplet)

For

$$j_1 = j_2 = j_3 = \dots = j_N = 1$$

and

$$\kappa_{i+1} = \kappa_i + 1 \quad (\Rightarrow J \equiv \kappa_N = N)$$

the expansion (135) becomes

$$\Delta \cdot D_{M M'}^J (\alpha \beta \gamma) = \sum_{\substack{m_1 + \dots + m_N = M \\ m'_1 + \dots + m'_N = M'}} \prod_{i=1}^N \sqrt{(1 + \delta_{m_i 0})(1 + \delta_{m'_i 0})} D_{m_i m'_i}^1 (\alpha \beta \gamma), \quad (141)$$

where Δ is given in (139) and each factor $D_{m m'}^1$ represents the W-matrix in the $j = 1$ representation written in terms of the Euler angles $\alpha \beta \gamma$, namely

$$D_{M M'}^1 (\alpha \beta \gamma) = e^{-iM\alpha} d_{M M'}^1 (\beta) e^{-iM'\gamma} \quad (142)$$

with

$$d_{M M'}^1(\beta) = \begin{pmatrix} \frac{1+\cos\beta}{2} & -\frac{\sin\beta}{\sqrt{2}} & \frac{1-\cos\beta}{2} \\ \frac{\sin\beta}{\sqrt{2}} & \cos\beta & -\frac{\sin\beta}{\sqrt{2}} \\ \frac{1-\cos\beta}{2} & \frac{\sin\beta}{\sqrt{2}} & \frac{1+\cos\beta}{2} \end{pmatrix}. \quad (143)$$

Remark B.1. Equations (138) and (141) turn out to be useful for evaluating in practice matrix elements of W -rotations acting on irreducible representation spaces. Notice in particular that matrix elements (141) can be actually obtained by considering the symmetric combination of two spins $= 1/2$, namely by exploiting (138) with $N = 2$. More generally, any $(2j_i + 1) \times (2j_i + 1)$ W -matrix (as those appearing in (135)) acts on a representation space which is irreducible under the action of $SU(2)$ and (according to Majorana splitting [66]) such eigenspace may be always viewed as a completely symmetric multiplet generated by $2j_i \frac{1}{2}$ spin kinematically independent "particles". By taking advantage of this remark we may factorize each $D_{m_i m'_i}^{j_i}$ in terms of (140), as discussed in relation with the estimate given in (31). \blacktriangle

B2. U -rotation matrices

In this appendix we collect from [14] some useful definitions and examples concerning rotation matrices expressed in terms of the direction of the rotation axis and of the rotation angles, namely alternative forms for the M -gates introduced in Section 3.2.

Let $\mathbf{n}(\Theta, \Phi)$ a unit vector in the direction of the rotation axis and ω the rotation angle. An element of an U -matrix is defined according to

$$U_{MM'}^J(\omega; \Theta, \Phi) \doteq \langle JM | \exp\{-i\omega \mathbf{n} \cdot \mathbf{J}\} | JM' \rangle \quad (144)$$

in a representation space labeled by the quantum numbers J, M . The W -rotation matrices introduced in (25) are related to (144) by

$$U_{MM'}^J(\omega; \Theta, \Phi) = \sum_{M''} D_{MM''}^J(\Phi, \Theta, -\Phi) e^{-iM''\omega} D_{M''M'}^J(\Phi, -\Theta, -\Phi). \quad (145)$$

For rotations around coordinate axes we find the expressions (the reduced W -matrices $d_{MM'}^J$ were introduced in (26) and given explicitly in (140) and (143) of Appendix B1 for $J = \frac{1}{2}, 1$).

- (x axis; $\Theta = \frac{\pi}{2}$; $\Phi = 0$):

$$U_{MM'}^J(\omega; \frac{\pi}{2}, 0) = D_{MM'}^J(\frac{\pi}{2}, \omega, -\frac{\pi}{2}) = (-i)^{M-M'} d_{MM'}^J(\omega) \quad (146)$$

- (y axis; $\Theta = \frac{\pi}{2}$; $\Phi = \frac{\pi}{2}$):

$$U_{MM'}^J(\omega; \frac{\pi}{2}, \frac{\pi}{2}) = D_{MM'}^J(0, \omega, 0) = d_{MM'}^J(\omega) \quad (147)$$

- (z axis; $\Theta = 0$):

$$U_{MM'}^J(\omega; 0, \Phi) = D_{MM'}^J(0, \omega, 0) = \delta_{MM'} e^{-iM\omega} \quad (148)$$

Acknowledgements

We are pleased to thank Vincenzo Aquilanti, Mauro Carfora, Silvano Garnerone and Tullio Regge for interesting discussions. We are in debt with M. Carfora also for his unexhaustible enthusiasm in helping us with the preparation of all figures, and with V. Aquilanti and C. Coletti for the permission to reproduce Fig. 21 from [27].

References

- [1] For reviews, see A. Steane, Rep. Prog. Phys. 61 (1998) 117; Yu.I. Manin, Classical computing, quantum computing, and Shor's factoring algorithm, Preprint `quant-ph/9903008`; D.P. DiVincenzo, C. Bennett, Nature 404 (2000) 247.
- [2] R. Jozsa, Entanglement and Quantum Computation, Preprint `quant-ph/9707034`;
- [3] A. Kitaev, Annals Phys. 303 (2003) 2.
- [4] M.H. Freedman, A. Kitaev, Z. Wang, Commun. Math. Phys. 227 (2002) 587; M.H. Freedman, M. Larsen, Z. Wang, Commun. Math. Phys. 227 (2002) 605; M.H. Freedman, A. Kitaev, M. Larsen, Z. Wang, Bull. Amer. Math. Soc. 40 (2002) 31.
- [5] A. Ekert, M. Ericsson, P. Hayden, H. Iwanami, J.A. Jones D.K.L. Oi, V. Vedral, J. Mod. Opt. 47 (2000) 2501; J.A. Jones, V. Vedral, A. Ekert, G. Castagnoli, Nature 403 (2000) 869.
- [6] S. Lloyd, Quantum Computation with Abelian Anyons, Preprint `quant-ph/0004010`.
- [7] E. Dennis, A.Yu. Kitaev, A. Landahl, J. Preskill, J. Math. Phys. 43 (2002) 4452.
- [8] S.B. Bravyi, A.Yu. Kitaev, Fermionic Quantum Computation, Preprint `quant-ph/0003137`.
- [9] P. Zanardi, M. Rasetti, Phys. Lett. A 264 (1999) 94.
- [10] J. Pachos, P. Zanardi, M. Rasetti, Phys. Rev. A 61 (2000) 010305(R).
- [11] A. Marzulli, M. Rasetti, Phys. Lett. A 306 (2002) 79.
- [12] A.P. Yutsis, I.B. Levinson, V.V. Vanagas, The Mathematical Apparatus of the Theory of Angular Momentum, Israel Program for Sci. Transl. Ltd., Jerusalem 1962.

- [13] L.C. Biedenharn and J.D. Louck, The Racah–Wigner Algebra in Quantum Theory, Encyclopedia of Mathematics and its Applications Vol 9, G–C. Rota Ed. Addison–Wesley Publ. Co. Reading MA 1981
Topic 9. Physical Interpretation and Asymptotic (Classical) Limits of the Angular Momentum Functions;
Topic 12. Coupling of N Angular Momenta: Recoupling Theory.
- [14] D.A. Varshalovich, A.N. Moskalev, V.K. Khersonskii, Quantum theory of Angular Momentum, World Scientific, Singapore, 1988.
- [15] R.P. Feynman, Int. J. of Theor. Phys. 21 (1982) 467.
- [16] R. Penrose, Angular Momentum: an approach to combinatorial space–time, in: T. Bastin (Ed.), Quantum Theory and Beyond, Cambridge Univ. Press, 1971, p.151.
- [17] S. Garnerone, A. Marzuoli, M. Rasetti, in preparation.
- [18] G. Ponzano, T. Regge, Semiclassical Limit of Racah coefficients, in: F. Bloch et al (Eds.), Spectroscopic and Group Theoretical Methods in Physics, North–Holland, Amsterdam, 1968, p. 1.
- [19] L.C. Biedenharn and J.D. Louck, Angular Momentum in Quantum Physics, Theory and Applications, Encyclopedia of Mathematics and its Applications Vol 8, G–C. Rota Ed. Addison–Wesley Publ. Co. Reading MA 1981.
- [20] T. Regge, Nuovo Cimento 19 (1961) 558.
- [21] J. Kempe, D. Bacon, D.A. Lidar, K.B. Whaley, Phys. Rev. A 63 (2001) 042307.
- [22] V. Fack, S. Lievens, J. Van der Jeugt, Comp. Phys. Comm. 119 (1999) 99.
- [23] V. Fack, S. Lievens, J. Van der Jeugt, Discr. Math. 245 (2002) 1.
- [24] A. Barenco, C.H. Bennett, R. Cleve, D.P. DiVincenzo, N. Margolus, P. Shor, T. Sleator, J. Smolin, H. Weinfurter, Phys. Rev. A 52 (1995) 3457.
- [25] E. Bernstein, U. Vazirani, SIAM J. on Comput. 26 (1997) 1411.

- [26] C. Moore, J. P. Crutchfield, *Theor. Comp. Sc.* 237 (200) 275.
- [27] V. Aquilanti, C. Coletti, *Chem. Phys. Lett.* 344 (2001) 601.
- [28] R. Askey, *Orthogonal Polynomials and Special Functions*, Society for Industrial and Applied Mathematics, Philadelphia PE 1975.
- [29] A. Marzuoli, M. Rasetti, Spin network setting of topological quantum computation, Preprint [quant-ph/0407119](#).
- [30] S. Lloyd, *Science* 273 (1996) 1073.
- [31] R.P. Stanley, *Enumerative Combinatorics Vol 2*, Cambridge University Press, Cambridge 1999.
- [32] L.H. Kauffman, *Knots and Physics*, World Scientific, Singapore 1991.
- [33] J. Ambjorn, B. Durhuus, T. Jonsson, *Quantum Geometry*, Cambridge University Press, Cambridge 1997.
- [34] T. Regge, R.M. Williams, *J. Math. Phys.* 41 (2000) 3964.
- [35] G. Carbone, M. Carfora, A. Marzuoli, *Nucl. Phys.* B595 (2001) 654.
- [36] V. Aquilanti, private communication.
- [37] V.G. Turaev, O.Ya. Viro, *Topology* 31 (1992) 865.
- [38] V.G. Turaev, *Quantum Invariants of Knots and 3-Manifolds*, Walter de Gruyter Berlin 1994.
- [39] S. Carlip, *Quantum Gravity in 2+1 Dimensions*, Cambridge University Press, Cambridge 1998.
- [40] D. Birmingham, M. Blau, M. Rakowski, G. Thompson, *Phys. Rep.* 209 (1991) 129.
- [41] M.F. Atiyah, *Publ.Math. Inst. Hautes Etudes Sci.* 68 (1989) 175.
- [42] F. Quinn, *Lectures on Axiomatic Topological Quantum Field Theories*, in: D.S. Freed et al (Eds) *Geometry and Quantum Field Theories*, IAS/Park City Math. Series Vol 1, Amer. Math. Soc. 1995.

- [43] V. Jones, *Bull. Am. Math. Soc.* 12 (1985) 103.
- [44] E. Witten, *Commun. Math. Phys.* 121 (1989) 351.
- [45] D. Beckman, D. Gottesman, A.Yu. Kitaev, J. Preskill, *Phys.Rev. D* 65 (2002) 065022.
- [46] F. Jaeger, D. Vertigen, D. Welsh, *Math. Proc. Cambridge Philos. Soc.* 108 (1990) 35.
- [47] M.R. Garey, D.S. Johnson, *Computers and Intractability, A Guide to the Theory of NP-completeness* W.H. Freeman and Co., New York 1979.
- [48] D. Deutsch, A. Barenco, A. Ekert, *Proc. R. Soc. London A* 449 (1995) 669; D.P. Di Vincenzo, *Phys. Rev. A* 50 (1995) 1015.
- [49] F. Wilczek, A. Zee., *Phys. Rev. Lett.* 52 (1984) 2111.
- [50] T.T. Wu and C. N. Yang, *Phys. Rev. D* 12 (1975) 3845; R. Jackiw, in: *Relativity Groups and Topology*, Les Houches 1983, 154pp, B.S. DeWitt, R. Stora (Eds.) North-Holland 1984.
- [51] M. Nakahara, *Geometry, Topology and Physics*, IOP Publishing Ltd. 1990.
- [52] J. Preskill, Fault-tolerant quantum computation, in: *Introduction to quantum computation and information*, Hoi-Kwong Lo, S. Popescu, T. Spiller Eds. World Scientific, Singapore, 1999.
- [53] L.H. Kauffman, S.J. Lomonaco, Braiding operators are universal quantum gates, Preprint **quant-ph/0401090**.
- [54] J. Fuchs and C. Schweigert, *Symmetries, Lie Algebras and Representations*, Cambridge University Press, Cambridge 1997.
- [55] Ya.A. Smorodinskii, L.A. Shelepin, *Sov. Phys. Usp.* 15 (1972) 1.
- [56] On-Line Encyclopedia of Integer Sequences, at <http://www.research.att.com/~njas/sequences/>
- [57] F. Buckley, F. Harari, *Distance in Graphs*, Addison-Wesley, Reading MA, 1990.

- [58] D.D. Sleator, R.E. Tarjan, W.P. Thurston, J. Amer. Math. Soc. 1 (1988) 647.
- [59] M. Li, J. Tromp, L. Zhang, J. Theor. Biol. 182 (1996) 463.
- [60] D. Robinson, J. Combin. Theory 11 (1971) 105; K. Culik, D. Wood, Inform. Process. Lett. 15 (1982) 39.
- [61] J.M. Pallo, Inform. Process. Lett. 73 (2000) 87.
- [62] J.M. Pallo, Inform. Process. Lett. 87 (2003) 173.
- [63] R.O. Rogers, R.D. Dutton, Congr. Numer. 120 (1996) 103.
- [64] S. Cleary, Inform. Process. Lett. 84 (2002) 333; S. Cleary, J. Tabak, Inform. Process. Lett. 88 (2003) 251.
- [65] B. DasGupta, X. He, T. Jiang, M. Li, J. Tromp, L. Zhang, in DIMACS Series in Discr. Math. and Theor. Comp. Science Vol. 55, Amer. Math. Soc. Providence (2000) 125.
- [66] E. Majorana, Nuovo Cimento 9 (1932) 43.

1

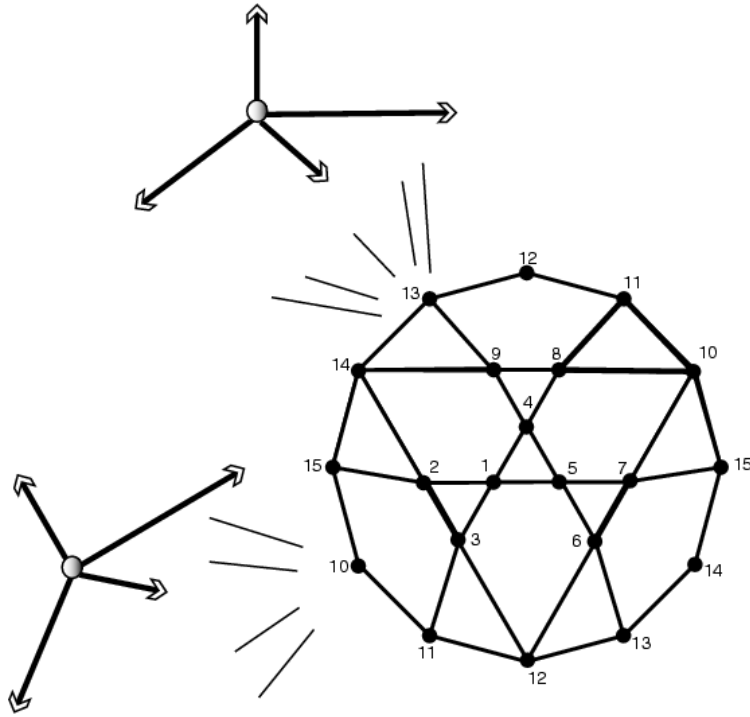


Figure 2: The computational setting based on the combinatorics of the Rotation graph $\mathfrak{G}_3(V, E)$ can be pictorially represented by blowing out each vertex into the corresponding computational Hilbert space and by looking at the gates as elementary operations on the base space and/or on the fiber (*cfr.* the remark at the end of this section and the analysis carried out in the next section).



Figure 3: Left: a marked 2-disk corresponding to the Hilbert space \mathcal{H}_{CS3} ($D^2, 3$ pts) with $\{a, b, c, d\} \in \{0, 1, 2, 3\}$. Right: the 2-disk supporting the topological qubit $V(D^2, 3$ pts).



Figure 4: Action of the braid group B_3 on the topological support of a single qubit.

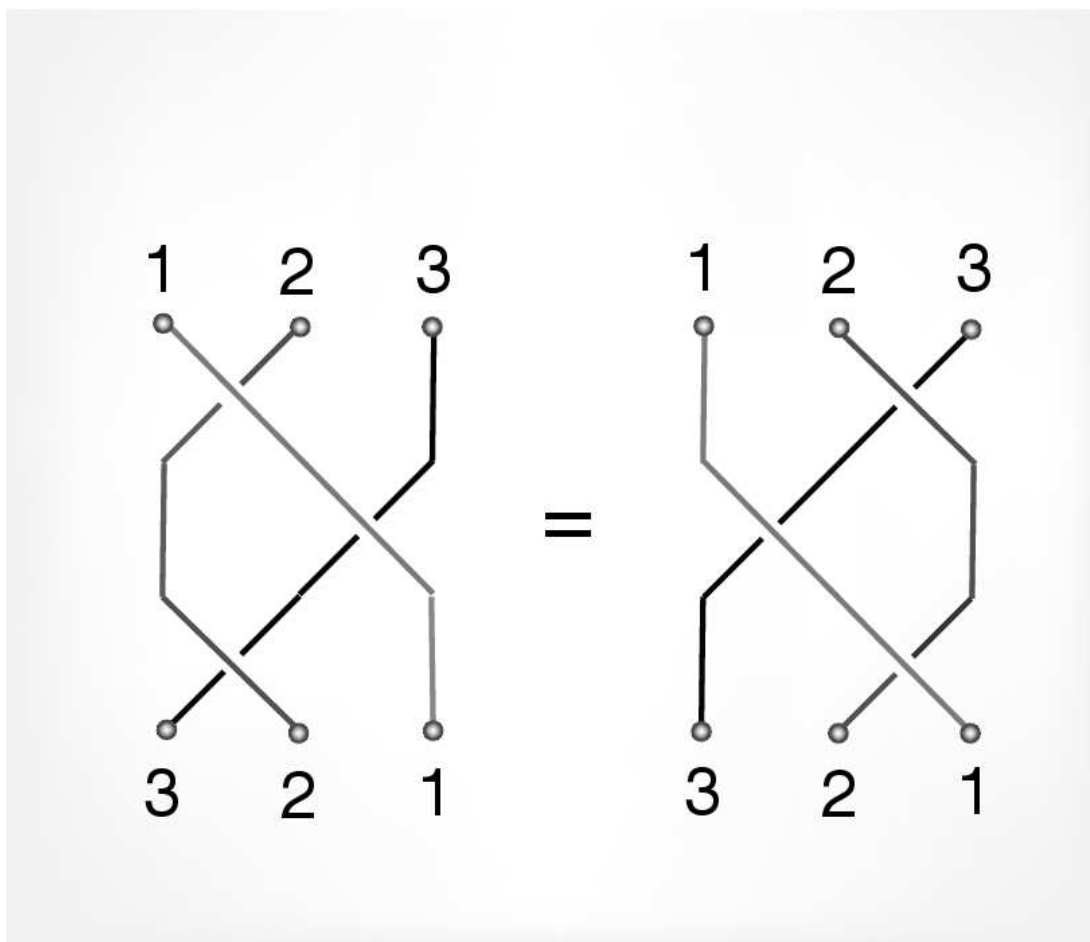


Figure 5: The Yang–Baxter equation $R_{12}R_{13}R_{23} = R_{23}R_{13}R_{12}$.

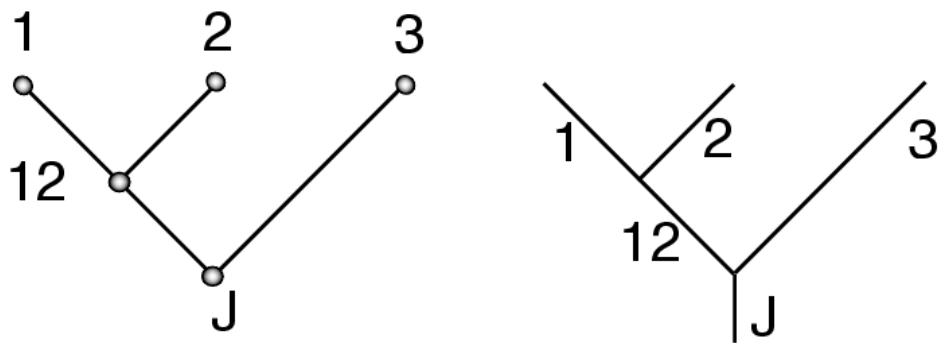


Figure 6: The fundamental tree T_{12} with labels on nodes (left) and the associated 3-valent graph t_{12} with labels on edges (right).

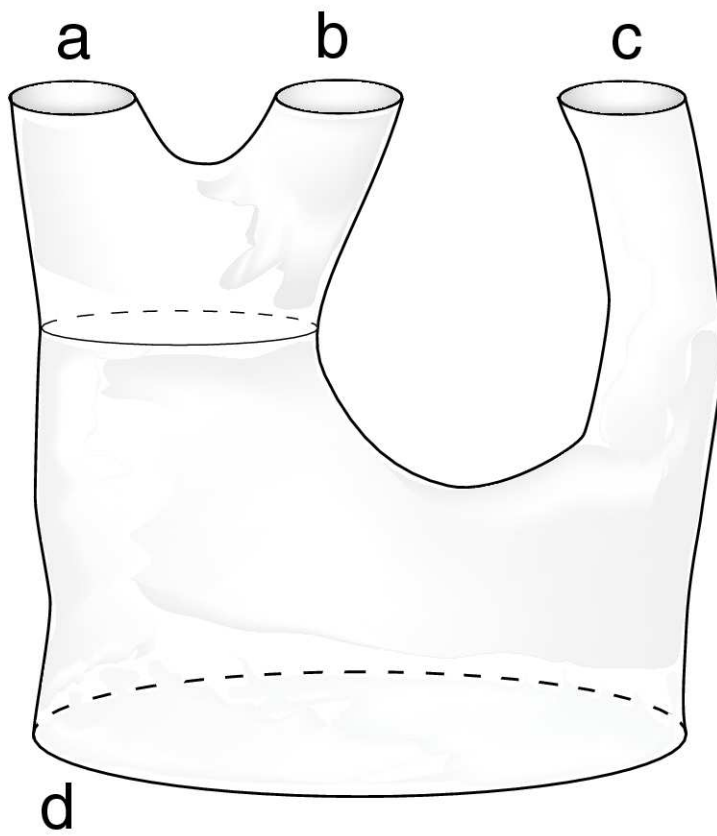


Figure 7: The punctured 2-sphere (S^2 ; a, b, c, d) with labels on the boundary circles.

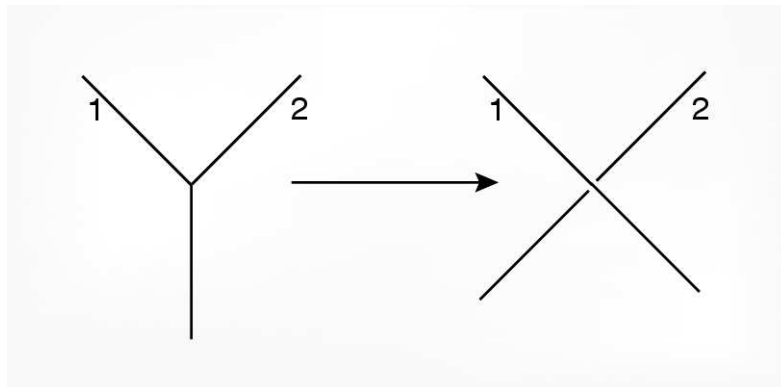


Figure 8: An interacting 3-valent vertex with two incoming edges is splitted by requiring that the first entry in the binary coupling overcrosses the second entry (and viceversa).

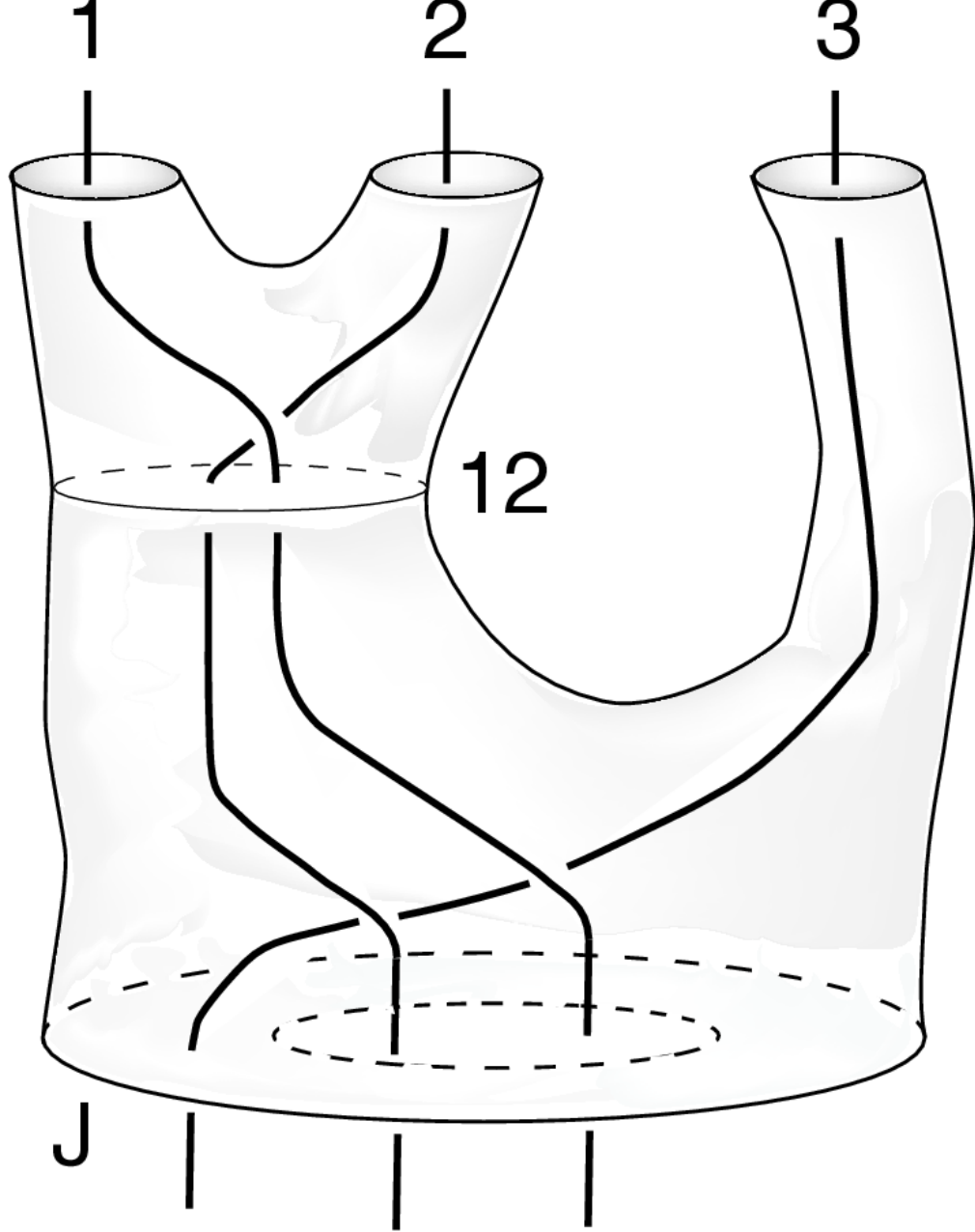


Figure 9: An embedding of the fundamental graph t_{12} into $(D^3, S^2)_{(a,b,c,d)}$ where we drop out the labels (a,b,c,d) on the boundary circles which appeared in Fig.7.

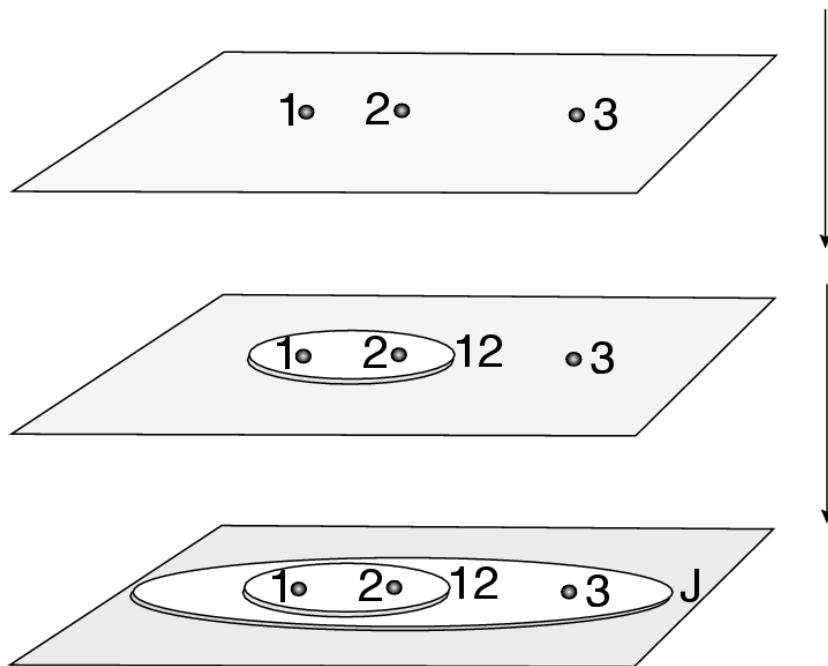


Figure 10: The level set (“time slicing”) of the configuration of Fig.9.

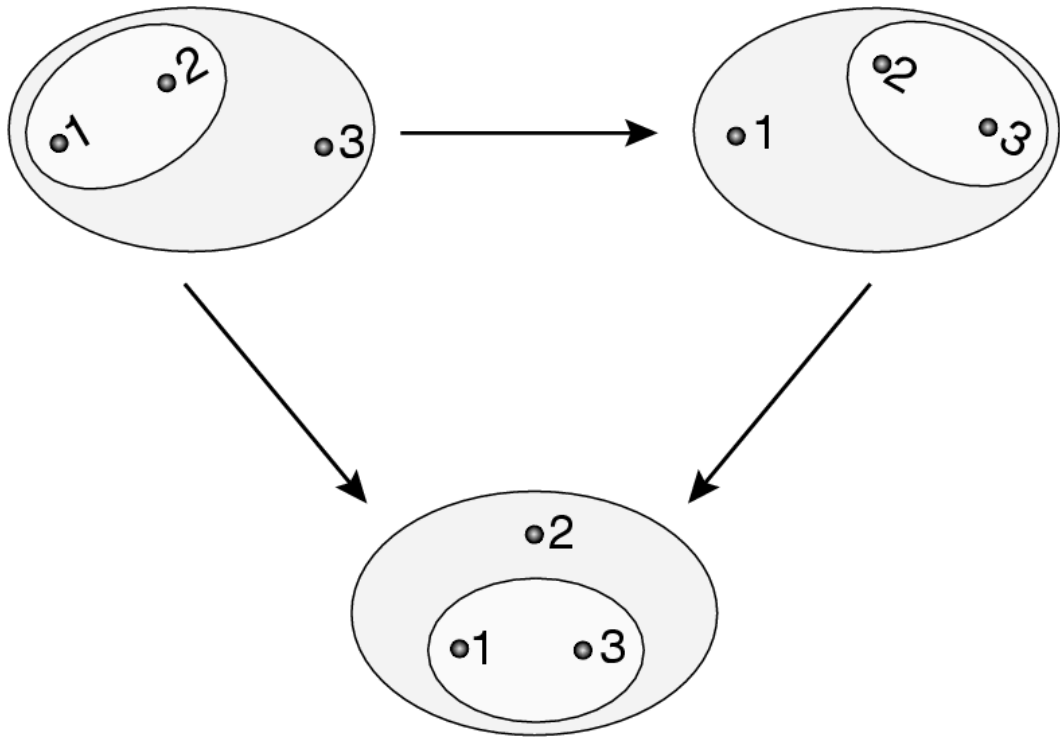


Figure 11: The triangular commutative diagram representing the Racah identity.

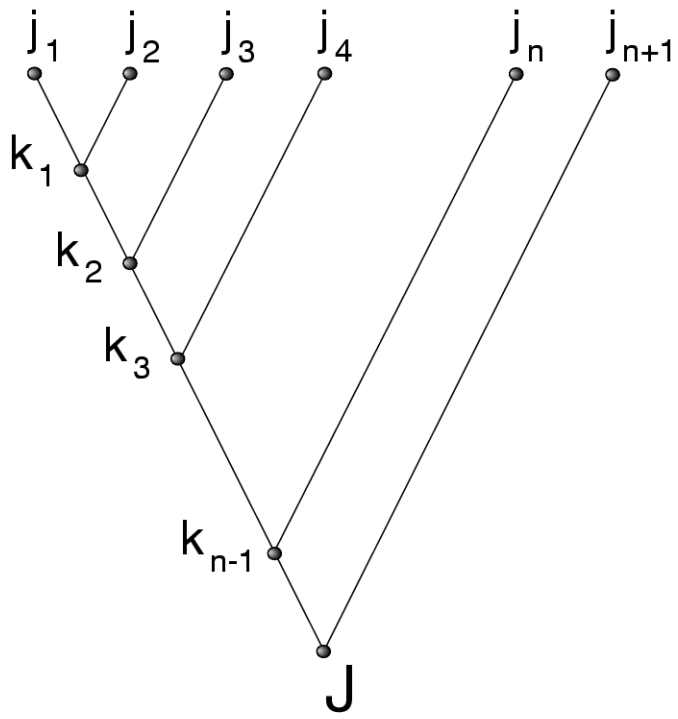


Figure 12: A particular rooted binary coupling tree on $(n + 1)$ leaves where incoming angular momenta are coupled sequentially.

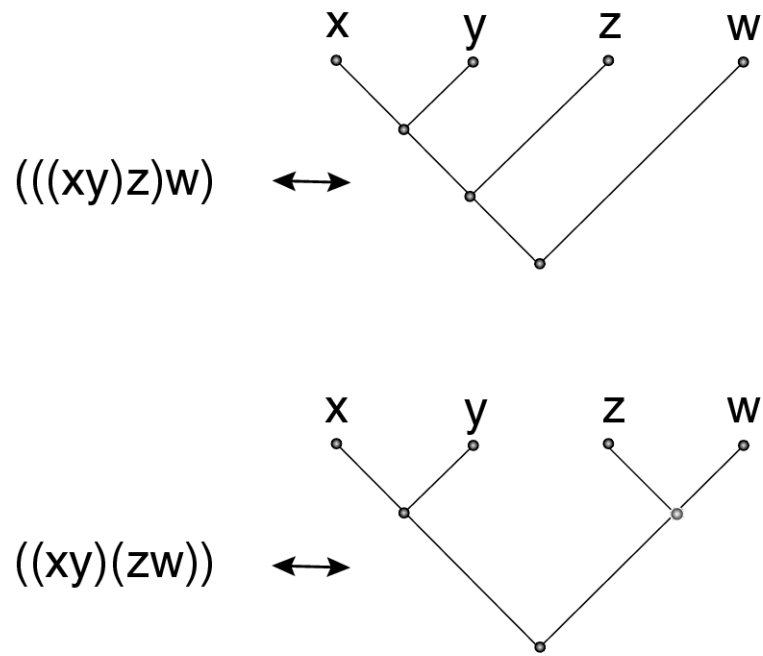


Figure 13: Explicit bijections between binary parenthesizations over an alphabet of 4 letters and rooted binary trees on 4 leaves. Here the ordering of $\{x, y, z, w\}$ is fixed and only two correspondences are depicted [the other ones arise from $(x(y(zw)))$; $((x(yz))w)$; $(x((yz)w))$].

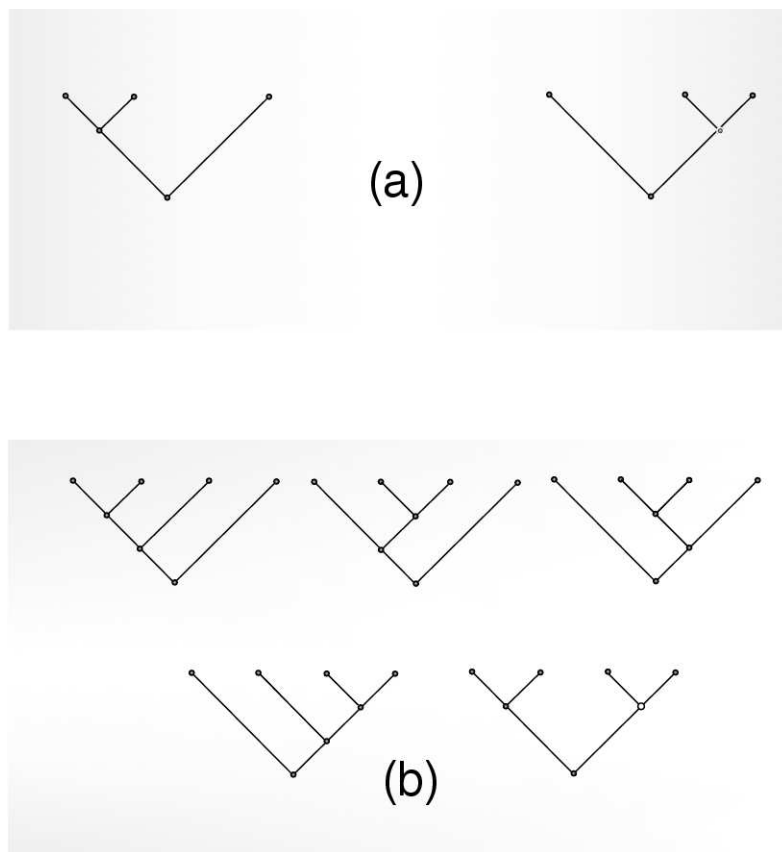


Figure 14: Plane unlabeled rooted binary trees on 3 leaves (a) and 4 leaves (b).

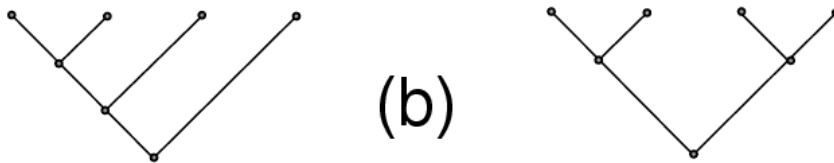
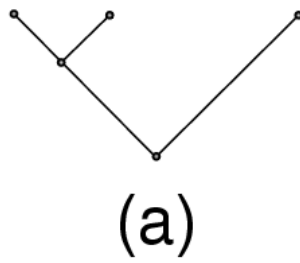


Figure 15: Not plane and unlabeled rooted binary trees on 3 leaves (a) and 4 leaves (b).

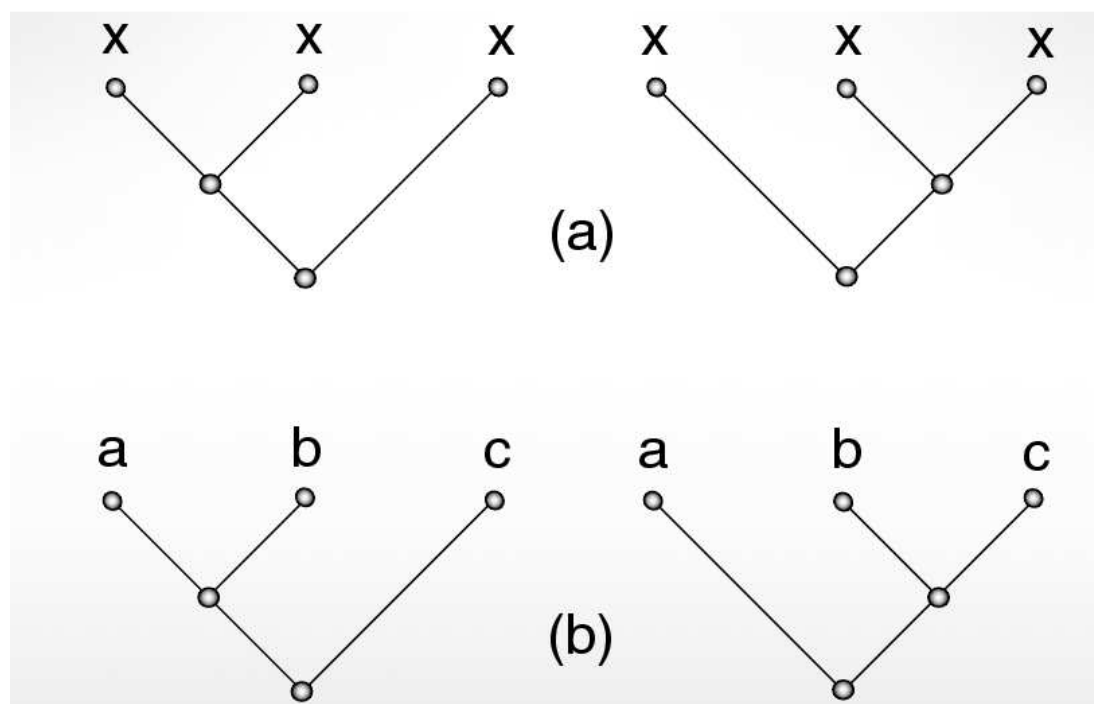


Figure 16: Presentation of Catalan trees on 3 leaves as labeled trees: a same label assigned to each leaf (a); a fixed sequence of distinct labels assigned to leaves (b).

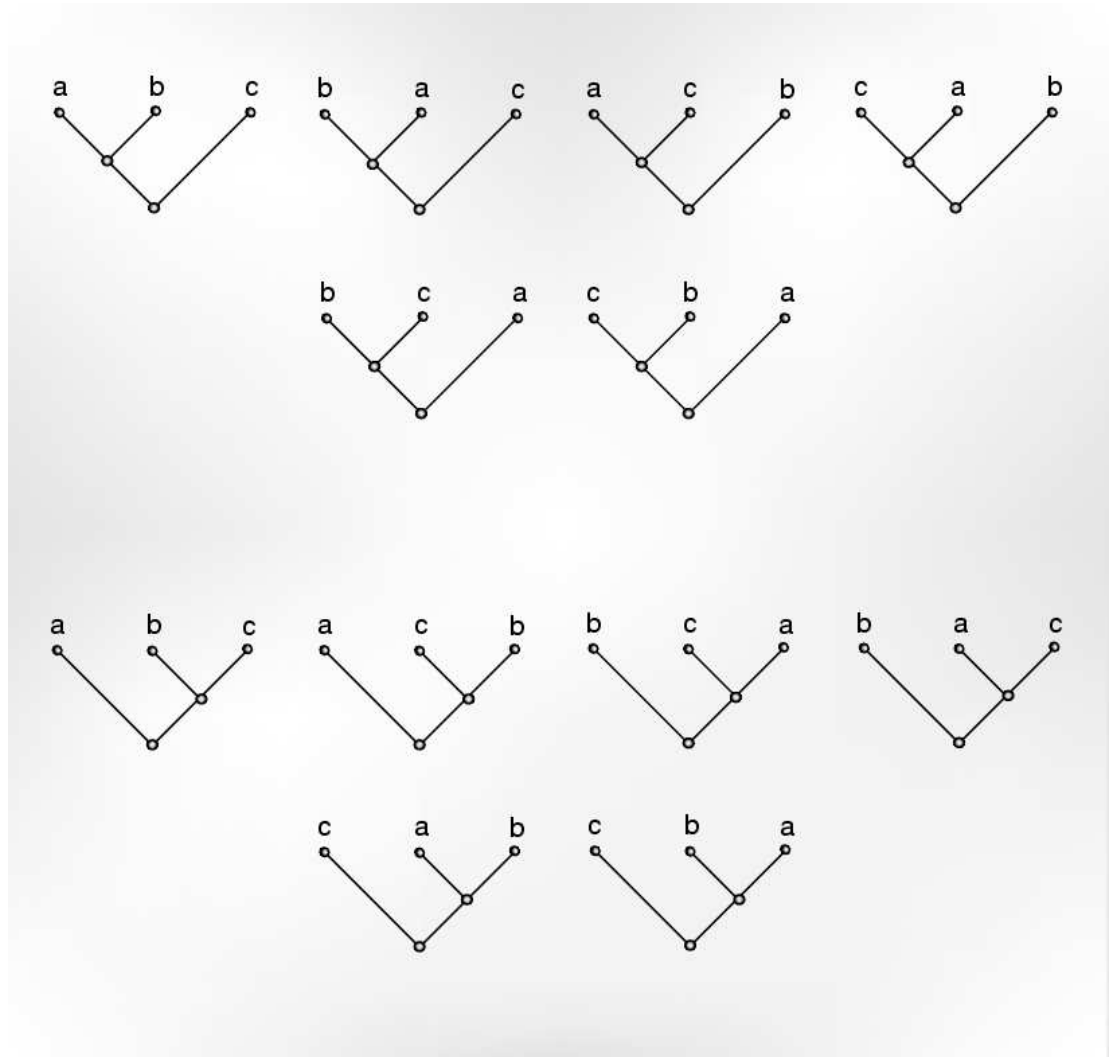


Figure 17: Plane rooted binary trees on 3 leaves labeled in all possible ways with distinct symbols.

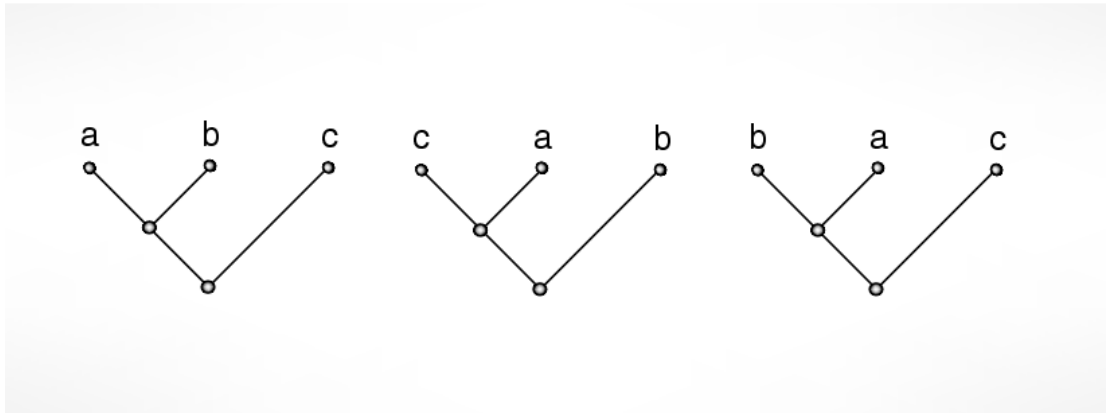


Figure 18: Not plane rooted binary trees on 3 leaves labeled with no distinction between left and right.

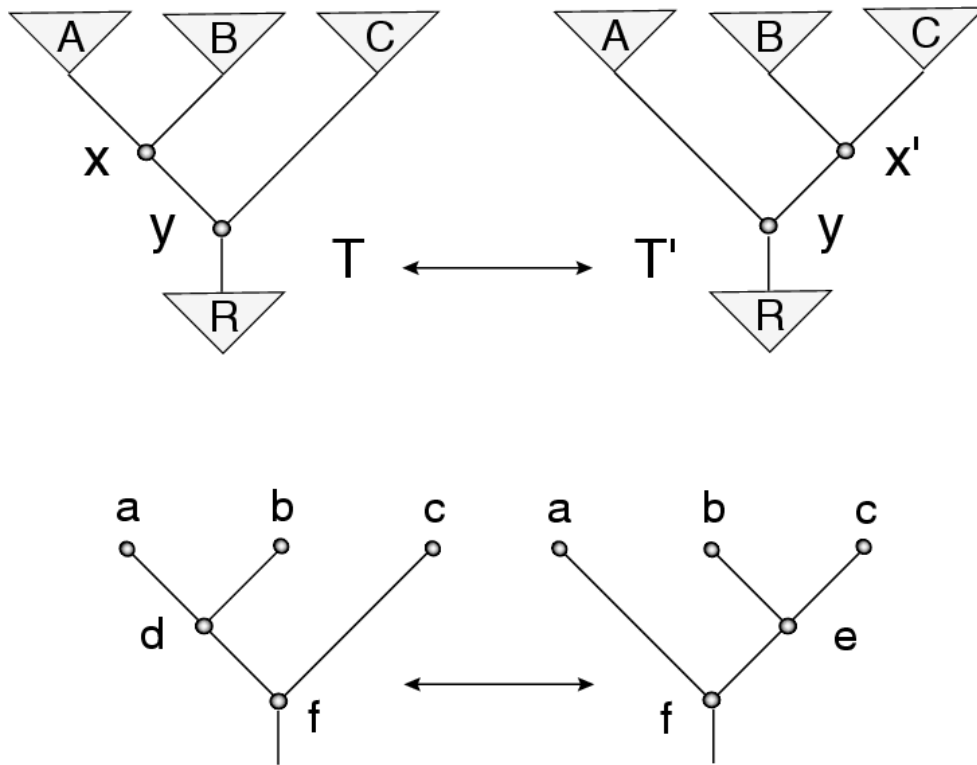


Figure 19: A general rotation (top) and a particular rotation (bottom) on rooted binary trees. A, B, C are generic subtrees, and R is a subtree containing the root.

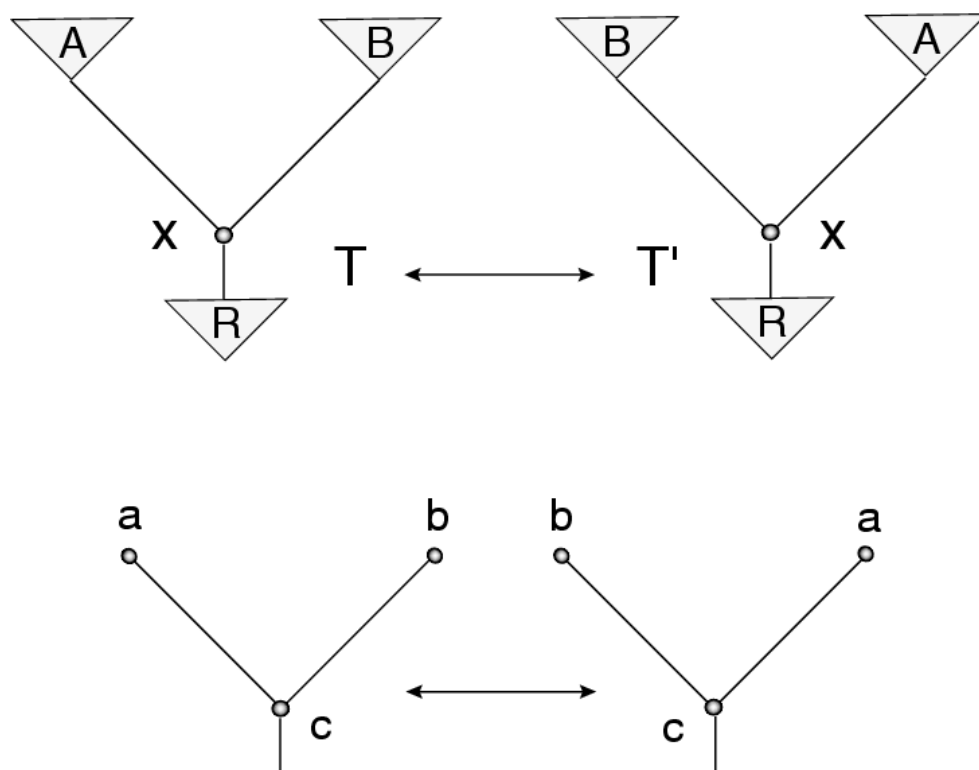


Figure 20: A twist on a generic tree (top) and a particular twist (bottom).

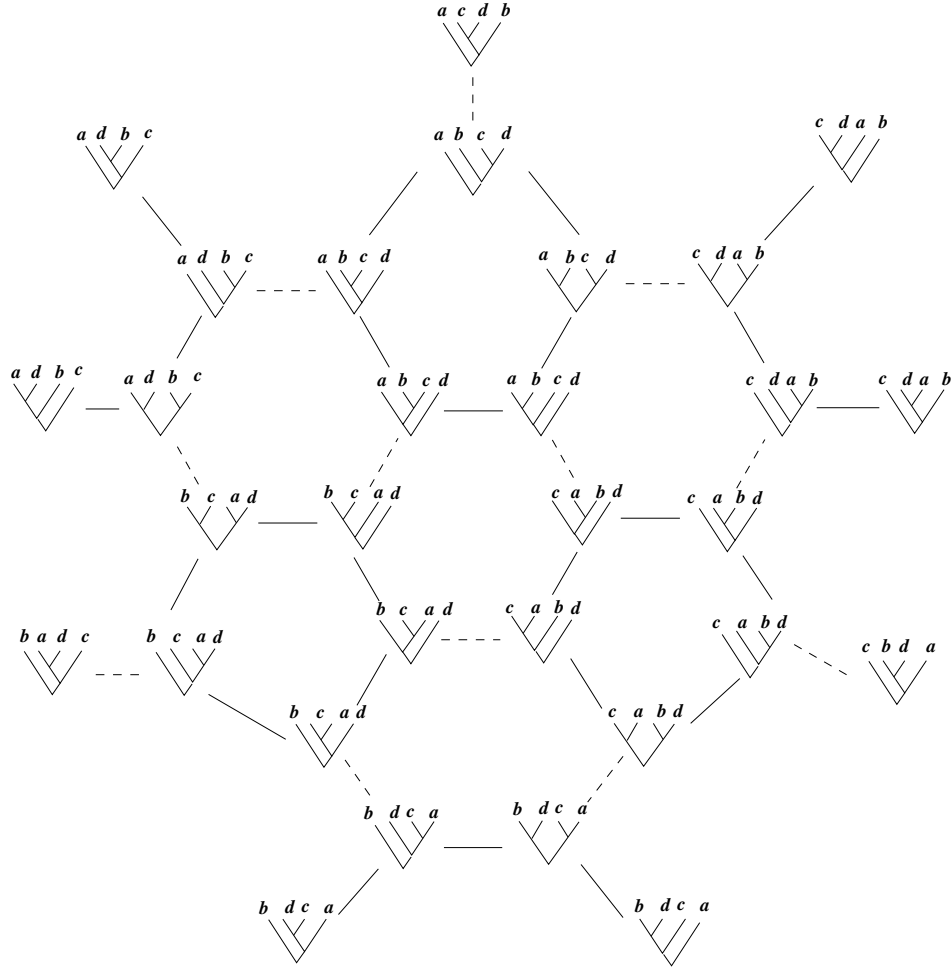


Figure 21: A portion of the Twist–Rotation graph $\hat{\mathfrak{G}}_3$ representing the vertex–edge set of a truncated icosahedron. Only 30 of the 60 vertices are shown, and the picture can be completed by taking the mirror image of each tree at the antipodal vertex. The remaining 60 vertices of $\hat{\mathfrak{G}}_3$ are arranged into an isomorphic graph which is obtained from the former one by exchanging a pair of labels, *e.g.* $(a, b) \rightarrow (b, a)$.

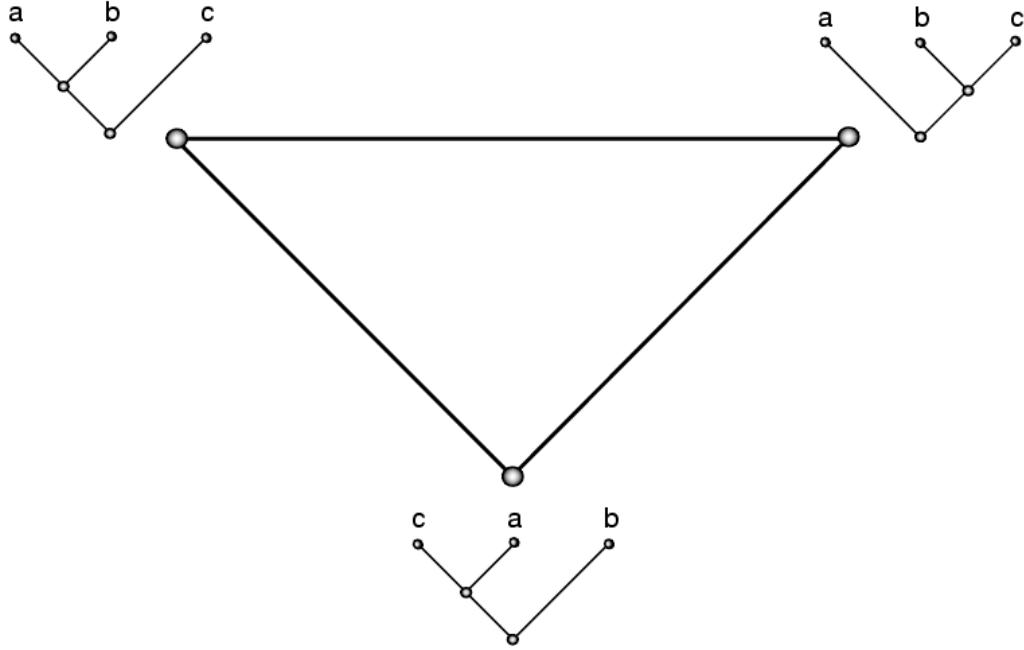


Figure 22: The Rotation graph \mathfrak{G}_2 is depicted as a triangle with binary trees attached to its vertices. Edges correspond to rotations (topologically) but – when dealing with binary coupling trees – they represent three Racah transforms related by the Racah identity (see also Section 4.1, Section 6 and Fig.11). Similar configurations are associated to triangular plaquettes in the Rotation graph \mathfrak{G}_3 of Fig.1.

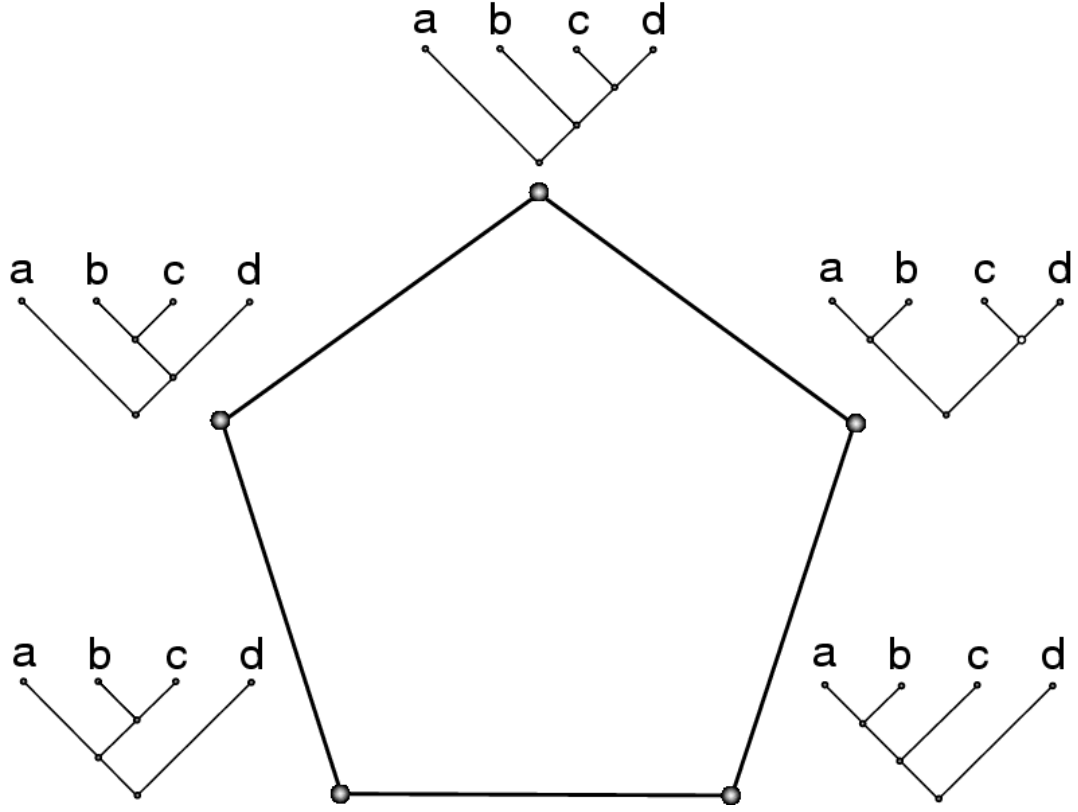


Figure 23: A pentagonal plaquette in the Twist–Rotation graph $\hat{\mathfrak{G}}_3$ of Fig.21 or in the Rotation graph \mathfrak{G}_3 of Fig.1. When binary coupling trees are considered, edges represent Racah transforms related by the pentagon (Biedenharn–Elliott) identity, see Section 4.1.